Dissertation
submitted to the
Combined Faculties for the Natural Sciences and for Mathematics
of the Ruperto-Carola University of Heidelberg, Germany
for the degree of
Doctor of Natural Sciences

presented by
M. Sc. Eva Mareike Hasel
born in Reutlingen, Germany
Oral-examination: 19.05.2017

Egfr signaling in *Oryzias latipes*

-

Characterization of inducible oncogene gain-of-function and receptor loss-of-function Medaka lines

Referees: Prof. Dr. Joachim Wittbrodt

Dr. Lázaro Centanin

Table of Contents

I. Summary

One of the major growth-promoting factors in animal development and growth is the epidermal growth factor receptor (Egfr). The Egfr pathway is involved in proliferation, cell survival, migration and differentiation and is one of the most commonly deregulated pathways in cancer. Medaka fish have two copies of the egfr gene, egfr a and b, which have so far not been analyzed for their particular function and redundancy.

To understand the role of Egfr signaling in the neural stem cell zones of the retina and the brain, we performed a whole mount in situ hybridization screen for egfrs, selected ligands as well as selected downstream signal transducers. We found that both egfrs are broadly and overlapping expressed during development and more specifically in proliferative zones of the brain and the ciliary marginal zone in hatchlings.

To determine the effect of enhanced growth signaling on the retinal stem and progenitor cells we created a versatile toolbox for targeted induction of Egfr-related oncogenes (Xmrk, myrAKT, and K-Ras12V) in cell types of interest. To this end, we tagged the Egfr variant Xmrk with a fluorescent protein and demonstrated its oncogenicity in a somitic overproliferation assay. A Cre-loxP based induction of oncogenes in single cells in somites and also in the retina was successfully achieved in transient and stable lines, and multiple lines were generated. The analysis of oncogenic effects on RSCs was however hampered by the loss of visible expression in later generations in the retina and brain.

To analyze the specific role of Egfra in development and growth I generated a CRISPR/Cas9 based knockout (KO) disrupting the open reading frame by GFP-plasmid insertion or deletion and analyzed the resulting phenotype. Egfra-KO fish develop and reproduce normally but have a defect in oogenesis. Oocytes derived from homozygous Egfra-KO females contain multiple sperm entry sites (micropyles), which causes polyspermy and therefore lethality. The characterization of the polyspermy phenotype, as well as the oogenesis defect in adult ovaries, points towards a role of Egfra in the communication between the granulosa cell layer and the oocyte to specify the micropyle.

By generation of genetic loss and gain of function tools for Egfra and related oncogenes, this work will contribute to understanding the general and the more specific role of Egfr signaling in growth and development of the Medaka fish.

II. Zusammenfassung

Der Epidermal growth factor (Egf) Rezeptor ist ein SchlüsselfAKTor in der Entwicklung und dem Wachstum von Tieren. Der Egf-Rezeptor Signalweg steuert Zellteilung, Zellmigration, Zellüberleben und Differenzierung und ist einer der am häufigsten deregulierten Signalwege in Tumoren. Der Medaka Fisch hat zwei Kopien des Rezeptors: a und b, deren Funktion bisher nicht bekannt ist. Des Weiteren ist unerforscht inwieweit sich beide Rezeptoren in ihrer Funktion unterscheiden oder ob sie redundant agieren.

Um die Rolle des Egf-Signalweges in den neuronalen Stammzellregionen der Retina und des Gehirns besser zu verstehen wurde ein *In Situ Hybridisierung* Screening durchgeführt. Hierfür wurden Sonden für die Erkennung der mRNA beider Egf-Rezeptoren sowie ausgewählter Liganden und Signalübertragungsproteine verwendet. Die Untersuchung hat ergeben, dass die Gene beider Egf-Rezeptoren großflächig und überlappend während der Entwicklung, jedoch später auch in den Stammzellzonen der Retina und des Gehirns abgelesen werden.

Um heraus zu finden ob ein erhöhtes Wachstumssignal eine Auswirkung auf das Verhalten retinaler Stamm- und Vorläuferzellen hat, haben wir eine Reihe von vielseitigen transgenen Fischlinien entwickelt, die es erlauben, Egf-Rezeptor verwandte Onkogene (Xmrk, myrAKT, and K-Ras^{12V}) in einzelnen Zellen oder Zelltypen zu exprimieren. Hierfür haben wir eine onkogene Variante des Egf-Rezeptors, Xmrk, mit einem fluoreszierenden Protein verbunden und die Fähigkeit der Rezeptorvariante, die Zellteilung anzuregen, in einem *in vivo* Zellteilungsassay bestätigt. Ein auf Cre-Lox Rekombination basierendes System ermöglichte es erfolgreich Onkogene in einzelnen Zellen in den Somiten und in der Retina zu exprimieren. Diverse induzierbare Onkogen-Fischlinien wurden generiert und getestet, jedoch wurde die Analyse der Onkogeneffekte auf retinale Stammzellen dadurch erschwert, dass in späteren Generationen der Onkogen-Linien keine sichtbare Expression des fluoreszierenden Onkogens mehr detektiert werden konnte.

Die spezifische Funktion des Egf-Rezeptors a in Entwicklung und Wachstum des Medaka Fisches wurde untersucht, indem das Gen mit Hilfe der CRISPR/Cas9

Technologie deAKTiviert wurde. Homozygote Träger beider Mutationen, eine GFP-Plasmid Insertion sowie eine Deletion von 12 Basen, wurden auf ihren Phänotyp hin untersucht. Egf-Rezeptor mutante Fische sind lebensfähig und in ihrer Fortpflanzung nicht beeinträchtigt; die Nachkommen homozygoter Weibchen weisen jedoch einen spezifischen Defekt bei der Oogenese auf. Homozygote Egf-Rezeptor a mutierte Weibchen produzieren Eier, die mehrere Mikropyle in ihrem Chorion aufweisen, die die Befruchtung der Eizelle mit mehreren Spermien ermöglichen (Polyspermie) und daher zum Absterben der Embryonen führen. In dieser Arbeit wurde der Phänotyp der Polyspermie sowie der Oogenesedefekt charAKTerisiert. Die Ergebnisse deuten darauf hin, dass der Egf-Rezeptor a eine wichtige Rolle bei der Kommunikation zwischen der Eizelle und der umgebenden Granulosa-Zellschicht spielt, die für die Ausbildung des Mikropyle verantwortlich ist.

Durch die Entwicklung genetischer „Gain- and Loss-of-Function“ Systeme für Egf-Rezeptor a und verwandte Onkogene wird diese Arbeit dazu beitragen, die spezifische Rolle des Egf-Signalwegs in Entwicklung und Wachstum des Medaka Fisches zu verstehen.

.

1. Introduction

One of the cardinal signaling pathways in animal development and growth is the epidermal growth factor receptor (Egfr) pathway. The Egfr, also known as ErbB1/HER-1 mediates proliferation, cell survival, migration and differentiation (Herbst 2004). A major challenge in studying the Egfr pathway is its diverse role in development and growth of multicellular organisms. The question how a single receptor can influence such a big range of developmental decisions is an issue that is studied for centuries. Other than most vertebrate, ray-finned fish (Teleostei) have two copies of the *egfr* (egfra and egfrb). The subfunctionalization or redundancy of the two receptors has not been studied in much detail so far. First steps to understanding the individual role of Egfra in fish are described in this work. Of particular interest is the function of Egfr signaling in the central nervous system (CNS) and more specific in the retina. Presented here is a toolbox that allows expressing Egfr related oncogenes in single clones of the freshwater Japanese Killifish *Oryzias latipes*, also known as Medaka.

The introduction covers different aspects of biology with relation to the Egfr and sets the base to understand the results subdivided into three chapters:

1. Expression of *egfrs*, ligand and signal transducer genes in the CNS
2. Egfr related oncogene expression systems for inducible expression in the retina
3. Egfra knock-out phenotype characterization: Defects in oocyte maturation

1.1 Structure and function of the Egfr

The first growth factor was identified and characterized by its ability to induce growth in epidermal tissues of mice and therefore called epidermal growth factor (Egf) (Cohen 1962). In the 1970s an Egf-binding trans-membrane glycoprotein was identified: the Egf-receptor (Egfr). The Egfr belongs to the ErbB family of receptor tyrosine kinases (RTK). Other members of this receptor family in mammals are ErbB2/Neu/HER-2, ErbB3/HER-3, and ErbB4/HER-4. Several biochemical studies demonstrated that the Egfr has an intrinsic kinase function which is specific for tyrosine residues (Buhrow, Cohen, and Staros 1982; Cohen et al. 1982; Ushiro and

Cohen 1980). To be activated the Egfr has to form homo- or heterodimers with other ErbB receptors (Tao and Maruyama 2008) or the Insulin-like growth factor receptor (Igrf) which is structurally very similar (Morgillo et al. 2006).

On their extracellular site, ErbB receptors are heavily glycosylated, and the cysteine-rich domains II and IV (see figure 1 A) can form several disulfide bonds. The other two extracellular domains (I and III) are responsible for binding of ligands. As other RTKs, ErbB receptors have a single transmembrane domain. The intracellular part (C-terminal region) contains several autophosphorylation sites as well as a juxtamembrane tail (Linggi and Carpenter 2006).

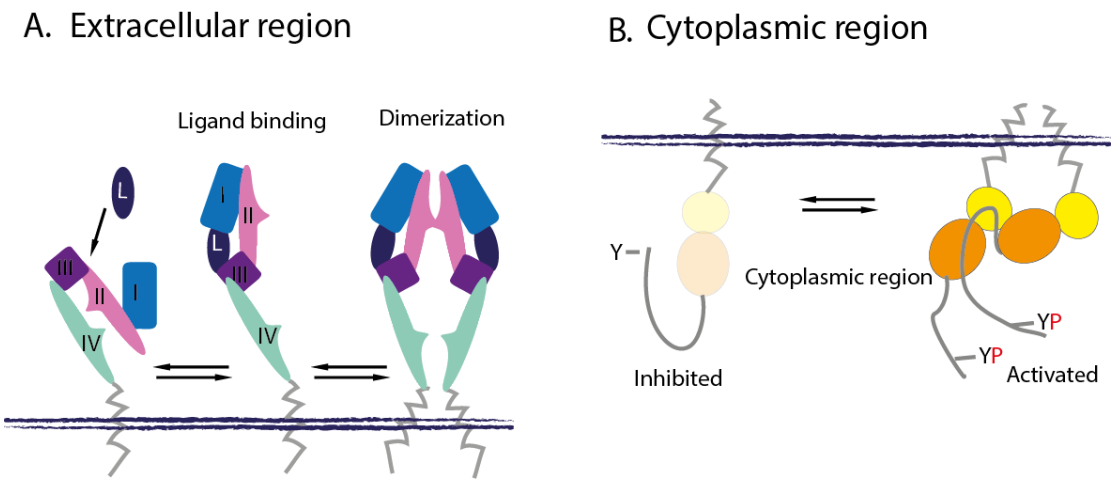

Figure 1: Schematic representation of the extracellular and intracellular domains of the Egfr upon ligand-binding induced activation. A. The Egfr has four domains, two ligand-binding domains (I and III) and two interaction domains (II and IV). Upon ligand binding, the receptor changes its conformation and can interact with one other receptor monomer. B. Upon dimerization of the extracellular interaction domains, the cytoplasmic domains phosphorylate each other on their tyrosine residues and become activated. The figure is redrawn from Linggi and Carpenter 2006.

Adding to the complexity of Egfr- signaling is that various structurally related ligands can bind the receptors extracellular domain. The vast majority of ligands namely Egf, heparin-binding Egf (Hb-Egf), transforming growth factor-α (Tgf-α), amphiregulin, epiregulin, epigen and betacellulin bind exclusively to the ErbB1 receptor (Linggi and Carpenter 2006). All of these ligands are translated into transmembrane precursors and become activated by proteolytic cleavage mediated by membrane-anchored metalloproteases of the ADAM family, a process known as ectodomain shedding. The ectodomain is then freed to act as a receptor ligand (Blobel 2005; Schlöndorff and Blobel 1999).

Ligand binding to the receptor domains I and III causes homo- and heterodimerization of two receptors which in turn activates the intracellular kinase domain (figure 1B). The kinase domains of dimerized receptors phosphorylate each other at specific tyrosine residues on the cytoplasmic tail. The phosphorylated tyrosine residues, in turn, serve as binding sites for Src homology 2 domain (SH2) containing proteins. The main SH2 domain containing proteins of the Egfr signaling pathway are Grb2 (Lowenstein et al. 1992), Son Of Sevenless (SOS) (Buday and Downward 2017), Src homology 2 domain containing (SHC) proteins (Pelicci et al. 2017; Ruff-Jamison et al. 1993) and Protein Lipase C-γ PLCγ (Margolis et al. 1990; Rotin et al. 1992), which in turn activate complex downstream signal transduction cascades (Schlessinger 2002; Yarden and Sliwkowski 2001). The output of activated Egfr signaling is diverse and depends on the type of ligand binding and dimer formed (Maria Sibilia et al. 2007).

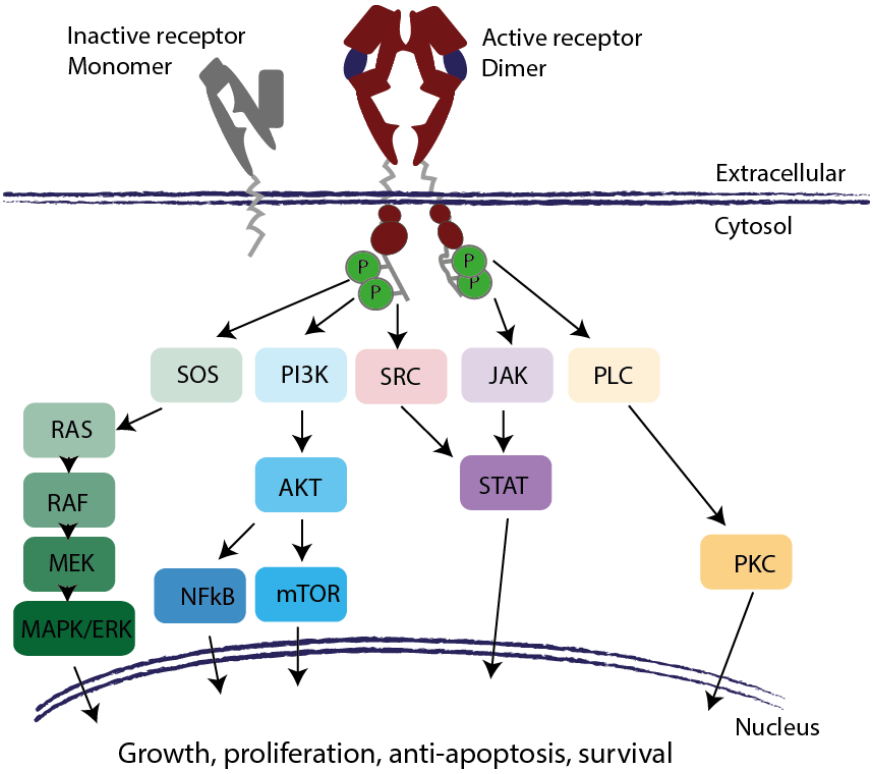

Figure 2 Simplified signal transduction pathways activated by the Egfr. The RAS/MAPK pathway is activated via SOS. NFkB and mTOR signaling are activated via PI3K and AKT. SRC and JAK both activate different STAT proteins. PLC activates PKC after interaction with autophosphorylated Egfr.

The Egfr controls vital functions of cells like survival, growth, cell division, motility, apoptosis and differentiation and thereby fulfills a fundamental role in development.

Several downstream signaling cascades mediate the diverse cellular processes induced by Egfr-ligand interaction. SH2-containing proteins bind to the phosphorylated tyrosine residues of the activated receptor and in turn activate downstream signal transducers as rat sarcoma (RAS), Protein kinase B (PKB/AKT) and Signal Transducers and Activators of Transcription (STAT) proteins and protein kinase B (PKB) (figure 2). The reactions elicited by the Egfr activation are specified by the ligand-receptor interaction and other co-factors (K. J. Wilson et al. 2009). On top of the diversity of ligands and downstream effectors, additional layers of regulation of EGFR signaling exist, that guarantee spatial and temporal control.

Intracellular Egfr-stimulated signal transducers are highly interlinked with other signaling pathways as the insulin-like growth factor (Igf) or the fibroblast growth factor (Fgf) pathway, which makes it difficult to dissect Egfr-specific functions. The study of the physiological role of the receptor was long hampered by the severity of the effects caused by enhanced or decreased activity of the receptor in various tissues of mammals (Maria Sibilia et al. 2007).

The presence of two Egfrs in Medaka might allow uncovering new roles of Egfr signaling in development and growth of vertebrates since a partial redundancy might allow generation of loss of function models and the sub-functionalization might permit the dissection of different roles in complex processes.

1.2 General physiological role of EGFR signaling

Egfr proteins are conserved in metazoans and have derived from a basic receptor ligand interaction pair as found in *Caenorhabditis elegans* (*C.elegans*) where LET-23 is the only receptor and LIN3 the only ligand *(Aroia*n *et al. 1990; Mog*hal and Stern*berg* 2003).LET-23 mediates two different kinds of processes dependent on the signal transducer used downstream of the receptor. The receptor stimulates the Ras/MAPK pathway to regulate cell fate specification during organogenesis on the one hand, on the other myoepithelial contractions during ovulation via IP3 mediated signal transduction (Moghal and Sternberg 2003). Looking at this simple version of the pathway in *C. elegans* already demonstrates the various ways in which Egfr signaling acts in development.

In *Drosophila melanogaster* only one ErbB receptor (DER) is present. In contrast to only one ligand in *C.elegans* however, five different ligands exist Spitz, Keren, Gurken, Agros and Vein. The downstream signaling cascade in flies is much simpler than in vertebrates with unbranched canonical Ras/MAPK activation being the default output of receptor activation. The fly Egfr receptor, DER, and its main ligands Spitz are broadly expressed. Nevertheless, EGFR signaling is spatially and temporally tightly regulated (B.-Z. Shilo 2005) to control various processes in the embryo and the larvae/pupae stage as cell and tissue fate during development, proliferation, and differentiation of cell types in wings, eyes, legs and ovaries (Schweitzer and Shilo 1997). While the multitude of developmental programs in the fruit fly are regulated by the Spitz ligand, Gurken is mainly involved in oogenesis related processes (Shilo 2003).

In vertebrates, the Egfr controls a similar spectrum of developmental programs. Loss of function studies, performed mainly in mice, helped to understand the vertebrate Egfr pathway in more detail. Egfr mutant mice die during different stages of development and are growth retarded. Mice that reach post-natal stages show abnormalities in the bone, brain heart, skin, hair follicle, and eyes. $Egfr^{-/-}$ embryos mostly die *in utero* because of placental defects and lung immaturity; surviving embryos have severe brain defects (Miettinen et al. 1995; M Sibilia and Wagner 1995; Threadgill et al. 1995). Knockouts of single receptor ligands lead to comparably mild

phenotypes indicating that there is high redundancy between ligands (Cook et al. 1997; Luetteke et al. 1994).

In fish, not many aspects of Egfr signaling have been investigated so far. In *Zebrafi*sh Egfr-signaling is essential for proper heart development (Goishi et al. 2003) as well as for oocyte maturation (Wang and Ge 2004; Yefei and Wei 2002). Novel genome editing tools like CRISPR/Cas9 allow fast and easy generation of loss of function mutants and enable researchers to dissect Egfr function in teleost species in more detail.

With the help of conditional alleles the receptor is now studied more specifically for its role in different tissues or processes (Lee and Threadgill 2009) for example in bone metabolism (X. Zhang et al. 2011), renal development (Z. Zhang et al. 2010) and skin innervation (Maklad et al. 2009). Although some studies are concentrating on the physiological functions of Egfr signaling the main focus of mammalian Egfr-related research is the role of the receptor in cancer and its potential as a target for anti-cancer therapy.

1.3 Egfr signaling out of control

The diversity of functions that the Egfr has in growth and development is reflected by the severity of effects resulting from deregulation of the pathway. Hyperactivity of Egfr-signaling is a common feature of many cancers by causing an unbalance between proliferation and differentiation of cells. Egfr itself can be found over-expressed for example in brain, colorectal, breast, lung, pancreatic and prostate cancers but can transform cells only in the presence of a ligand to stimulate an autocrine loop. Many cancers bear a somatic mutation that renders the receptor constitutively active for example by deletion of a part of the extracellular domain (Moscatello et al. 1995) or changes in the intracellular kinase domain. Constitutively activated Egfr signaling in cells that are not interrupted by induction of apoptosis will start dividing uncontrolled and adapt a more migratory phenotype. Tumor growth and metastasis are also often correlated with increased ligand and receptor levels (Überall et al. 2008).

Various cancer models in mice, rats and fish use Egfr related oncogenes to induce over-proliferation and thereby tumor formation. These oncogenes are for example constitutively active forms of the receptor itself or hyperactive downstream signaling components as K-Ras, AKT or Braf. K-Ras variants are used to induce cancer in the pancreas (Friedlander et al. 2009), lung (Kim et al. 2005) and brain (Bachoo et al. 2015. Oncogenic AKT is used as a trigger for brain tumors (Holland et al. 2000). Xmrk (*Xiphophorus* melanoma receptor kinase), a mutant form of the egfrb, is used to transform melanocytes (Schartl et al. 2010) as is a mutant for of BRAF (Dhomen et al. 2009) and other mutant forms of Egfrs induce glioblastoma (Bachoo et al. 2002).

1.4 Teleost as cancer models

Teleost fish, like Zebrafish and Medaka, are used to model human diseases for approximately 25 years. Tumors of various tissues, which develop spontaneously or after induction of mutations by radiation or chemicals, resemble those of humans, histologically and genetically (Feitsma and Cuppen 2008). Many fish tumor models based on chemical treatment, xenotransplantation, knockout of genes or transgenesis were established (Feitsma and Cuppen 2008; H. Feng et al. 2007; Le et al. 2007). The generation of transgenic lines, often expressing mammalian oncogenes, overcame the disadvantages of tumor models based on random mutation screens: the frequency of

off-target mutations, the unpredictability of the outcome and the amount of fish necessary.

An example for a transgenic tumor model is the Medaka melanoma model (Schartl et al. 2010) based on the expression of the potent oncogene, the *Xiphophorus* melanoma receptor kinase (Xmrk). *Xmrk* is a mutated variant of the *egfrb* proto-oncogene that is unique to the genus *Xiphophorus* (Wittbrodt et al. 1989). The oncogenic receptor occurred during the diversification of the genus from a duplication event (Weis and Schartl 1998) and is favored by sexual selection for the hyperpigmentation it causes in male carriers (Fernandez and Bowser 2010). If uncoupled from a repressor by hybrid back-crosses, expression of *xmrk* leads to the formation of a spontaneous, lethal melanoma (Ahuja and Anders 1976).

If transgenically expressed under the pigment cell-specific *microphthalmia-associated transcription factor (mitf)* promoter in Medaka, *xmrk* causes malignant melanomas with a prevalence of 100% in homozygous carriers without any additional mutation (Schartl et al. 2010). The oncogenicity of this specific Egfr-variant is due to two activating mutations in the extracellular domain of the receptor which render it constitutively activated in a ligand-independent manner (Dimitrijevic et al. 1998; Winnemoeller, Wellbrock, and Schartl 2005). Because Egfr is upstream of various downstream signaling cascades, it is not surprising that *in vitro* and *in vivo* Xmrk is able to induce several characteristics of neoplastic transformation. Xmrk induces strong cell proliferation and anti-apoptotic signals, inhibition of differentiation and survival of melanocytes in cell culture as well as in Medaka (C Wellbrock et al. 1998; Claudia Wellbrock et al. 2002; Claudia Wellbrock, Fischer, and Scharti 1998). Various tissues of fish embryos are sensitive to cancerogenic transformation through *xmrk* expression; it is, therefore, a gene with enormous oncogenic potential (Geissinger et al. 2002; Winkler et al. 1994). Melanomas, as well as hepatocellular carcinomas stimulated by *xmrk* expression, share molecular signatures with respective human cancers and cancer cell lines (Teutschbein et al. 2010; Zheng et al. 2014). A tetracycline-inducible system (Tet-ON) has been used to express *xmrk* in the liver to induce hepatocellular over-proliferation. These "carcinomas" develop within a couple of weeks with a 100% penetrance when fish are constantly treated. The liver, however, regresses to normal size as soon as the treatment is stopped. The "carcinomas" are

thus *xmrk*-dependent as is the activity of downstream signal transducers Stat5 and Erk (Li et al. 2012).

Oncogenic versions of the small GTPase protein Ras as the K-RAS^{G12V} are often mutated in the GTPase domain leading to a constant signaling GTPase. This Ras-variants are used for cancer models to induce for example pancreatic cancers (Friedlander et al. 2009). K-RAS^{V12} was also expressed in a GAL4-UAS transactivator system in Zebrafish to induce proliferation of endothelial cells (Alghisi et al. 2013) and brain tumors (Mayrhofer et al. 2016). The clonal mouse tumor models are either based on the expression of an oncogene, knockout of an endogenous tumor suppressor gene or a combination of both in single cells. Widely adapted for activation of the oncogene is the excision of a floxed STOP cassette. An inducible and lineage-specific expression of a recombinase guarantees spatial and temporal control of oncogenes (Rappaport and Johnson 2014). Several Cre-Lox based inducible clonal tumor models exist in mice, but so far there is no genetic fish model expressing *xmrk* or any other oncogene in a clonal manner

1.5 CNS- and retina-specific effects of Egfr signaling and oncogenes

Looking at the incidence number of cancer in different tissues and the correlation to enhanced Egfr signaling it becomes apparent that different cell types react differently to Egfr-related oncogene expression. Some cell types will develop malignant tumors (Schartl et al. 2010) while other tissues react with enhanced proliferation (Li et al. 2012) and terminal differentiation (Aguirre, Rubio, and Gallo 2010) or even apoptosis (Rush et al. 2012). In humans, most adult cancers arise in tissues in which cells are regularly replaced by adult stem cells, such as skin (Blanpain and Fuchs 2006) and intestine (Barker et al. 2009). In other adult tissues as the CNS, more specifically the retina, cancers develop very rarely or never which might be due to the lack of proliferating cells. Subsets of cells isolated from the pigmented ciliary margin of the mouse retina can however clonally proliferate in vitro and differentiate into various retinal cell types if stimulated with Egf or Fgf (Tropepe 2000). In contrast to mammals, teleost fish like Zebrafish and Medaka have adult retinal stem cells (RSCs) that are active throughout the life of the fish and are implicated in maintenance,

growth, and regeneration of the eye (Amato, Arnault, and Perron 2004; P. Raymond et al. 2006) and could thus be responsive to the occurrence of oncogenic mutations in the Egfr pathway. Yet, cancers or even over-proliferation of the neural retina never occur as far as the literature reports, suggesting a very tight control of growth in the retina that cannot be disturbed easily.

The Egfr plays a central role in the development of the *D. melanogaster* eye. Its role in vertebrate eye development and growth has so far not been elucidated to a high extend. Various signaling pathways as insulin (Boucher and Hitchcock 1998), Hedgehog, Tgf-ß, Wnt (Meyers et al. 2012) and Fgf (Martinez-Morales et al. 2005) signaling play and important role in eye development and growth.

Enhanced Egfr signaling in the neural stem cells (NSCs) of mouse brains shifts the balance between NCS and their progenitors towards the neural progenitor cell (NPC) pool reducing self-renewal of NSCs. Egfr signaling, together with Notch, mediates the balance between these two cell populations (Aguirre, Rubio, and Gallo 2010). Notably, in this case, the over-activity of Egfr alone is not enough to stimulate tumor formation but rather drives the stem cell pool towards terminal differentiation.

The result of Egfr loss in mammals is progressive, wide-ranging neurodegeneration due to apoptosis of neurons and glial cells (astrocytes and oligodendrocytes) (Kornblum et al. 1998; M Sibilia et al. 1998).

1.6 The retina in teleost fish

Development and organization of the eye are highly conserved among vertebrate species. The events leading to the formation of the mature NR out of an epithelial monolayer happen in a very stereotypic manner. The retina is the most available part of the CNS and is therefore a traditional model to study neurogenesis and behavior of NSCs. The single layer of neuroepithelium develops into a laminated tissue with seven major cell types (six neural and one glial cell type), each of which takes a well-defined position in the retina (Figure 3 A and B). By this retinal cells form a highly organized structure of three nuclear layers divided by two plexiform layers (Livesey and Cepko 2001). The nuclei of rod and cone photoreceptors make up the outer nuclear layer (ONL) in which light is photoconverted into membrane potentials. The neural impulses are then transmitted through a relay in the inner nuclear layer (INL) to the retinal ganglion cells (RGCs). In the ganglion cell layer (GCL). RGCs project the signals through their axons bundled in the optic nerve towards the optic tectum (OT).

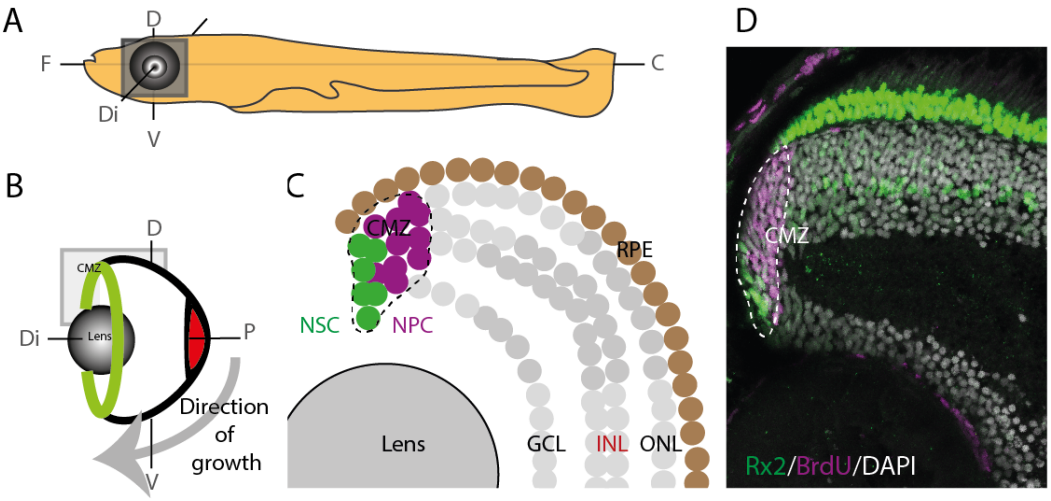

Figure 3: Different views on the retina and the CMZ of the Medaka hatchling. A. Schematic representation of the Medaka hatchling. B Eye of the Medaka fish represented to understand the orientation of retinal growth. Cells are added at the CMZ (green ring) around the lens so that the direction of growth is from the proximal embryonic retina (red) to distal. The gray square represents the section plane shown in C. C. Schematic drawing of the CMZ. Rx2-positive RSCs, at the most distal part of the CMZ, are depicted in green, highly proliferative retinal progenitor cells (RPC) are depicted in magenta. The CMZ and the differentiated neural retina (gray) are surrounded by a single cell layered retinal pigmented epithelium (RPE, brown). D. Section through a retina of a hatchling incubated in BrdU for three days. Stem cells, photoreceptors and Müller glia cells (MGCs) expressing Rx2 are stained in green. BrdU labeling the dividing RPCs are depicted in magenta. F=frontal, V=ventral, D=dorstal, Di = distal , C=caudal, CMZ=ciliary marginal zone, RSC=retinal stem cell, RPC= retinal progenitor cell, GCL=ganglion cell layer, INL=inner nuclear layer, ONL=outer nuclear layer, RPE=retinal pigmented epithelium

The INL accommodates the bipolar-, horizontal-, amacrine and Müller-glia cells (MGCs). MGCs, being the only non-neurogenic cells, are the radial glia of the retina (Bernardos et al. 2007; Urlinger et al. 2000) and fulfill special functions. They span the whole neural retina and act to support retina homeostasis. Upon injury, MGCs can act as multipotent RSCs (Bernardos et al. 2007; P. A. Raymond et al. 2006) and can even be stimulated to re-enter cell cycle by expression of Atoh7 (Lust et al. 2016) or stimulation with HB-EGF (Wan, Ramachandran, and Goldman 2012).

The actual RSCs of the adult fish retina are located in the ciliary marginal zone (CMZ) a ring of cells in the outermost periphery of the retina (Figure 3A, green ring). As the NR grows, the CMZ moves outwards, and newly formed neurons are added to the outer rim close to the lens. This temporal organization of the retina, leaving old neurons in a central position and young neurons in the periphery, makes the position of a neuron a direct temporal read-out. The homeobox transcription factor retina-specific homeobox gene 2 (rx2) can be used as a bona fide marker for RSCs (Figure 3D) (Reinhardt et al. 2015) but is also expressed in photoreceptors and MGC. As the RSCs divide they give rise to faster cycling RPCs that then terminally differentiate into neurons or MGCs and take their place in the structured retina.

Transplantation experiments, using fish lines that express fluorescent proteins ubiquitously, could prove that multipotent adult stem cells located in the CMZ form arched-continuous stripes (ArCoS) independently in the NR and the retinal pigmented epithelium (RPE) (Centanin, Hoeckendorf, and Wittbrodt 2011). The RPE is a single epithelial layer essential for proper functioning of the retina (Ramón Martínez-Morales, Rodrigo, and Bovolenta 2004), grows in a coordinated fashion with the NR and shares the developmental origin. However, the RPE stem cell is not concordant with the NR stem cell even though location in the CMZ and growth patterns are similar (Centanin, Hoeckendorf, and Wittbrodt 2011).

More recently it could be verified by long-term analysis of induced color-recombined RSCs that these cells retain their ability to divide throughout the life of the fish asymmetrically (Centanin et al. 2014). Using stem cell specific (Rx2 driver) or heat shock inducible Cre-driver lines (Rx2:: Cre-ERT2/hsp70:: Cre) and a fish ubiquitously expressing a floxed labeling cassette (Livet et al. 2007) recombination towards an

easily detectable H2B-GFP label in single stem cells let to the formation of colored ArCoS. The history of a clone derived from a single RSC can be analyzed by the shape of the ArCoS (Centanin et al. 2014; Centanin, Hoeckendorf, and Wittbrodt 2011). The ArCoS assay is a great tool to study the effect of genetic factors, more precise the expression of oncogenes, on the behavior of single RSCs and RPCs and their descendants.

The vertebrate neural retina seems to be immune to the occurance or the effect of oncogenic mutations, given the fact that tumors originating from this tissue have not been described. The growing NR must thus have active mechanisms that prevent over-proliferation since it is of great importance for proper functioning of the eye that the stereotypic organization is not disturbed. The only tumor arising from the retina is retinoblastoma caused by a bi-allelic mutation of the Retinoblastoma (Rb) gene. This tumor exclusively occurs in children from immature retinoblasts with proliferative capacity. In mammals, the noticeable absence of retinal cancers might thus be due to the lack of proliferating cells in the retina. In vitro however, the receptor ligand Egf stimulates proliferation and differentiation of murine RSCs (Angénieux, Schorderet, and Arsenijevic 2006).

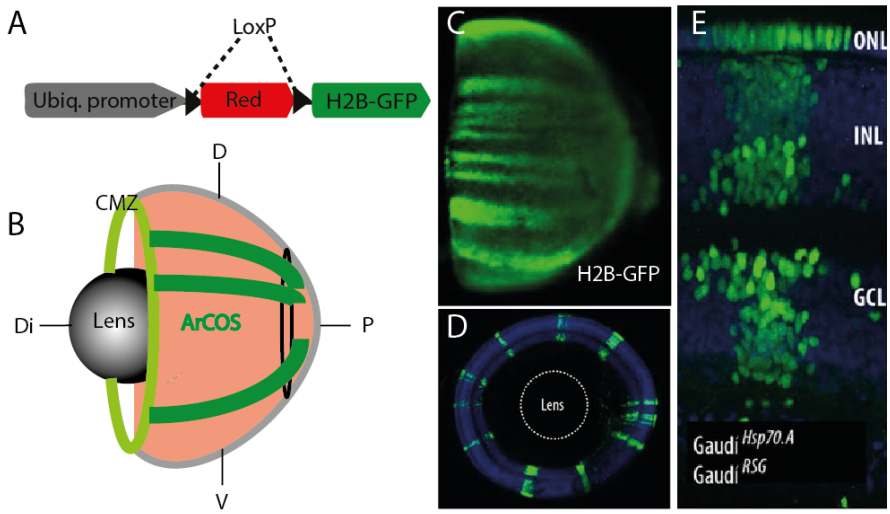

Figure 4: ArCoS assay used to label single RSC clones used to demonstrate the preference for asymmetric division mode of RSCs. A. Genetic layout of the labeling cassette expressing the default DsRed and upon recombination in single cells express H2B-GFP as a clonal label. B. Schematic representation of ArCoS formed by single labeled clones spanning from the embryonic retina (proximal ring) to the CMZ (green ring around lens). C. Example of a whole retina with several ArCos. D. Section through the entire retina showing several ArCoS. E H2B-GFP labeled clone, containing cells of all three nuclear layers. Di=distal, D=dorsal, P=proximal, V=ventral, ArCoS=arched continuous stripes, ONL=outer nuclear layer, INL=inner nuclear layer, GCL=ganglion cell layer. Panel C-E were adapted from (Centanin et al. 2014).

1.6.1 Egfrs and its ligands in teleost fish

The mammalian EGFR is the only receptor of the ErbB1 class of Erb RTKs, and not much had been known about egfrs in fish until the beginning of the '00s. Except for the *Xiphophorus xmrk* gene, that was described in 1989 no other teleost Egfr had been isolated until 2004, even though a proto-oncogenic version of Xmrk (INV-*xmrk*/*egfrb*) was described before (Dimitrijevic et al. 1998).

In 2004 Gómes et al. published the isolation and characterization of another *Xiphophorus* egfr gene (egfra) and suggested a fish-specific duplication of an ancestral receptor gene (Gómez et al. 2004). Another local gene-duplication of egfrb in the *Xiphophorus* genus then let to the occurrence of xmrk. The expression of egfra in different tissues of *Xiphophorus* is much closer to the expression patterns of the Egfr in mice then is the pattern of egfrb expression. Another hint that egfra might be functionally more related to the mammalian Egfr is its ability to react to stimulation with human EGF (hEGF) which does not stimulate egfrb (Gómez et al. 2004). During development of Medaka, the egfrs are expressed in a dynamic pattern as could be shown by using a human antibody (AB) against the more conserved tyrosine kinase domain (Boomsma, Scott, and Walters 2001).

The two egfrs in teleost are a result of the fish-specific genome duplication of (FSGD) 320-350 million years ago after which many duplicates disappeared again, but some were retained because of neofunctionalization or subfunctionalization of the gene copies (Meyer and Van De Peer 2005; Postlethwait et al. 2004). Whether one or the other is the case for egfra and egfrb or whether they are completely redundant is not known so far. In contrast to the receptors, only one copy of each ligand is conserved in fish except for the two *hb-egf* genes in Zebrafish (Kassahn et al. 2009; Laisney et al. 2010). Even though all Egfr ligands were retained in teleosts as in tetrapods, the sequence conservation is rather weak. The comparison between tetrapod and teleost egfr gene sequences revealed that highest similarities could be found in the intracellular tyrosine kinase domain and greatest difference in the extracellular domain. The ligand-binding domain displays little identity between teleost and tetrapods and even between different teleost's itself, suggesting the co-evolution of ligands and receptor ligand binding site (Laisney et al. 2010). This might also be a hint for a possible sub-functionalization between the two teleost *egfrs*.

Egfr transcripts are deposited in the oocyte since high expression of both receptors in stage 8 Medaka embryos, and only low zygotic expression could be detected. RT-PCR analysis of egfr transcripts revealed that *egfra* and *egfrb* are similarly expressed in muscles, testis, brain eye and heart and different in spleen, kidney, skin (egfra higher) and gills liver and ovary (*egfrb* higher) (Laisney et al. 2010). The same pattern could be observed in *Xiphophorus* (Gómez et al. 2004) and might be due to a tissue specific subfunctionalization of the receptor.

Relevant answers about the subfunctionalization and redundancy of the two egfrs are to be gained by loss-of-function approaches that are feasible in times of easy genome editing techniques as CRISPR/Cas9. Described in this work is an egfra loss-of-function Medaka line in which a surprising function during oogenesis of egfra is revealed. The course of oogenesis and the known functions of egfr in this process are in the following described in more detail.

1.7 Oogenesis and Egfr signaling

One organ in which Egfr-signaling is known to play a significant role in different species is the ovary, especially during the process of oogenesis (FregosoLomas et al. 2013; Jamnongjit, Gill, and Hammes 2005; Schweitzer and Shilo 1997; Wang and Ge 2004; Yefei and Wei 2002).

Most teleost fish are oviparous, meaning that they produce yolk-containing eggs instead of living offspring. For the generation of these eggs, three different ways are described: synchronous, group-synchronous and asynchronous ovarian development. While in Zebrafish oocytes develop in a group-synchronous way, Medaka oocyte maturation happens asynchronously, so that all stages of developing oocytes are present at all times (Wallace and Selman 1981).

1.7.1 Oogenesis

The differentiation of a primary oocyte into an egg is accompanied by significant structural and functional changes (Lubzens et al. 2010), and the process in which an oocyte matures can be divided into four major phases. The follicular layer, the cells supporting and regulating oocyte development and growth, develops along with the oocyte. From a single cell layer, the follicle in teleosts develops into a two cell layer in which the oocyte is directly surrounded by interconnected granulosa cells which in turn are surrounded by the theca cell layer.

The process of oogenesis in Medaka was subdivided into ten stages based on the internal and external structure and morphology as seen by electron microscopy by Iwamatsu et al. (Iwamatsu et al. 1988) and schematically illustrated in figure 5.

In the previtellogenic stage, oocytes of the chromatin nucleolar stage (Stage I), ranging in size between 20 and 60μM, can be found next to the ovarian epithelium. In stage I and II (perinucleolar stage) the oocytes lack a chorion and are surrounded by a single layer of flat follicular cells. The animal-vegetal axis of oocytes is defined in the earliest stages of oogenesis by the presence of the yolk nucleus, also known as the balbiani body (BB), on the vegetal side of the developing egg. In stage III (egg-envelop-rudiment stage) oocytes reach a diameter of 100 μM and start developing their egg envelope, the chorion. In the last previtellogenic stage (stage IV) oocytes reach a size

between 120-150 μM and their nucleus can grow up to 90 μM in diameter (Kinoshita et al. 2009)

In stage IV oocyte maturation starts, the primary oocyte leaves the diplotene stage (first meiotic prophase) and resumes meiosis. The maturation process and meiosis resumption is triggered by pulses of gonadotropic hormone and leads to changes in the ooplasm and the nucleus (Suwa and Yamashita 2007). Several nucleoli localize along the nuclear membrane and oil droplets appear in the cytoplasm of late previtellogenic oocytes. Along the newly formed chorion, the attaching filaments start to form (Kinoshita et al. 2009).

During the vitellogenic phase, nutrients and information for the developing embryos are stored in the yolk. To sustain the rapid growth of the yolk and eggshell the oocyte has a high rate of endocytosis to take up vitellogenin (Lessman 2009). The oocyte nucleus (germinal vesicle) is located in the center of the primary oocyte, but upon receiving the maturation, trigger migrates to the animal pole of the oocyte where germinal vesicle breakdown (GVBD) takes place after which the first polar body becomes expelled (Suwa and Yamashita 2007). Oocytes grow enormously from 150 μM in the early yolk vesicle stage (Stage V) up to 800 μM in diameter in the late yolk formation stage (Stage VIII). From the early to the late yolk formation stage (Stage VII and VIII) yolk globules appearing around the yolk vesicles fuse to each other to occupy most of the yolk.

In the post-vitellogenic phase (maturation stage IX) the yolk mass makes up most of the oocyte and yolk vesicles (oil droplets) are pushed against the egg envelope at the outer part of the cytoplasm. The egg envelope is well developed and still in close contact with the follicular layer and the oocytes grows another 400 μM in diameter from 800 to 1200 μM. When the oocytes arrest again in metaphase of the second meiotic division (metaphase II) the oocyte has reached maturation state.

In the ovulation stage (Stage X) oocytes ovulate into the ovarian cavity by separating from the follicular layer (Kinoshita et al. 2009).

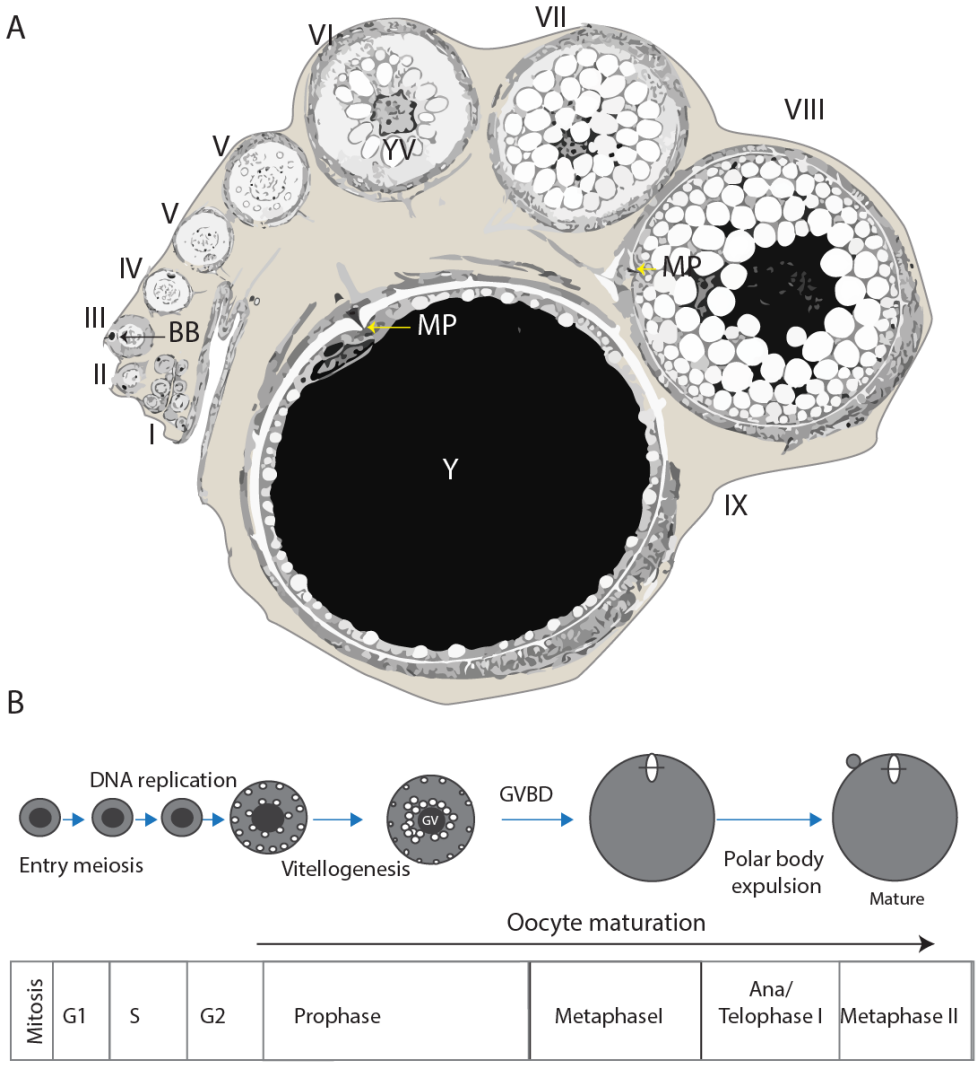

Figure 5: Different stages of Medaka oogenesis. A. Schematic drawing of a Medaka ovary with different stages of oocyte development. B. Phases of the cell cycle in which the oocyte is at the different stages of development. The cell cycle is resumed in secondary oocytes at stage IV. The mature oocytes arrest in meiosis II after germinal vesicle break down (GVBD) and first polar body expulsion. BB=Balbiani body, YV= yolk vesicle, MP= micropyle, Y=yolk, GV=germinal vesicle. Figure A redrawn from (Kinoshita et al. 2009) and B from (Lubzens et al. 2010)

1.7.2 Egfr signaling in oocyte-follicle interaction

The complex interaction between the follicular layer and the oocyte itself is crucial for oocyte growth and maturation at all stages. The oocyte and the follicle have many gap junctions that allow chemical and electrical communication. It recently became apparent that oocyte-derived growth factors stimulate the activity of follicle cells and in turn, the follicle regulates all stages of oocyte development (Lubzens et al. 2010).

The events triggered in the follicular layer as well as in the ooplasm are complex, and many signaling cascade, as G-proteins and cAMP changes, MAPK signaling, calcium

signaling, inositol triphosphate and protein kinase A and PKC signaling, are involved (summarized in (Lessman 2009)). Egfr activity stimulates some of these pathways. How the two Egfrs present in fish might fulfill this variety of duties of oocyte maturation and crosstalk between the oocyte, and the follicular layer remains to be elucidated.

1.7.3 Formation of the chorion and the micropyle

Since fish embryos develop externally, they have a protective layer, the chorion that develops around the maturing oocytes. The chorion does not only serve as a protective barrier for the embryos but also is the primary factor that guarantees that only one sperm fertilizes the oocyte. The only entry point for sperm is a small funnel-like channel in the chorion of most teleosts, the micropyle (MP). The animal pole of the maturing oocytes is characterized in the beginning by being opposite of the balbiani body (BB) and later by the presence of the MP. The MP if formed by a specialized granulosa cell in the early vitellogenic phase.

The sequence of events of the formation of the MP was described in electron microscopic detail by Iwamatsu et al. (Nakashima, S; Iwamatsu 1989). During the previtellogenic phase, thecal and granulosa cells are minuscule. When the primordium of the chorion is formed in stage III, all follicular cells appear to be the same. As the yolk nucleus begins to swell during oocyte maturation, attaching filaments at the vegetal pole become visible and a micropylar cell (MC) can be distinguished from neighboring granulosa cells at the animal pole. While other granulosa cells are joined by desmosomes to which bundles of tonofilaments are attached, the MC has a large package of tonofilaments in the cytoplasm in contact with the cell nucleus. In Stage V the chorion develops into a two-layered structure with a thin inner and a thicker outer layer. Large bundles of tonofilaments become visible in the perinuclear cytoplasm of the MC on the site facing away from the oocyte. In stage VI of oocyte development, the yolk vesicles occupy a significant part of the cytoplasm. The MC differentiates into a mushroom-shaped flat cell in which the nucleus is localized away from the chorion. The MC develops a long cytoplasmic process which protrudes through the chorion layers.

The MC also loses contact to surrounding connected granulosa cells (Nakashima, S; Iwamatsu 1989). Large bundles of tonofilaments occupy the cytoplasm between the nucleus and the cell process. Through rotation of the oocyte within the follicle the inner surface adapts its characteristic spiral surface as can be seen in figure 6.

So far nothing is known about the event that leads to differentiation of a single MP cell and how the oocyte senses that an MP has formed.

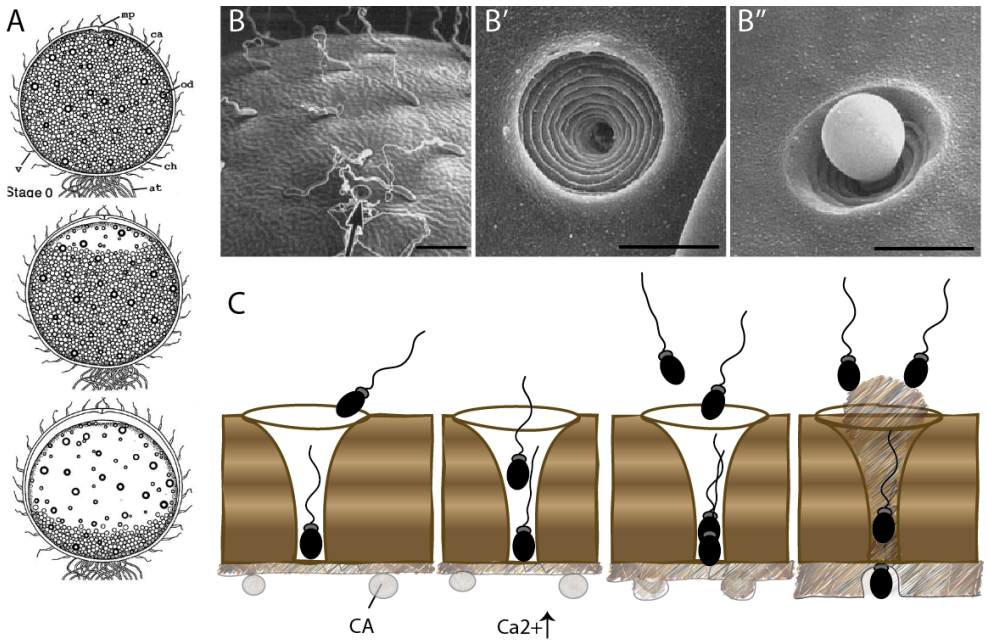

Figure 6: Appearance and function of the micropyle (MP) in the chorion of *Oryzias latipes*. A. The appearance of the oocyte before and directly after fertilization. Upon sperm entry, though the MP the oocyte membrane becomes separated from the chorion and oil droplets move to the vegetal pole of the fertilized eggs. Pictures are taken from (Iwamatsu 2004). B. Electron microscopy pictures of the chorion B, and the MP before fertilization B' and after B'' C. Polyspermy block in teleost. As a sperm enters the MP channel and attaches to the oocyte membrane the membrane becomes depolarized and Ca2+ becomes released. The gamete fuses with the oocyte membrane and cortical alveoli (CA) are exocytosed which leads to separation of oocyte membrane and chorion. The perivitelline fluid flows up the MP channel and forms a plug which closes the MP. B and C are taken and redrawn from (Iwamatsu et al. 1991) Scale bar in B 100 µm, in B' and B'' 10 µm.

2. Aims

In this study we looked at different aspects of Egfr signaling in the Japanese Killifish Medaka by using gene expression studies, clonal overexpression tools and reverse genetic approaches. Egfr signaling is a central pathway in in development and growth and therefore found deregulated in various diseases, yet in fish the pathway has so far not been studied to a great extend. Fish have gained increasing attention as models for human disease and it is therefore important to understand the physiological role of the Egfr in normal development. Growing throughout their live fish are ideal models to study growth signaling in physiology and disease. The retina of fish is a popular model to study neurogenesis in fish but so far the role of Egfr-signaling in CMZ has not been studied.

The first objective was to investigate the function of Egfr signaling in the retinal stem cell niche. For that we first studied the expression patterns of receptors, ligands and signal transducers in the retina and compared these patterns to expression in the NSC niches in the brain. With this we intended to elucidate the role of the pathway in the development and growth of the CNS and more specifically of the retina.

The second aim was to characterize the reaction of RSCs to the expression of Egfr-related oncogenes. We addressed two main questions: does Egfr signaling play a role in maintenance and function of the retinal stem cell niche and can enhanced Egfr signaling change the behavior of RSCs. For this purpose we developed a genetic toolbox for transient and clonal expression of xmrk, K-Ras^{12V} and myrAKT.

As a third aim we tried to understand the specific role of Egfra in Medaka by generating and characterizing a CRISPR/Cas9 based *egfra* knockout fish and analysing the resulting phenotype.

3. Results and Discussion

3.1 Expression study of components of the Egfr signaling pathway in the CNS of *O.latipes*

To set a base for understanding the role of Egfr signaling in the growing retina and brain we performed a whole mount in situ hybridization (WISH) screen for Egfrs, Egfr-ligands and critical downstream targets of the receptor in the eye and brain of Medaka. Based on previous studies about Egf-receptors and -ligand expression in different tissues (Laisney et al. 2010), I designed probes against *egfra*, *egfrb*, as well as the receptor ligands *egf*, *hb-egf* and *tgfa*. These ligands were selected for their relative abundance in the eye and stem cell lines when compared to their expression in the brain (Laisney et al. 2010). Additionally, I designed *in situ* probes against key players of Egfr main downstream signaling pathways components, *k-ras*, *AKT1* and *AKT2*, *stat5a* and *b* and *stat3* to confirm the existence of these signal transducers in the CMZ and proliferative regions in the Medaka brain.

In collaboration with Clara Baader, we investigated the expression patterns of Egfr signaling components during developmental stage 24 and 32 (critical stages in eye development) and in more detail in hatchlings, which have developed primary brain structures and the retina.

3.1.1 Expression of Egfr signaling components in the retina

The Egfr pathway is essential for maintaining the balance between proliferation and differentiation in various stem cell niches. In neural stem cells (NSCs) Egfr signaling is essential for proliferation and survival (Aguirre, Rubio, and Gallo 2010; Wagner et al. 2006). In the post-embryonic retina of fish, Egfr signaling was not studied in depth.

We found that both *egfrs* are actively transcribed in the CMZ (marked by dashed box in figure 7). *Egfrb* is expressed broader than *egfra*, also in early transiently amplifying zone next to the differentiated retina. Amacrine cells, the ciliary zone, and the cornea also express both receptors. The only investigated ligand that was found transcribed in the CMZ is *hb-egf and also egf but at a lower level*. The probes for all three ligands,

however, stain the ciliary zone and the cornea adjacent to the CMZ (figure 7B). The chorion surrounding the neural retina is strongly stained for all performed in situs and is therefore probably unspecific. Strong staining of the choroid layer makes in difficult to distinguish expression in the retinal pigmented epithelium

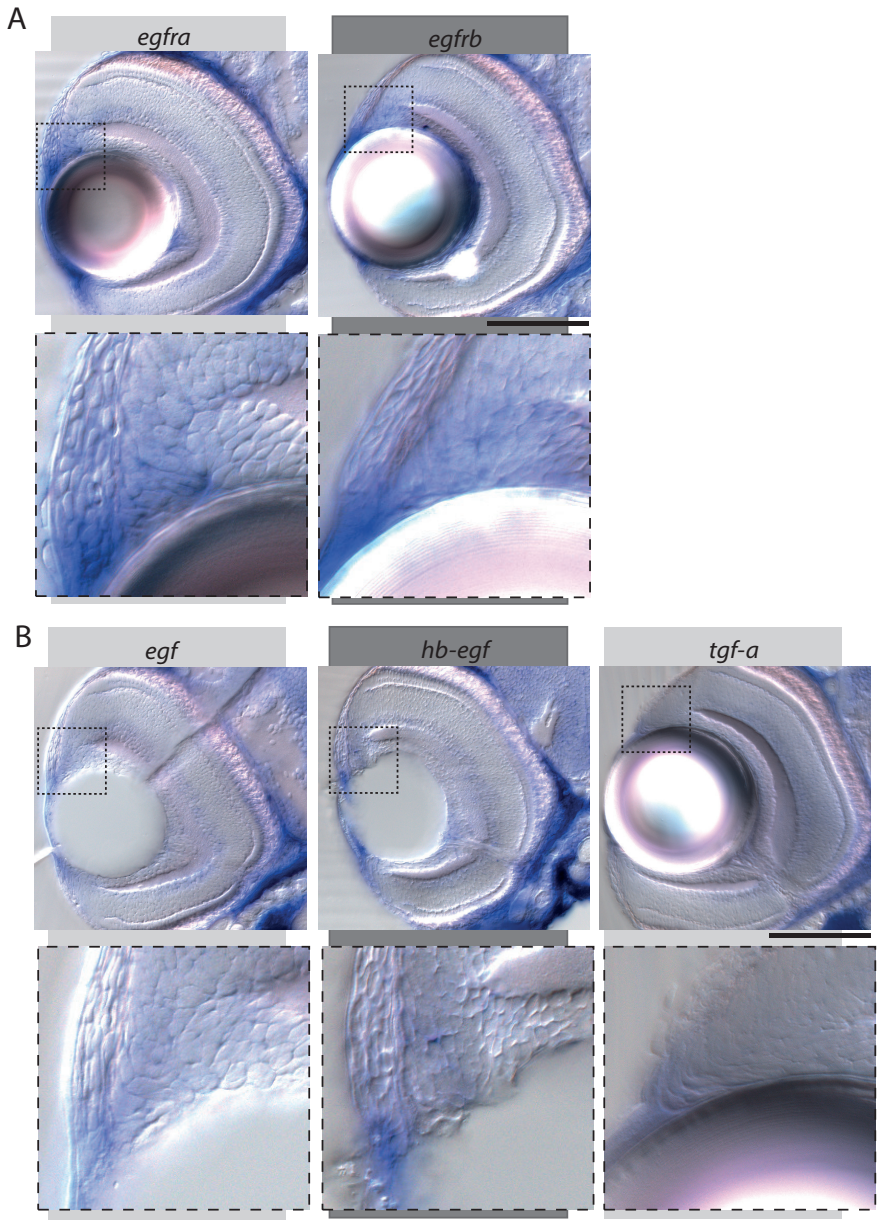

Figure 7: Expression of mRNA of *egfra* and *b* and its ligands in the retina of Medaka larvae. WISH was performed using probes directed against *egfra, egfrb, egf, hb-egf, and tgf-a.* Stained WISH embryos were cut into 25 µm thick transversal vibratome sections. Sections of the retina displayed here were chosen at the level of the optic nerve to have a central picture of the CMZ. *Egfra* and *b* are expressed in the CMZ and the cornea. *Egf* and *tgf-a* are transcribed in the cornea but not the CMZ, whereas *hb-egf* is expressed in the cornea and the CMZ. The dashed boxes contain a detailed view of the CMZ, four times enlarged. Scale bar is 200 µm.

The presence of both receptors transcripts in the CMZ indicates that Egfr signaling is functioning in the RSCs and reacts to paracrine signals from adjacent tissues. The hb-egf ligand might also operate in an autocrine fashion in RSCs. In the cornea, Egfr has significant wound healing and homeostasis functions in mammals (Nakamura, Sotozono, and Kinoshita 2001; Zieske et al. 2000).

Although not much is known about Egfr signaling in the vertebrate eye and RSCs, the Egfr was shown to be involved in the MC-mediated regeneration of the Zebrafish retina (Wan, Ramachandran, and Goldman 2012). *Hb-egf* is also expressed in MC in chicken and mouse and stimulates proliferation of MGCs upon injury by N-Nitrosodimethylamie (NDMA) (Todd et al. 2015). The proliferation of MCs is induced most effectively by a combination of Egfr signaling and Insulin in NDMA treated retinae that upregulated *egfr* expression due to the treatment. The same way of induction works in the ciliary body of chicken retinae where human EGF (hEGF) or hFGF together with insulin induce strong proliferation and neurogenesis (Fischer and Reh 2003). It is thus probable that similar mechanisms are at work in the RSCs of Medaka. In other stainings, I could see dotted *hb-egf* expression in the INL implicating that it is expressed probably in MGCs in Medaka (data not shown).

We looked at the expression of signal transducers of Egfr signaling and found that the mRNAs of most downstream signaling components (all but *stat5a*) are transcribed in cells of the undifferentiated region of the retina. Most restricted to the stem cell zone are the expression patterns of *AKT1* and *stat5b* that were found exclusively in the outermost tip of the CMZ where Rx2-positive RSCs are located. The *AKT2* gene, on the other hand, is strongly transcribed in the whole undifferentiated region of the CMZ as well as INL and GCL. *Stat3* and *k-ras* display similar expression patterns in the CMZ and additionally *k-ras* is strongly expressed in the amacrine and the ganglion cell layer as well as in the ciliary body and the cornea while cells in this region only weakly express *stat3*. *Stat5a* is expressed obverse compared to its homolog stat5b; it is transcribed only in the differentiated part of the retina.

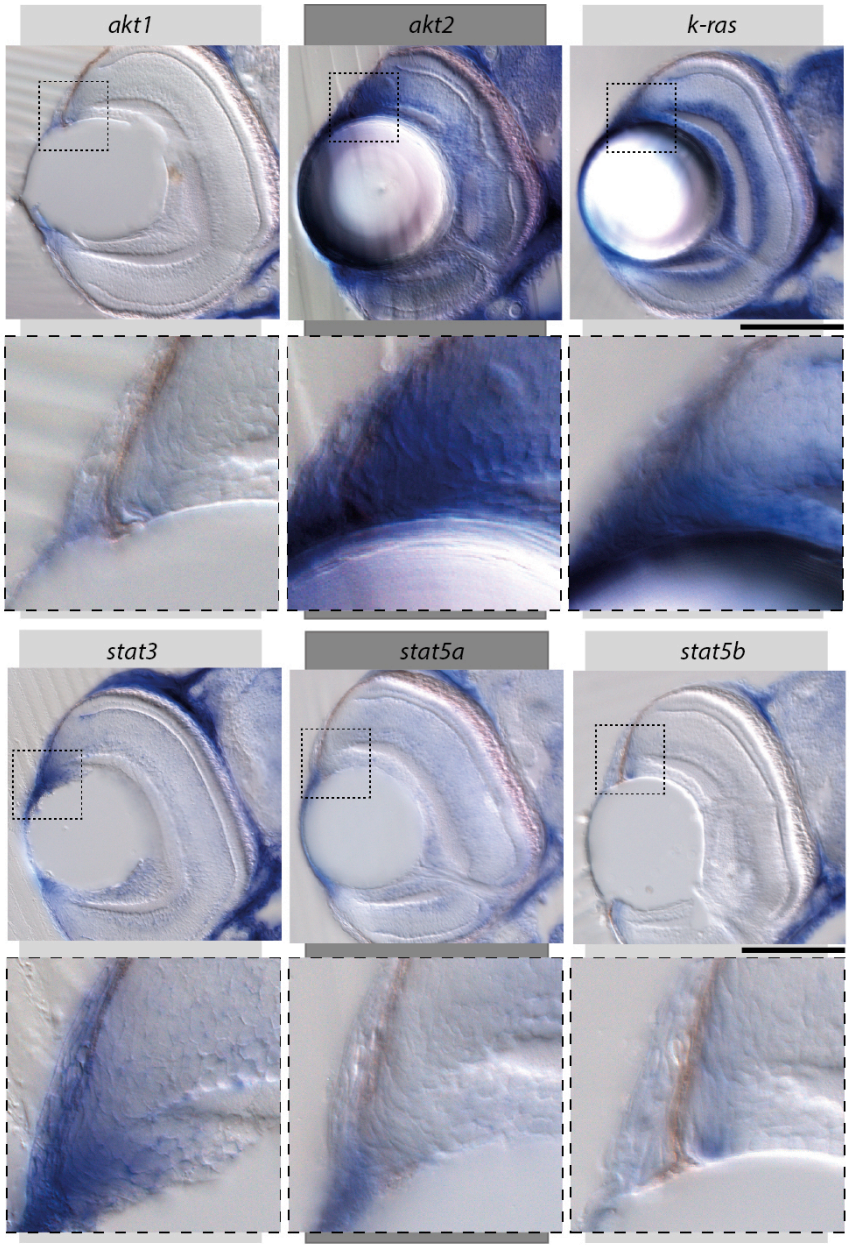

Figure 8: Expression of mRNA of *AKT, k-ras and Stat genes in the retina of Medaka.* WHISH was performed using probes directed against *AKT1, AKT2, k-ras, stat5a, stat5b and stat3*. Stained WISH embryos were cut into 25 µm thick transversal vibratome sections. Sections of the retina displayed here were chosen at the level of the optic nerve to have a central picture of the CMZ. The dashed boxes contain a detailed view of the CMZ, four times enlarged. *AKT1* and *stat5* b are explicitly described in the outermost tip of the CMZ. The *stat3* and *AKT2* genes are transcribed in the entire CMZ, the ciliary body and the cornea. *AKT2* is additionally transcribed in the ganglion and the inner nuclear layer, as is *k-ras*. *Stat5a* is transcribed in the cornea and only weakly in the differentiated part of the retina. Scale bar is 200 µm.

Most of the investigated signal transducers are also downstream of RTK other than the Egfr, like insulin-like growth factor receptor (Igfr) or fibroblast growth factor receptor (Fgfr), with known function in retinal development and RSCs. Human derived insulin-related factors (insulin, insulin-like growth factor 1 and 2) but not EGF can stimulate proliferation of RPCs in the CMZ of goldfish retina cultures

(Boucher and Hitchcock 1998). RTKs other then Egfr might thus be the primary regulators of proliferation in the CMZ although both Egfrs are expressed in the region and phosphorylated Egfr is used to identify activated NSCs in the CNS (Codega et al. 2014). The use of human ligands for Egfr to study the pathway might be misleading since ligand as well as the ligand-binding domain sequences are only partially conserved between teleosts and tetrapods (Laisney et al. 2010).

Based on this result I took a closer look at the activity of one of the central pathways downstream of the Egfr, the Ras/Mapk/Erk pathway. I stained sections of hatchlings with a Phospho-p44/42 MAPK (Erk1/2) (pErk) antibody and found that it was activated in amacrine cells and photoreceptors but not in the CMZ (figure 9A). The brain shows a dynamic pattern with varying intensity of pErk in neural cells adjacent to, but never in the SVZ, where NSCs are located (figure 9 b). The expression zones of *k-ras* (GCL, INL) matches the pattern observed for its activated downstream target ERK, in photoreceptors k-ras was however not expressed. This ERK activation is probably Egfr independent following described mechanism in which the depolarization of neurons leads to Ca^{2+} influx which in turn activates the Ras/MAPK pathway and downstream transcription factors as CREB (*cAMP response element-binding protein)*(Thomas and Huganir 2004). pErk patterns are very dynamic; it can be used to localize active neurons (Randlett et al. 2015). In this context, the Ras/MAPK pathway is probably not activated via the classical route (RTK dependent) but rather via membrane depolarization in a Ca^{2+} dependent manner as described in (Thomas and Huganir 2004). These pErk patterns are probably similarly active in neurons of the brain and amacrine cells. Amacrine cells depend on MAPK, PI3K and JAK/STAT for their survival and die if these pathways are inhibited (Kunzevitzky, Almeida, and Goldberg 2010). It is not clear how these pathways are activated, but Egfr has probably no relevance in Erk activity of retinal neurons. Egfrs might exert their possible function in the CMZ and the brain via the PI3K/AKT pathway and the STAT pathways which are more specifically expressed in the CMZ and the brain (see next chapter). *In vivo* as well as *in vitro* studies indicate that for proliferation in the CMZ different RTKs are likely to interact (Boucher and Hitchcock 1998; van der Veeken et al. 2009) and so they probably fulfill a partially redundant function.

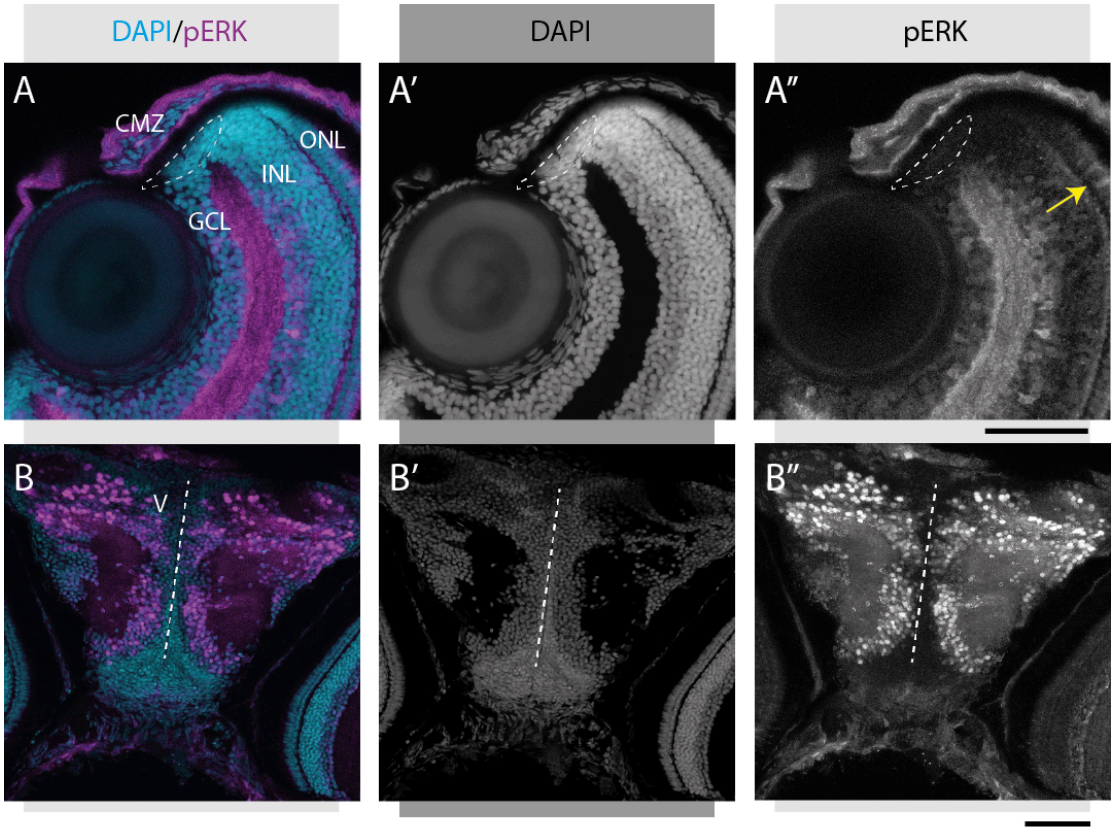

Figure 9: Erk is phosphorylated in retinal neurons and brain but not the CMZ. Sections of Medaka hatchlings were stained for phosphorylated Erk (magenta) and DAPI (cyan). A. In the retina of a Medaka hatchling, Erk is activated in all three neuronal layers, the CMZ surrounded by a dashed line. B In the telencephalon pErk is present in many neurons but not in in the subventricular zone. The ventricle is indicated by a dashed line. CMZ= ciliary marginal zone, GCL= ganglion cell layer, INL= inner nuclear layer, ONL= outer nuclear layer, V= ventricle. The scale bars are 50 µm.

3.1.2 Expression of Egfr signaling components in the brain of Medaka larvae

Just like the retina, the brain hosts neurogenic stem cell zones namely the subventricular zone (SVZ) along the lateral ventricle (Kuroyanagi et al. 2010) and the peripheral area of the optic tectum (OT) (Alunni et al. 2010; Nguyen et al. 1999). The OT grows in a similar way as the retina, temporally and spatially ordered populations of proliferative, postmitotic, and mature cells (Alunni et al. 2010; P. Raymond et al. 2006).

We compared the expression pattern of Egfr signaling components that we observed in the retina to the way in which they are transcribed in the brain. We especially looked for overlapping or adjacent expression of the receptors and the ligands in known proliferative regions of the brain and differences in patterns of downstream signaling components that might hint towards the main functional pathway in certain brain areas. We found that *egfra* and *egfrb* were expressed broadly in the brain and had some regions of higher expression in proliferative zones of the brain like the SVZ and the outer margin of the OT. Similar expression levels of both *egfrs* in the brain were also observed by Laisney et al. (Laisney et al. 2010). *Egfra* has a very distinctive area of high expression in the forebrain around the frontal starting point of the ventricle and slightly increased expression along the central ventricle and the uppermost central part of the OT (figure 10). *Egfrb* is expressed stronger than *egfra* along the central and lateral ventricles.

The Egfr-ligands investigated in this screen show distinct patterns of expression. *Egf* has an articulate expression domain along the ventricles (central and lateral), this expression starts early and is clearly visible already at stage 32 (figure 12) and also in adult sections (data not shown). There is a weak expression of *egf* in the central part of the OT decreasing gradually towards the sides. For the other ligands (*hb-egf* and *tgf-a*) we observed rather broad and indistinct expression throughout the brain. *Hb-egf* is expressed strongly in the ear and also in the skin and connective tissue. *Tgf-a* has increased expression levels in the caudal part of the OT. Altogether these results fit the RT-PCR based expression study performed with adult Medaka tissues where *egf* expression in the brain is significantly higher than in the rest of the tissues and *hb-egf* and *tgf-a* are lower expressed than in other tissues (Laisney et al. 2010).

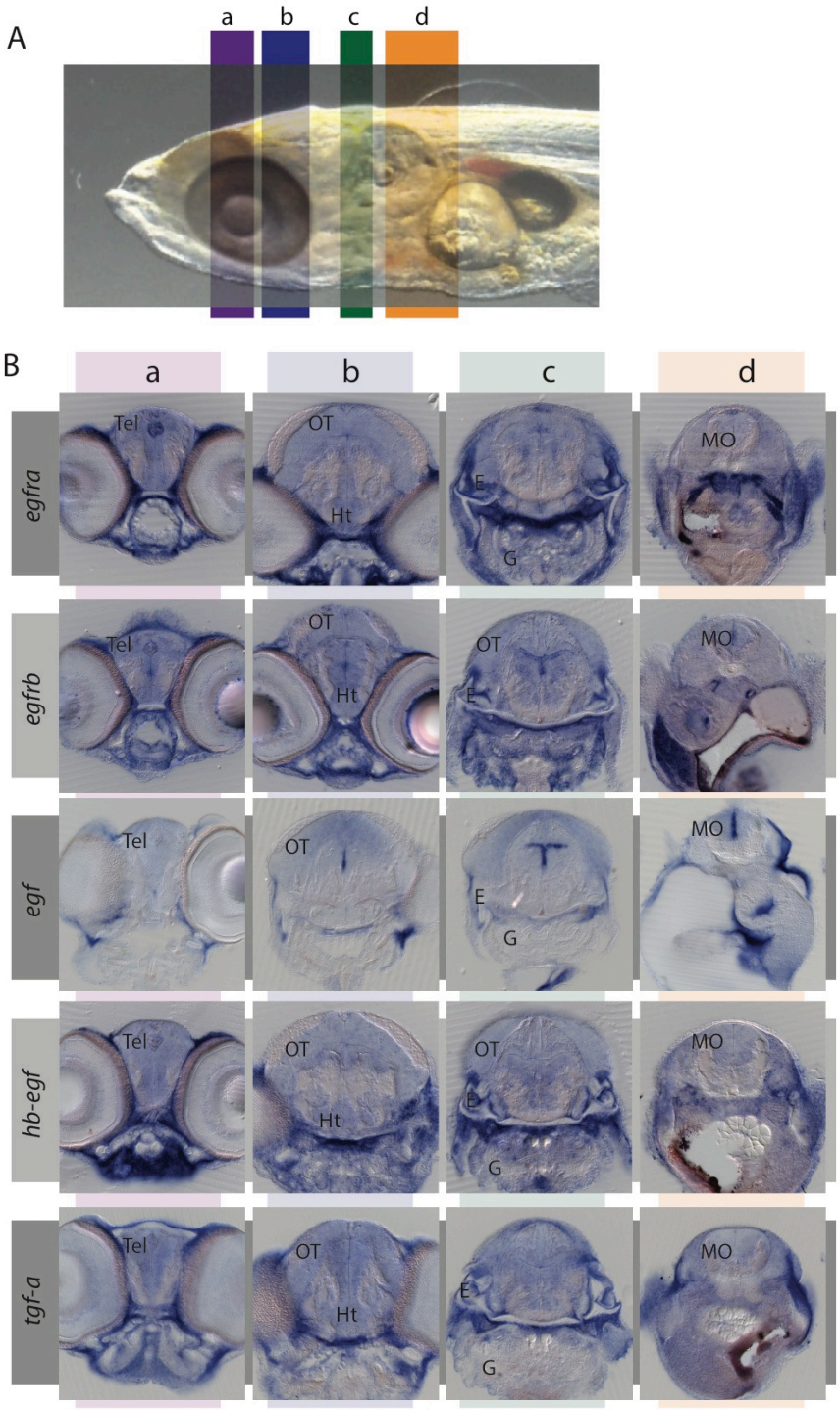

Figure 10: Expression pattern of *egfrs* and its ligands in transverse brain sections of Medaka hatchlings. Medaka hatchlings of the Heino strain were used for WISH stainings with antisense probes against *egfra*, *egfrb*, *egf*, *tgf-a* and *hb-egf*. Stained hatchlings were cut transversally into 25 µm sections. A. Lateral view of a Medaka fish with the colored region for the approximate location of sections (a-d). B. Sections of different brain regions (a-d) of WHIS embryos stained for egfrs and ligands. egfra and b are broadly expressed in the brain but slightly enhanced in the SVZ. Egfra is stronger directly surrounding the start of the ventricle (a) in the telencephalon and egfrb is higher expressed directly at the ventricles (b and c). Egf is very specifically transcribed next to the ventricle in the midbrain (b-d). Hb-Egf and tgf-a are broadly expressed in the brain, tgf-a slightly increased in the margin of the optic tectum (c). OT=optic tectum, Tel=telecephalon, Ht= hypothalamus, MO= medulla oblongata, E=ear, G=gills. Scale bar is 200 µm.

As mentioned before Egfr can be used as a marker for active stem cells in the SVZ of mammals (Codega et al. 2014). In the fish brain, the most probable candidate for the activation of Egfrs in the SVZ is egf. *Tgf-α* or one of the neglected egfr ligands (such as betacellulin, neuregulin and amphiregulin) might stimulate the Egfrs in the OT and the rest of the brain. Interestingly we could not find a similar strong expression of *egf* around the CMZ which hints towards a different ligand-receptor interaction pair in the CMZ and the OT compared to the SVZ.

The expression of downstream pathways showed high similarities between retinal and brain patterns as can be seen in figure 11. Specifically expressed in proliferative zones are *AKT1*, *stat3* and *stat5a*. *K-ras* is strongly expressed throughout the brain with slightly increased expression in proliferative zones; the same holds true for *AKT2*. This expression pattern indicates that both factors are activated Egfr-independently and rather fulfill survival and metabolic functions as described in (Wagner et al. 2006). The two *AKT* kinase isoforms are expressed in different patterns in the Medaka brain, even though structurally very similar they are described to have specialized functions that might even advert each other (Heron-Milhavet et al. 2011).

The most probable Egfr activated signal transducers that exert a proliferative function in the SVZ are *AKT1*, *stat3* and *stat5* since these genes are transcribed enhanced in NSC zones. Little is published on the natural role of Stat genes in the proliferative zones of the brain. However, tumors originating from the brain, so-called gliomas, often depend on hyperactive Stat3 and 5b to sustain their proliferation (Fan et al. 2013; Gressot et al. 2015; Sherry et al. 2009; Xiong et al. 2009). Wagner et al. showed that Egfr signaling is essential for the survival of astrocytes but not neurons in the cortex; neurons, however, need astrocytes for their survival. While $Egfr^{-/-}$ midbrain astrocytes can sustain neuronal survival, cortical $Egfr^{-/-}$ astrocytes cannot but their survival can be rescued by RasV12 expression (Wagner et al. 2006). The broad expression of K-Ras observed here in the brain also implicates that K-Ras has an essential function in survival of neurons in Medaka.

Based on the literature and our *in situ* data we assume that Egfr signaling plays a role in NSCs in the brain and the retina, there is, however, a difference in the stimulating ligand since *egf* is expressed very specifically in the SVZ but not in other stem cell zones of the CNS. Downstream effectors of Egfr signaling, probably stimulated in

concert with other signaling pathways, are the PI3K/AKT and Stat pathways in the stem cell zones rather than the broadly used Ras/MAPK pathway.

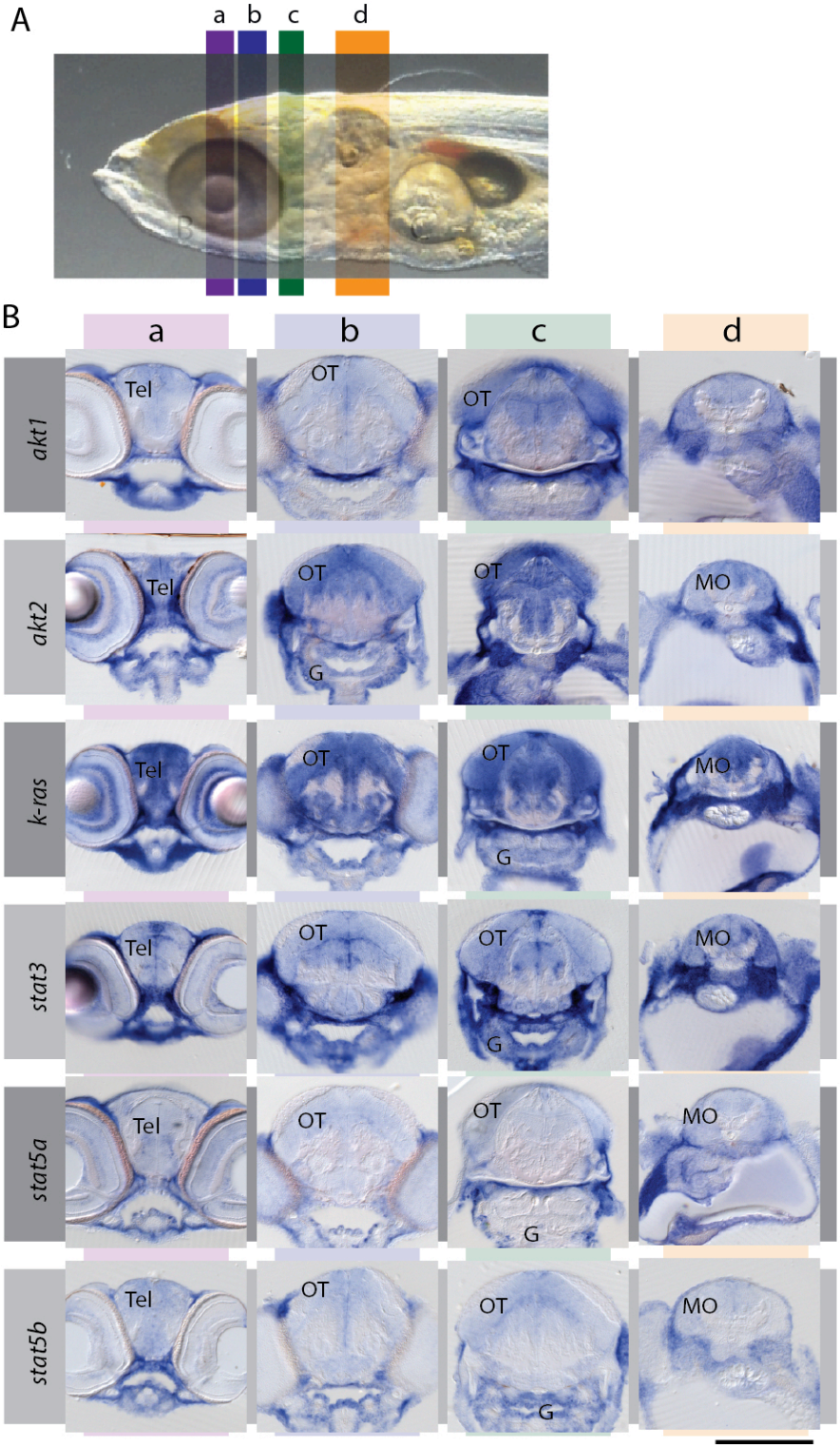

Figure 11: Expression pattern of *egfrs* related downstream signaling components in transverse brain sections of Medaka hatchlings. Medaka hatchlings of the Heino strain were used for WISH stainings with antisense probes against *AKT1*, *AKT2*, *k-ras*, *stat3*, *stat5a* and *stat5b* and sectioned 25 µM thick. A. Lateral view of a Medaka fish with the colored region for the approximate location of sections (a-d). B. Sections of different brain regions (a-d) of WISH embryos stained for

different signal transducers in the egfr signaling cascade. *AKT1* is expressed mainly in the dorsal and lateral margins of the OT (c) and slightly along the ventricles (b & c). *AKT2* and *k-ras* are strongly transcribed throughout the brain with enhancing expression in the dorsal margin of the OT (c). *Stat3* is expressed specifically in proliferative regions of the brain (SVZ and OT margin in a-c). Stat5a and b are weakly transcribed in the brain, stat5b shows enhance expression along the ventricles (b & c). OT=optic tectum, Tel=telecephalon, Ht= hypothalamus, MO= medulla oblongata, E=ear, G=gills. Scale bar is 200 µm.

3.1.3 Expression of Egfr signaling components during development

We also looked at the expression of Egfr signaling components during development to uncover processes mediated by only one receptor, ligand or signal transducers. All tested genes of the Egfr signaling pathway are expressed throughout the head region of embryos at stage 24 when retina and lens are patterned, but the CMZ is not yet formed (figure 12 and 13). In stage 24 the expression of *egfra* is ubiquitous, *egfrb*, however, is expressed stronger in the forming lens and the central brain. Expression of the retina-specific transcription factor *rx2* that was included as a positive control is strong throughout the retina since the CMZ has not yet formed (figure 12.A). At stage 32 the expression patterns become more restricted, *egfrb* is mainly transcribed in the choroid layer, parts of the otic vesicle, along the optic nerve and distinct structures in the brain. *Egfra* is transcribed more broadly in the brain and somewhat enhanced in the ventricle region. In the newly formed CMZ in stage 32 embryos, we could not see the same increased expression observed in the CMZ in hatchlings

The Egfr ligands show a broad expression pattern at developmental stage 24. The expression is slightly enhanced at the midbrain/hindbrain boundary as can be seen in figure 12B. *Egf* expression seems to be overall weak at early stages and only when brain ventricles are formed it starts to be transcribed in the SVZ (figure 12B). *Tgf-α* and *hb-egf* have similar expression patterns; rather ubiquitous at stage 24 and then mainly in the skin of stage 32 embryos. The retina at that stage shows some expression of the receptors but no obvious expression of ligands. Receptors and ligands are both expressed in the brain region (forebrain and midbrain/hindbrain boundary) and can contribute to development and growth. *Egfrb* is overall stronger expressed and becomes more restricted to certain areas in the brain suggesting a more distinct function of this receptor compared to *egfra*.

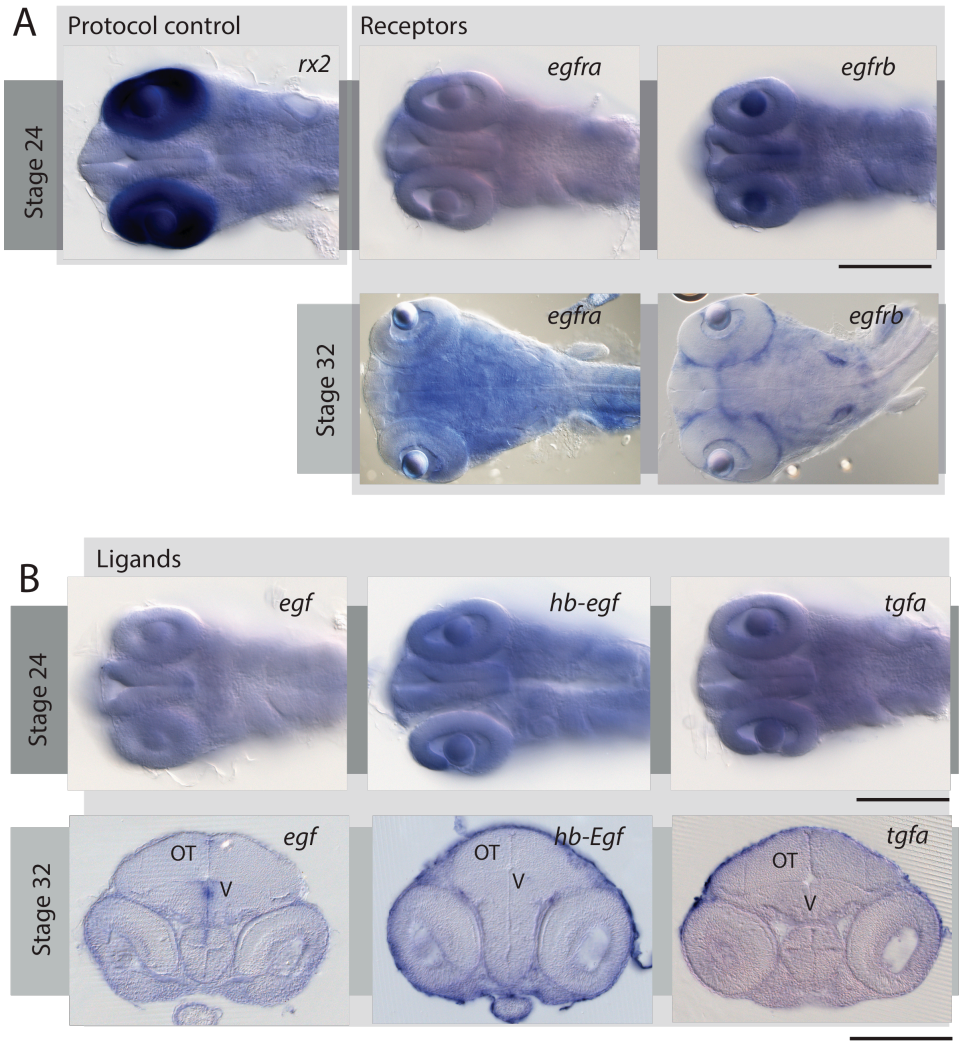

Figure 12: Broad expression of *egfrs* and ligands at St.26 and more restricted expression at stage 32. Whole mount in situs (WISH) using antisense probes for detection of Egfra and b (A) as well as the receptor ligands *egf*, *hb-egf* and *tgfa* (B). The Rx2 antisense probe was used as a technical control. A. *Egfra* and *b* are broadly expressed at Stage 26. *Egfrb* is widely expressed Stage 32 WISH were photographed in whole mount for *egfrs* and vibratome-sectioned in 25 µm thick sections for *egfr*-ligands. A central brain section has been chosen for display of Egfr-ligand expression at stage 32. *Hb-egf* and *tgfa* are expressed primarily in the skin and *egf* along the brain ventricle. Scale bar is 200 µm.

We also checked for the presence of mRNA of downstream components of the Egfr signaling pathway to understanding where and through which pathway Egfr signaling might function in CNS development.

We detected strong expression of all investigated Egfr-related downstream genes throughout the head region of stage 24 embryos (figure 13) which is not surprising since at that stage most cells of the embryo are dividing and growth happens all over. Stats, AKT and K-ras are downstream of most growth signaling receptors like Fgfr and Igfr and might function in any of these.

The mRNA expression of most investigated downstream components becomes more restricted to proliferative brain regions or tissues at stage 32. *AKT1* is mainly expressed in proliferative zones of the brain namely along ventricles (central and lateral) and the tectal plate while *AKT2*, on the other hand, is expressed more ubiquitously in the whole brain and retina. These differences in expression and also in function have been described before (Heron-Milhavet et al. 2011).

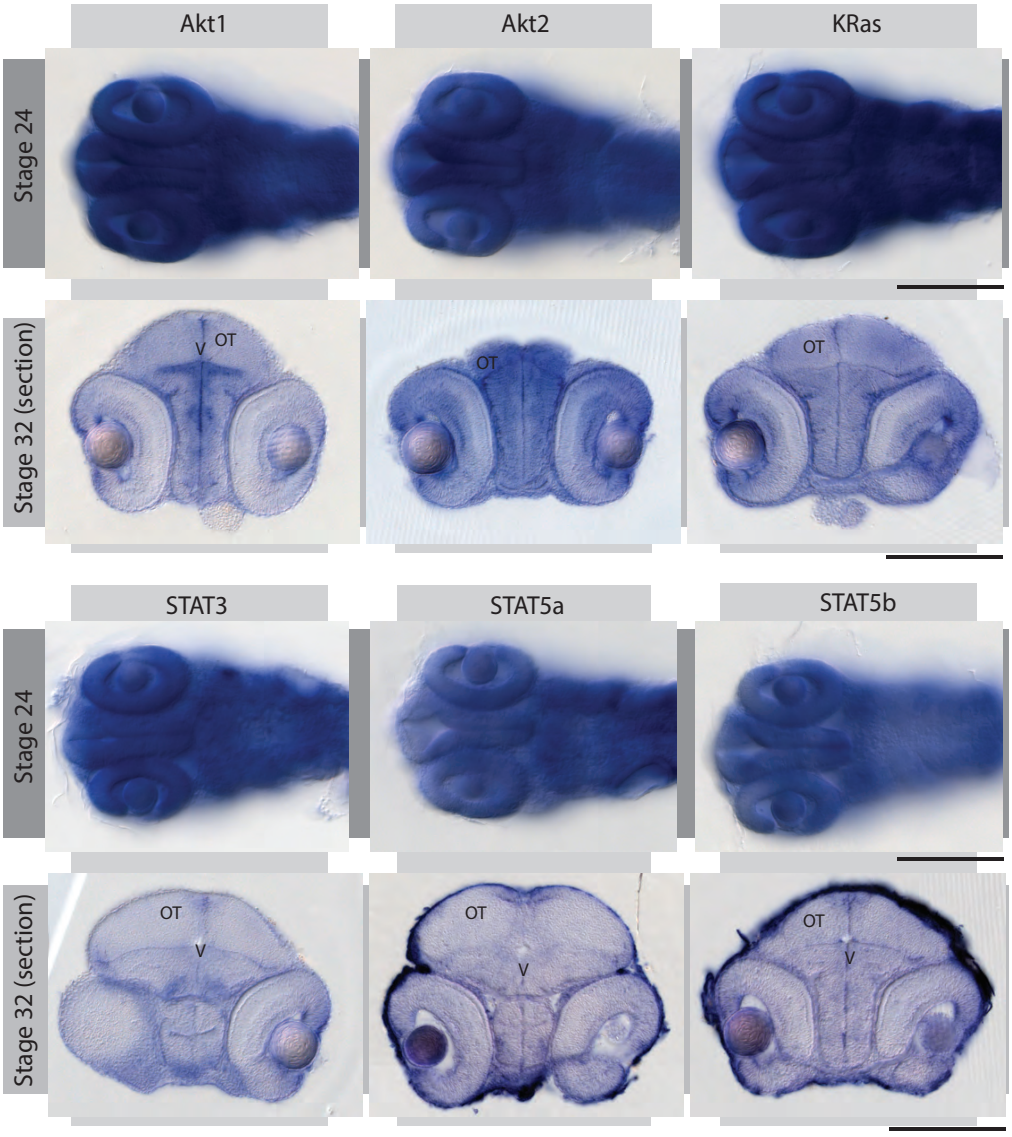

Figure 13: Expression of downstream components of the Egfr signaling cascade, AKTs, Ras and STATs. Whole mount in situs (WISH) using antisense probes for detection of AKT1, AKT2, K-Ras, STAT3, STAT5a and STAT5b were performed for stage 24 and 32 embryos. Stage 32 WHISH embryos were photographed after vibratome-sectioning (25 µm thick sections), and a central section was chosen for display. Scale bar is 200 µm.

K-ras is broadly expressed in the whole head but more enhanced along the border areas, like ventricles, around the eyes and in the area of the newly formed CMZ. Stat3 mRNA could be found along the lateral ventricle at the margin of the OT and in more ventral brain regions of the stage 32 embryo. Both *stat5* genes (a and b) show strong expression in the skin and proliferative zones in the brain and the forming CMZ.

For all investigated components we could observe that during development most of the investigated growth-signaling components become gradually more restricted to proliferative zones in the brain of Medaka embryos. Co-expression of ligands *hb-egf* and *tgf-α* with the *egfrb* and all tested downstream components could be observed in the tectal plate. The indistinct expression of *egfrs* during development has been described before in other species (Gabay, Seger, and Shilo 1997; Threadgill et al. 1995; Zhang et al. 2010) and reflects the broad implication of the pathway in development, growth and maintenance of multicellular organisms.

3.2 Generation of an Egfr-signaling related toolbox for oncogene expression in *O.latipes*

The Egfr signaling pathway is amongst the most commonly deregulated pathways in tumors. During my Ph.D. project, we created a genetic toolkit for the expression of oncogenes in the retina and other tissues of Medaka to investigate the effect of oncogene expression on retinal stem cells (RSCs). We raised various fish lines for inducible expression of the oncogenic Egf-receptor Xmrk, as well as for the human oncogenes K-RAS^{V12} and myristoylated AKT (myrAKT). Xmrk has been identified as a very potent oncogene that can transform melanocytes into malignant melanomas and induce over-proliferation in hepatocytes (Li et al. 2012). So far Xmrk has only been used in a limited number of genetic settings mainly being expressed by tissue-specific promoters (Patton and Nairn 2010; Schartl et al. 2010) or under control of transactivator response elements (Li et al. 2012; Zheng et al. 2014). We managed to clone the 3,5 kb open reading frame (ORF) of *xmrk* into various inducible genetic contexts in which its expression can be traced by a fluorescent tag. Additionally, we acquired published constructs containing human K-RAS^{V12} and myrAKT from the lab of Marina Mione (Alghisi et al. 2013) and cloned them in the same construct setups. We tested the functionality of new Xmrk-variants with an assay based on strong heat-shock inducible expression in injected embryos.

3.2.1 Transient expression of oncogenes in Medaka hatchlings

For a transient high expression of Xmrk, I cloned two constructs that were aimed for strong Tet-OFF-transactivator (tTA) based expression of the oncogene, as described in (Gossen et al. 1995). I generated a construct in which two TET-response elements (Knopf et al. 2010) are mirrored to drive expression of *xmrk* on one site and a stable GFP-tagged H2B variant on the other site. This construct was injected together with another construct expressing tTA after an HSP70 promoter. Constructs are schematically represented in figure 14A.

I observed strong fluorescence of *H2B-GFP* in early embryos without applying heat treatment. Embryos that showed *H2B-GFP* expression in yolk cells often had a tumor-like accumulation of cells and died (figure 14B) meaning that Xmrk can elicit a

proliferative response. Injected embryos with a mosaic expression of *H2B-GFP* soon developed irregularities in the tail muscle mass (figure 14C). Within one-week post hatch (wph) these H2B-GFP-postive irregularities grew out to easily visible bumps of somites (figure 14D). This outgrowth can only be due to Xmrk-activity since it was never observed in any other H2B-GFP expressing line in the lab. We realized that expression of *xmrk* and H2B-GFP is independent of the transactivator tTA since it proved to be dysfunctional by mRNA injection (experiment performed by Isable Krämer) data not shown. The two constructs displayed in figure 14A were co-injected and therefore likely co-integrated in a way that the hsp70 promoter element can drive expression of *H2B-GFP* and *xmrk* from the minimal promoter elements that are part of the DualTet RE, independent of the binding of tTA.

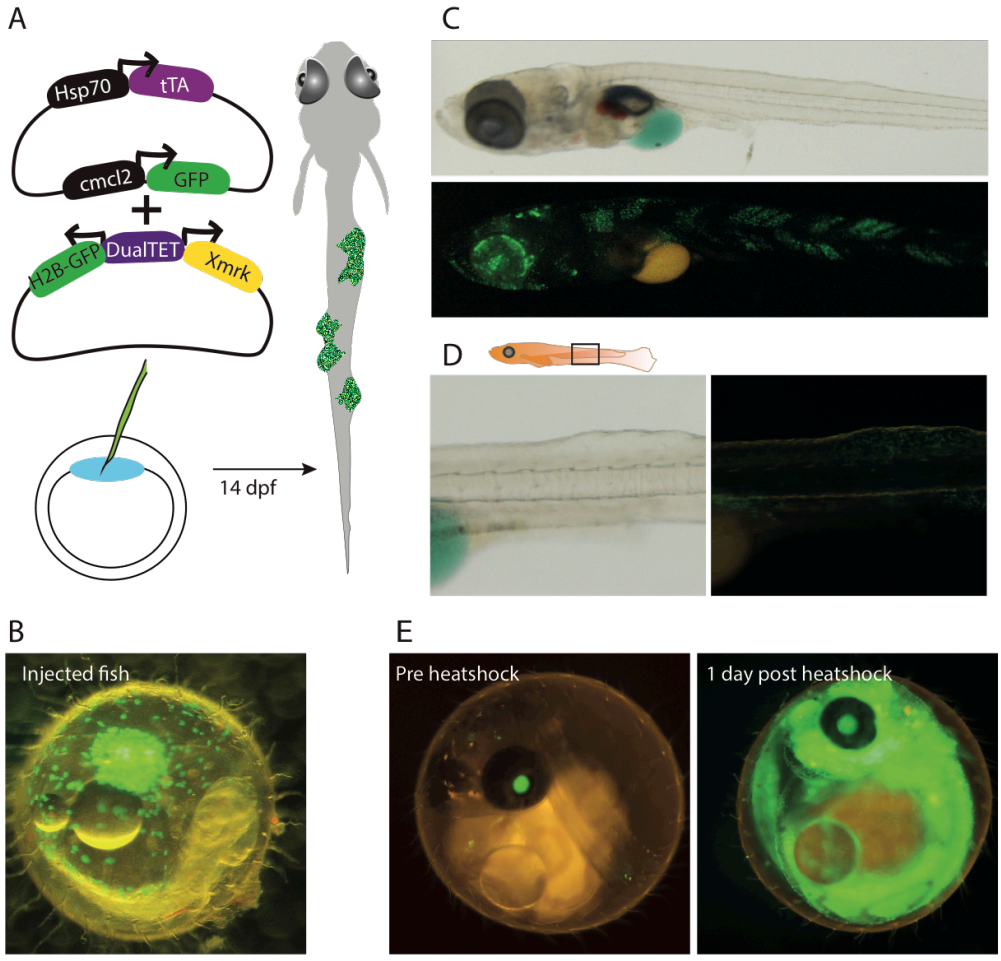

Figure 14: Inducible and trans-activator independent expression of Xmrk and H2B-GFP lead to over proliferation in somites. A. Two constructs were co-injected in single cell stage embryos: DualTetRE driving H2B-GFP on one site and Xmrk on the other side and a Hsp70 promoter driving a tTA protein with a cmlc2-promoter driving GFP in the heart as insertion marker. Death rates of injected H2B-GFP expressing embryos were high. B. Surviving embryo that showed mosaic expression of H2B-GFP in the lens and somites one dph with irregularities in somite growth in tails. C. Five dph larvae show substantial overgrowth of muscle tissue at places where H2B-GFP is expressed

Fish with somitic tissue abnormalities never displayed any other obvious phenotypes even though a remaining H2B-GFP signal could be seen in many other tissues (retina, lens, brain and skin). Fish with muscle ver-growth retained a thicker tail when compared to wild type (WT) siblings but did not develop any further overgrowth. We, therefore, conclude that an initial pulse of Xmrk can induce muscle growth but the situation becomes stabilized as the fish grows into adulthood, thereby resembling human Embryonal rhabdomyosarcoma (ERMS) a disease originating from immature muscle-progenitors (Breitfeld and Meyer 2005). The injection of a *K-RAS*^{12D} containing transgene in Zebrafish causes a similar phenotype with tumors forming in larvae with a mosaic expression of the transgene in satellite cells (muscle stem cells). Muscle overgrowth in Zebrafish becomes visible after 10dpf, which is comparable to the time frame that we observed here for Medaka. In the transgenic Rag2:: K-RAS^{12D} ERMS model the expression of the oncogene is persisting in the satellite cells and tumors grow invasive and are fueled by satellite cancer stem cells (Langenau et al. 2007). In our model, however, the over-proliferation seems to be due to an initial strong pulse after which muscle cells lose or adapt to enhanced growth signal, and no invasive growth takes place. The high expression from injected plasmids is probably due to a feedback loop of oncogenes with the stress-responsive hsp70 promoter element: Xmrk causes over-proliferation, which leads to stress, and more expression activity of the hsp70 promoter leading to more *xmrk* expression.

Even though we did not use a muscle specific promoter the only tissue that showed a proliferative phenotype at this stage are the muscle cells. Hsp70 proteins have a known function in the muscle tissue reaction to exercise (Gomes Heck et al. 2012). A persisted stress response was also described for the somatic tissue of *Xenopus laevis* embryos after slight heat-shock (Lang et al. 2000). A baseline expression from the hsp70 promoter in fish under moderate stress conditions is thus not surprising.

In the following generation, fish showed default expression of H2B-GFP in the lens due to the baseline activity of the promoter in this tissue that we observe in other hsp70- lines and which was reported in Zebrafish (Blechinger et al. 2002). When a heat treatment is applied to the F1 DualTetRE:: *H2B-GFP*/*xmrk*_ hsp70::*tTA*_ cmlc2::GFP (in the following named HSindX_H2B-GFP) embryos always showed ubiquitous expression of H2B-GFP within less than 24 hours post heat shock (hpHS)

(figures 14E and 15). The cardiac myosin light chain 2 (cmlc2) promoter drives expression specifically in the heart and is used here as a screening marker. Fish heat-shocked before hatching failed to do so and died, which might either be due to the Xmrk or the high H2B-GFP expression since in a control experiment where embryos only expressed H2B-GFP and no Xmrk some HS embryos also failed to hatch. In induced embryos, H2B-GFP expression can be found in all tissues and cell types as demonstrated in figure 15 for the brain (A' &B), eye (B'), skin (B'') muscles, gut, and neuromasts (B''').

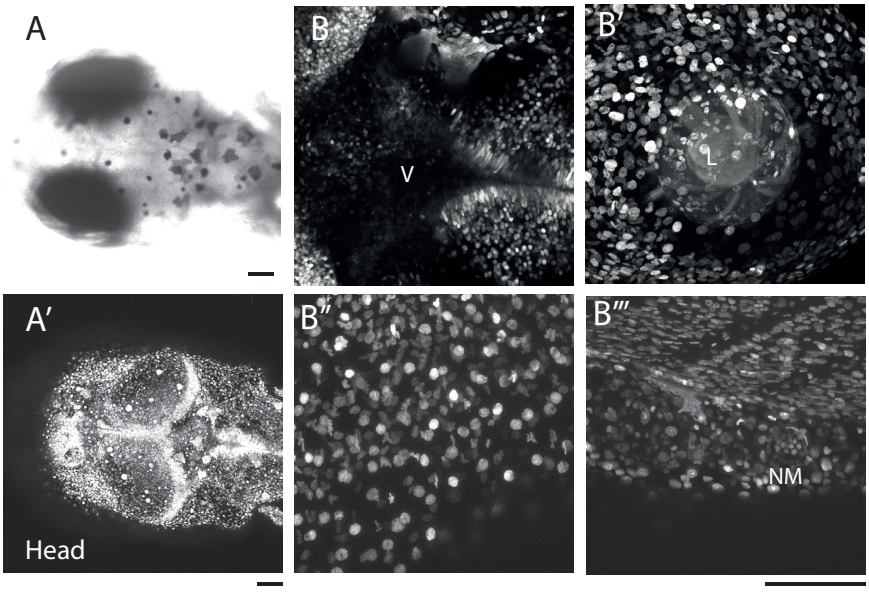

Figure 15: *In vivo* imaging of *DualTet::xmrk/H2B-GFP_Hsp70:.tTA_cmlc2::*GFP line expressing H2B-GFP in every nuclei after heat shock treatment. A. *In vivo* imaging of head region. A'. Brain structures can be distinguished based on the density of nuclei. B. Central brain ventricle and surrounding neurons. B'. The eye is expressing H2B-GFP in choroid layer. B''. Tail fin. B'''. Somites, gut, and neuromast are expressing H2B-GFP. Scale bar is 100 µm.

Xmrk expression in this context cannot be visually traced so that the impact of the oncogene can only be judged by looking at the tail appearance of hatchlings. Tails of HS fish grew thicker but stopped to grow any further. The HS-induced expression and translation of Xmrk protein are probably much slower than the H2B-GFP expression since the ORF of *xmrk* is three times the length. Hatchlings that were heat-shocked survived and did not display phenotypes, from that we conclude that short-term expression of Xmrk is insufficient to cause over-proliferation of cells.

H2B-GFP in a very stable label of cells since it integrates into the chromatin and even when transcribed transiently persists for a long time, H2B-GFP can therefore also be used for label retention studies (Foudi et al. 2009) or to analyze chromatin dynamics

(Kanda, Sullivan, and Wahl 1998). Not much is known about the stability of Xmrk, cell culture experiments, however, show that ErbB1 receptors are endocytosed relatively quickly and degraded by ubiquitin ligase stimulated pathways (Levkowitz et al. 1998). Since a tight regulation of growth signaling is essential for proper development, growth, and maintenance, we assume that potent mechanisms act on the fast degradation of Xmrk similar to endogenous Egfrs.

I also tested the induction of Xmrk and H2B-GFP expression in the *HSindX_H2B-GFP* line by locally applied heat-shock with an IR-lego system as described in (Deguchi et al. 2009; Kamei et al. 2009). For this, we kept *HSindX_H2B-GFP* embryos in heat-stable conditions until hatch and then anesthetized and mounted them with methylcellulose (to prevent heat shock by warmed up agarose) on to an inverse spinning disc microscope coupled to an infrared (IR) laser (1480nm). Fish were mounted in a way that regions of interest were closest to the objective to reduce energy loss (figure 16A). The target area was then selected using the bright field channel and applied laser pulses with an energy of 60-100 mW for 1 to 3 seconds until we could see twitching of cells. We applied the IR-laser heat shock only to the eye (around the lens) and the tail (around the site where the spinal cord ends) of the left side of the fish to use the other as a control.

One day after IR-laser treatment hatchlings were imaged under a regular fluorescent binocular. I observed H2B-GFP-positive cells around the lens of only the left eye of fish (N=3) and never in the right eye (figure 16B). Also, the tail fin showed a dispersed region of H2B-GFP positive cells. H2B-GFP was also expressed in the somites (figure 16B), even though no direct HS was applied. The embryos subjected to IR-Lego treatment were fixed and sectioned to stain for the presence of nuclear GFP. In the left eye of the fish, we could see GFP-positive nuclei throughout different layers of the retina. The applied HS thus led to expression not only in the choroid layer but also within the retina itself. No GFP expression could be observed in the right eye except for the lens.

Described pilot experiments for the transient expression of Xmrk together with H2B-GFP of a mirrored HS-responsive element shows that the line can be used to test short-term effects of enhanced Egfr signaling. The use of the line is however limited

by the lack of a direct readout of Xmrk expression; we, therefore, worked on fluorescent tagging of the Xmrk gene, which will be described in the following.

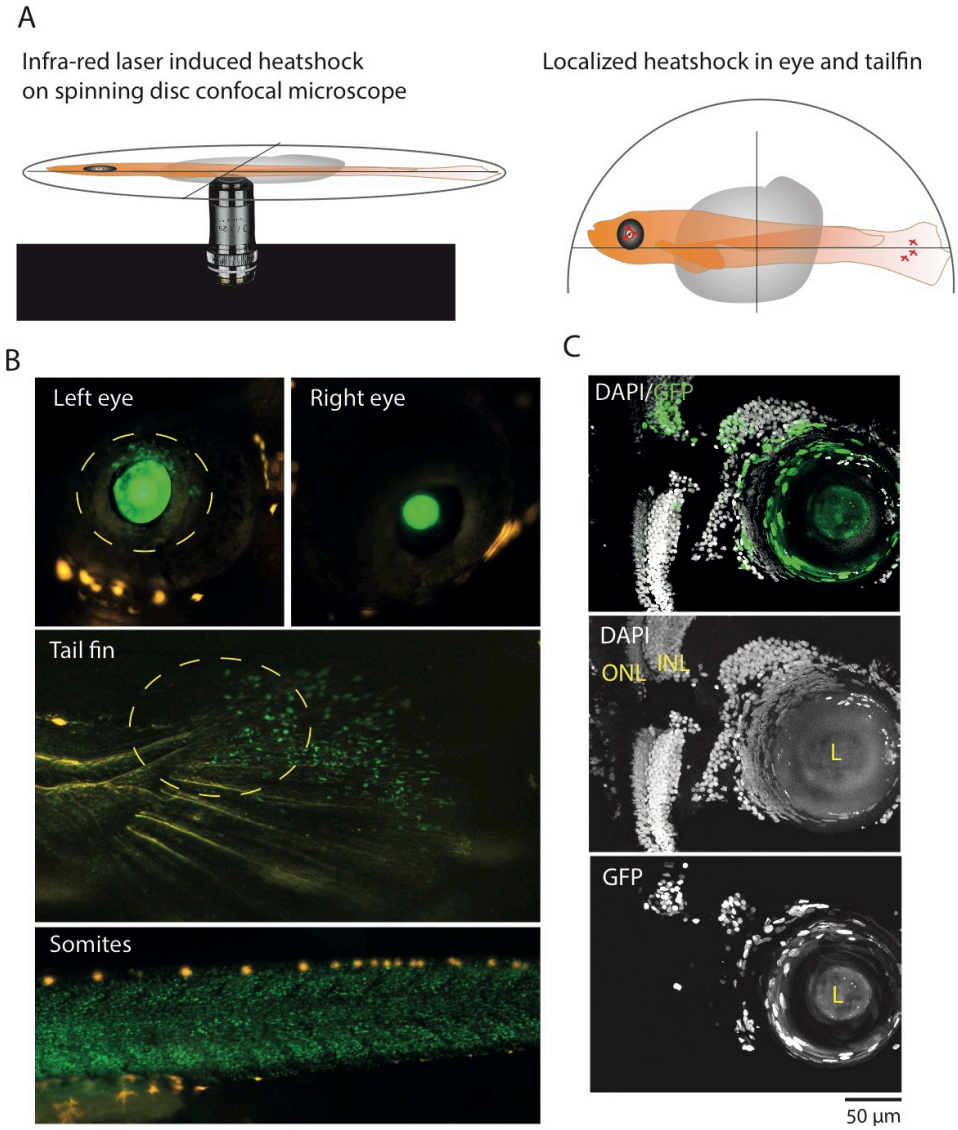

Figure 16: : Local heat shock causes expression of H2B-GFP/Xmrk in the *DualTETRE::xmrk/h2b-fp_Hsp70::tTA* fish line. A. The schematic graph is representing of the IR-lego setup. Medaka larvae are paralyzed and mounted on top of an inverted spinning disc confocal microscope, which is connected to an infrared laser to induce local heat-shocks. Red crosses indicate locations of induced heat-shocks. Heat-shocks were only induced on the left side of the fish; the right side was used as a control in larvae represented in B, N=3. B. Expression of H2B-GFP could be detected directly around the lens of only the left eye of the fish. The tail fin also showed activation of the constructs gene expression around the locations where local heat-shocks were induced at three positions. Somitic recombination could be observed independently in heat-shocked and no-HS fish. C. Cryosection of the retina of the fish shown in B. H2B-GFP transcription was induced in several layers of the retina, even though the heat shock was localized to the CMZ region close to the lens. The lens as the somites always showed expression of H2B-GFP independent of the heat-shock.

3.2.2 Tagging Xmrk with fluorescent proteins

Xmrk expression cannot be detected in vivo or in fixed tissue since so far no FP-tagged versions are available and commercial antibodies (Abcam) are only suited for Xmrk detection on western blots. Clara Becker and I collaborated in generating genetic constructs that allow a visual readout of Xmrk expression. For that, we C-terminally tagged Xmrk with FPs using either a flexible linker (FL, $(GGGS)_3$ (Arai et al. 2001; Trinh et al. 2004) or a T2A sequence (schematic representation in figure 17A). For testing the functionality of tagged Xmrk variants, we used the DualTetRE system again as described before in figure 14. We thus cloned plasmids with an *H2B-GFP* ORF on one side and the cyan fluorescent protein (CFP)-tagged versions of *xmrk* on the other side of a DualTetRE (*HSindX-FL-CFP_H2B-GFP and HSindX-T2A-CFP_H2B-GFP*). These plasmids were then co-injected with the *Hsp70::tTA_cmlc2::*GFP plasmid into single cell WT embryos. As a control, we injected the same plasmids in which *xmrk*-CFP is replaced by an *mCherry*. We did not apply any HS but could observe the same mosaic expression as described for *HSindX* _H2B-GFP. When injected embryos hatched, we saw that in muscle cells the FP signal localized according to our expectation. Cells expressing H2B-GFP also showed membrane localized CFP in the case of the FL tagged version of Xmrk and cytoplasmic localization of CFP in the T2A variant (figure 17B, upper row). We confirmed the correct localization of CFP tagged to Xmrk with either T2A or FL in fixed tissue sections (figure17B, lower row).

For all three dualTetRE constructs (Xmrk-FL-CFP, Xmrk-T2A-CFP, and mCherry) we found some embryos that showed expression of H2B-GFP and either CFP or mCherry and raised them until hatch. We discovered that T2A-tagged, as well as FL-tagged Xmrk, was able to induce irregularities in muscle growth that were not present when embryos were injected with the mCherry control. The expression of CFP correlated with regions of somatic overgrowth indicating that C'-terminally tagged versions of Xmrk retain their functionality. Example results are depicted in figure 17C.

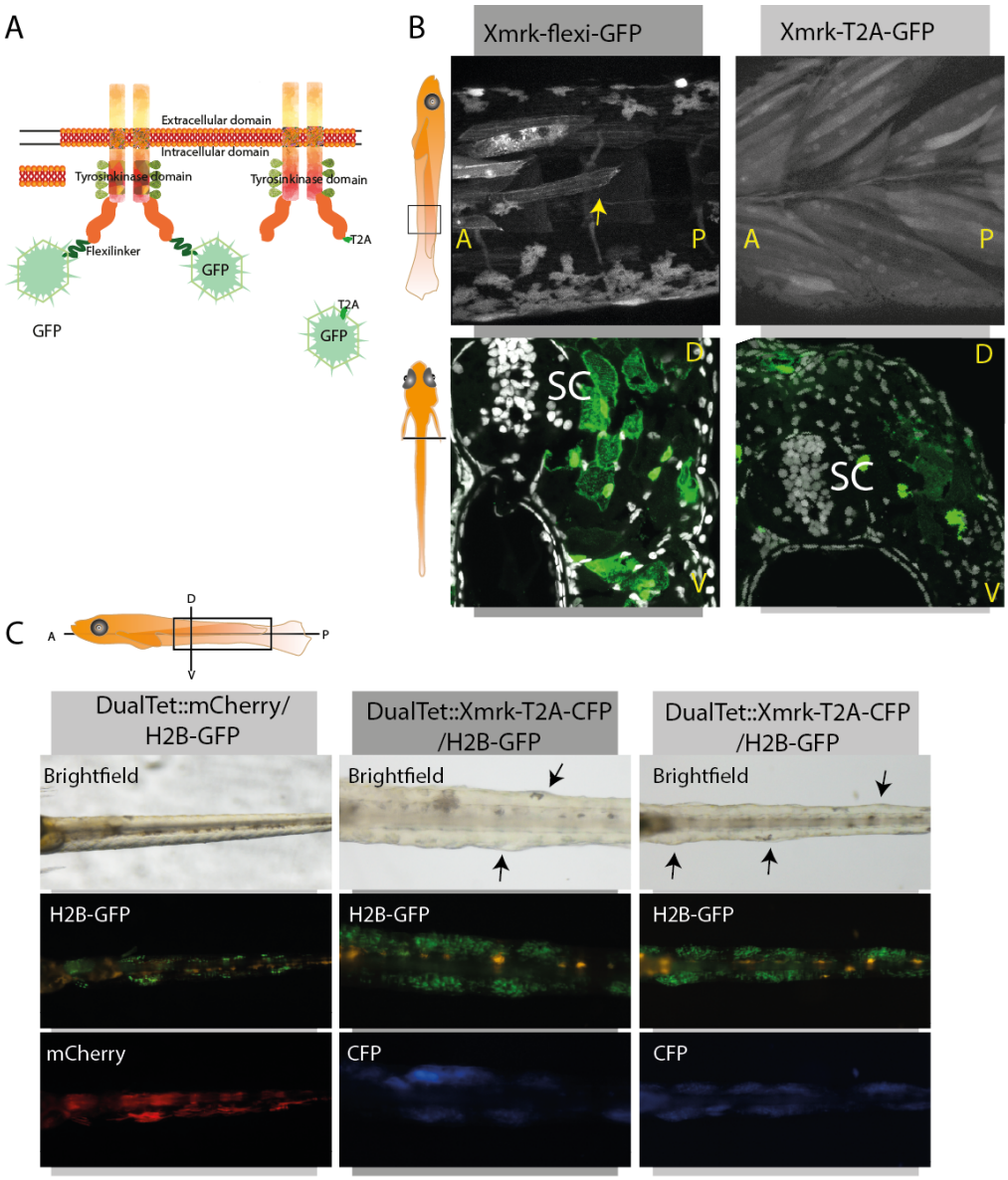

Figure 17: C-terminal FP-tagged versions of Xmrk via T2A and FL are functional oncogenes. A. Representation of the tagged Xmrk proteins. The flexi-linker is a direct linker that stays connected to the receptor after its localization to the membrane. In the T2A tagged version of the Xmrk gene, GFP would be retained in the cytoplasm after translation since the T2A sequence causes ribosome-skipping. B. *In vivo* imaging of somites and sectioning both confirmed the expected localization of tagged receptor variants. C. Functionality test of tagged Xmrk. DualTETRE::Xmrk-(FL or T2A)-CFP/H2B-GFP or DualTETRE::mCherryH2B-GFP co-injected with Hsp70:tTA_cmlc2:GFP in single cell embryos. Ten dpf somatic overgrowth was only observed in Xmrk-linker-CFP expressing fish and not in DsRed expressing fish. A=anterior, P=posterior, D=dorsal, V=ventral.

We also created DualTetRE based constructs for the HS-induced expression of eGfp-K-RAS$^{(V12)}$ and eGfp-myrAKT and obtained the same results concerning overgrowth of tail tissue (not shown). To correlate the expression of oncogenes with DNA replication events, we incubated injected fish in BrdU. The experimental setup as depicted in figure 18A was as following: we co-injected fish with *DualTet:tagged*

oncogene/H2B-GFP (*xmrk, myrAKT, and K-RAS*^{V12}) and *Hsp70::tTA _cmlc2::*GFP constructs and let them grow until hatch. As a control, we injected the same plasmids with a *mcherry* gene instead of an oncogene. Since the phenotype occurred without any heat-treatment, we did not apply an HS. After hatching, larvae were incubated two days in BrdU and then fixed and stained against GFP/CFP and BrdU. All three oncogenes were localizing predominantly in the membrane of H2B-GFP positive cells. We also detected cells which expressed only H2B-GFP. This can be because H2B-GFP is significantly more stable than any of the oncogenes. We saw increased muscle mass co-localizing with high membrane or cytoplasmic GFP expression (data not shown). However, we could not directly correlate GFP-positive nuclei with the presence of BrdU-positive nuclei. BrdU-positive nuclei could be mainly detected in the skin, the spinal cord (along the ventricle) and regions between muscle sections (figure 18B-E).
Even though we could see remarkable growth in muscle volume at sites of expression of the constructs we could not judge from this experiments whether the excess tissue mass is due to cell growth or proliferation. Due to the particular organization of somite tissue in multinucleated muscle fibers, it is hard to relate the nuclei to a specific fiber and sectioning of the fish does not allow judging proliferation dynamics based on BrdU-positive nuclei. The two days BrdU-pulse might also have been to short since most of the proliferation likely happened during development before hatch. An actin staining performed to see thickness and number of muscle fibers did not show any distinct differences between oncogene-expressing and other muscle fibers (results not shown).

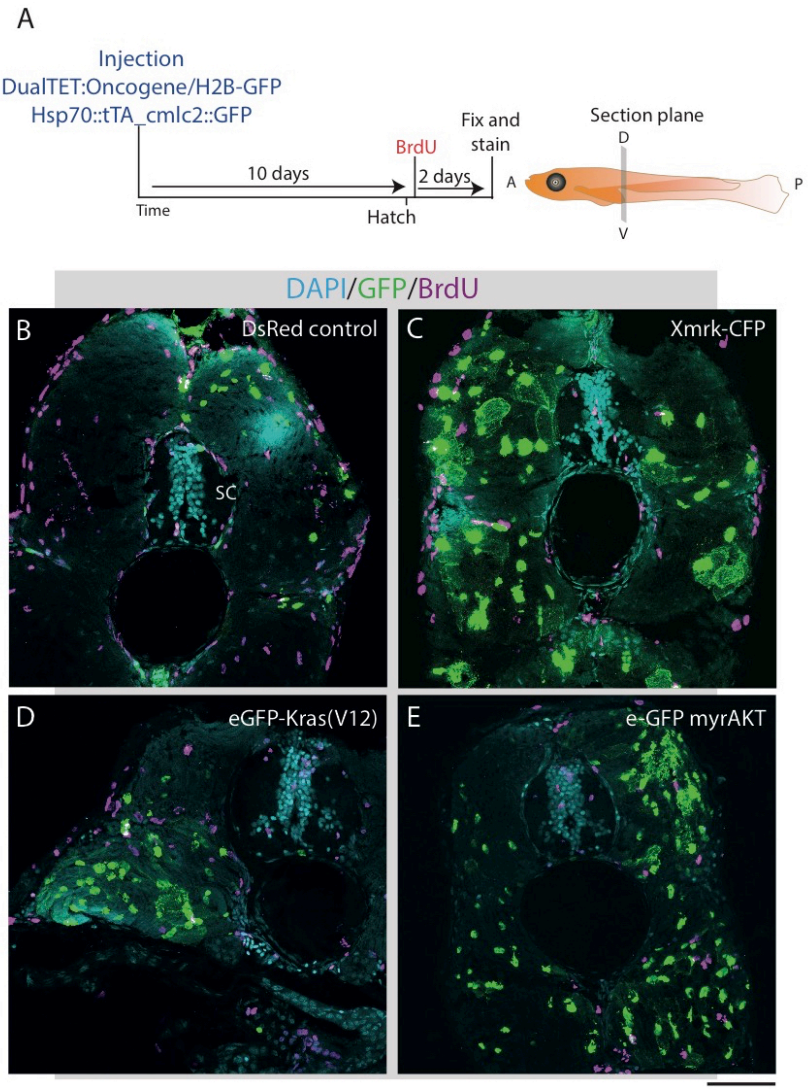

Figure 18: Expression of GFP-tagged oncogenes does not correlate with BrdU positive nuclei. A. schematic representation of the experimental setup, the DualTET::oncogene/H2B-GFP and Hsp70::tTA were co-injected, and embryos were raised until hatch. Hatchlings showing GFP expression were incubated for two days in BrdU and then stained for GFP and BrdU. Section through the tail of GFP positive embryos injected with Hsp70::tTA and DualTET::DsRed/H2B-GFP (B), DualTET::Xmrk-FL-GFP/H2B-GFP (C), DualTET::eGFP-K-RAS(V12)/H2B-GFP (D) or DualTET::eGFP-myrAKT/H2B-GFP (E). 18 µm sections were stained with a-GFP (green), a-BrdU (magenta) and DAPI (cyan). Scale bar is 50 µm.

3.2.3 Creation of a tool box for expression of oncogenes in single cells

After confirmation of the functionality of tagged versions of Xmrk we (Clara Becker and me) generated a genetic toolkit for the inducible Cre-mediated expression of FP-tagged Xmrk, K-RAS^{12V}, and myrAKT. For this, we used golden gateway cloning (Kirchmaier, Lust, and Wittbrodt 2013) to assemble plasmids containing a ubiquitin promoter (*D. rerio*), an mCherry STOP cassette flanked by loxP sites followed by the tagged versions of oncogenes and a triple polyA sequence. The construct design followed the example of published red-switch-green constructs by Lazaro Centanin (Centanin et al. 2014). As shown in figure 19A, the gene cassette is flanked by I-SceI restriction sites to allow optimal random integration into the Medaka genome (Thermes et al. 2002). The ubiquitous promoter was used to guarantee the versatile use of the transgenic fish lines in combination with tissue-specific Cre-drivers. mCherry expression was used as an insertion and ubiquitousness marker. Transgenic fish lines generated with defined constructs are named RS (red switch) followed by respective oncogene-FP fusions, being: *Xmrk-T2A-GFP, Xmrk-FL-GFP, eGFP-K-RAS^{12V}*, and *eGFP-myrAKT*.

For expression of oncogenes from the RSOncogene constructs, the *mcherry* STOP-cassette needs to be exist by Cre-mediated recombination of loxP sites. For temporal control, Cre is fused to an ERT2 promoter that is activated by binding tamoxifen (TMX). Another possibility of temporal control of Cre expression is to drive Cre fused to a nuclear localization signal (NLS) under an HS-protein activated promoter (Hsp70). We injected the RS-oncogene constructs in the *Hsp70::Cre-NLS_cmlc2::GFP* fish line to test the functional recombination after HS treatment of mCherry and cmlc2:: GFP positive embryos. In most cases, we could see broad recombination in somites of treated fish for *RSXmrk-FL-GFP* and *RSXmrk-T2A-GFP* as shown in figure 19C. Membrane localization of *Xmrk-FL-GFP* was confirmed by staining sections of positively recombined fish (figure 19C lower right picture).

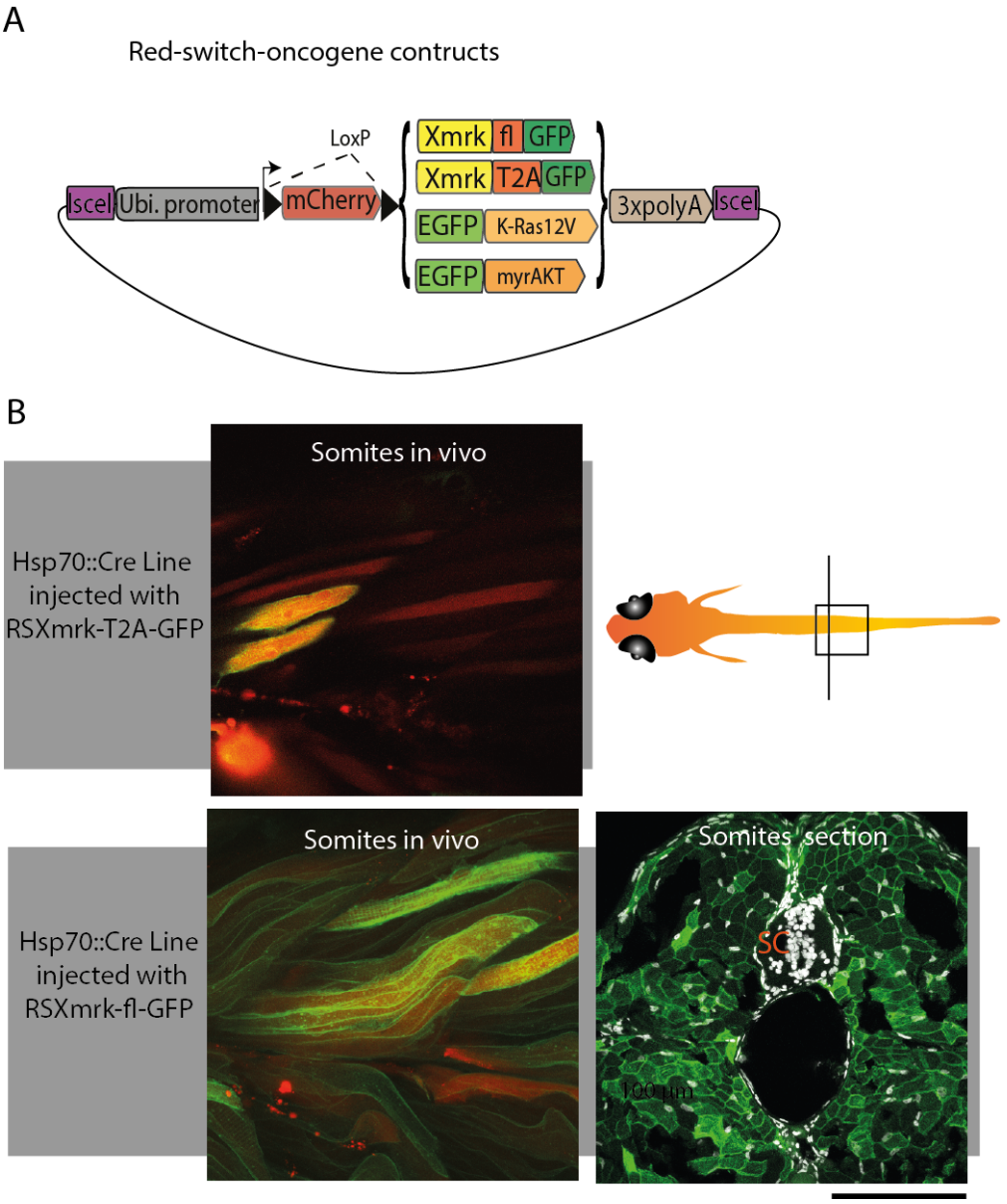

Figure 19: Toolbox for expression of oncogenes in single cells after Cre-mediated recombination. A. Constructs generated for the expression of Xmrk, Xmrk-FL-GFP, Xmrk-T2A-CFP, eGFP-K-Ras, eGFP-myrAKT after recombination of an mCherry stop cassette flanked by loxP sites under the control of a ubiquitin promoter and followed by a triple polyA site. B. Examples of recombination by injection of oncogene plasmids into HSP70:: Cre line. Xmrk-T2A-GFP expressed in muscle cells, shown by *in vivo* imaging (upper row). Xmrk-FL-GFP localizes to the membrane of somitic cells here shown *in vivo* and on a transverse section through the tail of a hatchling stained with an a-GFP antibody (green) and DAPI (white) SC=spinal cord, RS=red-switch. Scale bar is 100 µm.

The ability of tagged oncogenes to induce proliferation transiently was confirmed by Narges Aghaallaei. She injected a combination of *RSXmrk-FL-GFP* and *RSeGFPK-RAS^{V12}* together with the *Hsp70::Cre_cmlc2::GFP* plasmid and imaged the fish at 10 dpf (figure 20A). In mosaic embryos, she observed somatic over-proliferation as described before for the *HSindOncogene _H2B-GFP* constructs (figure 20B). Fish did not show over-proliferation in any other tissue either because they are not expressed

there, or other tissues need stronger and more prolonged exposure to oncogenic growth signaling to cause a visible proliferative response.

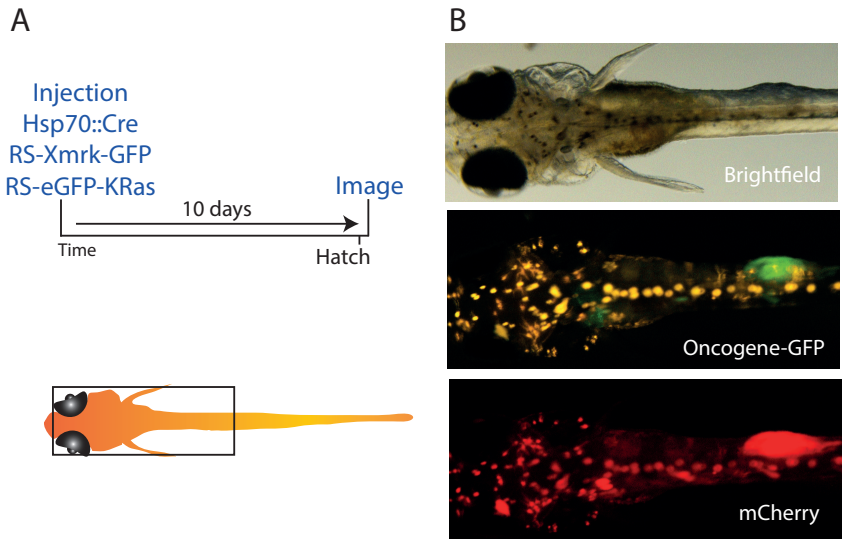

Figure 20: Co-injection of RSXmrk and RSK-RAS12V with Hsp70:Cre plasmids cause over-proliferation in recombined muscle cells. A. Schematic representation of the experimental setup with co-injected constructs. Embryos were grown until hatch and imaged. B. Some co-injected fish showed over-proliferation in muscle cells that expressed GFP and mCherry at somatic bumps. Experiment and imaging performed by Narges Aghaallaei.

A significant challenge in raising the RSOncogene lines was the screening for ubiquitousness of mCherry. The *D. rerio* ubiquitin promoter used for the expression of the oncogene cassette is only rarely integrated into the Medaka genome in a way that it is truly ubiquitously used. The expression in muscle fibers is always much higher than in the rest of the body and sometimes the only place of expression. This differential activity of the Ubi promoter in Medaka contrasts with the results found by Mosimann et al. who initially isolated the regulatory element. When integrated through Tol2 mediated transgenesis (Abe, Suster, and Kawakami 2011; Suster et al. 2009) in Zebrafish the 3,5 kb Ubi regulatory element leads to high ubiquitous expression of transgenes throughout development and adulthood over several generations (Mosimann et al. 2011).

For each construct (*RSXmrk-T2A-GFP, RSXmrk-FL-GFP,RSeGFP-K-RAS*^{12V} and *RSeGFP-myrAKT*) we selected several founder fish based on the mCherry expression in tissues other than muscles (brain, retina, fins & heart). F0 fish were crossed to WT cabs and offspring with ubiquitous expression of all constructs were raised. Selected oncogene lines are summed up in table 1 with the respective stock numbers of their F1 and F3 generation.

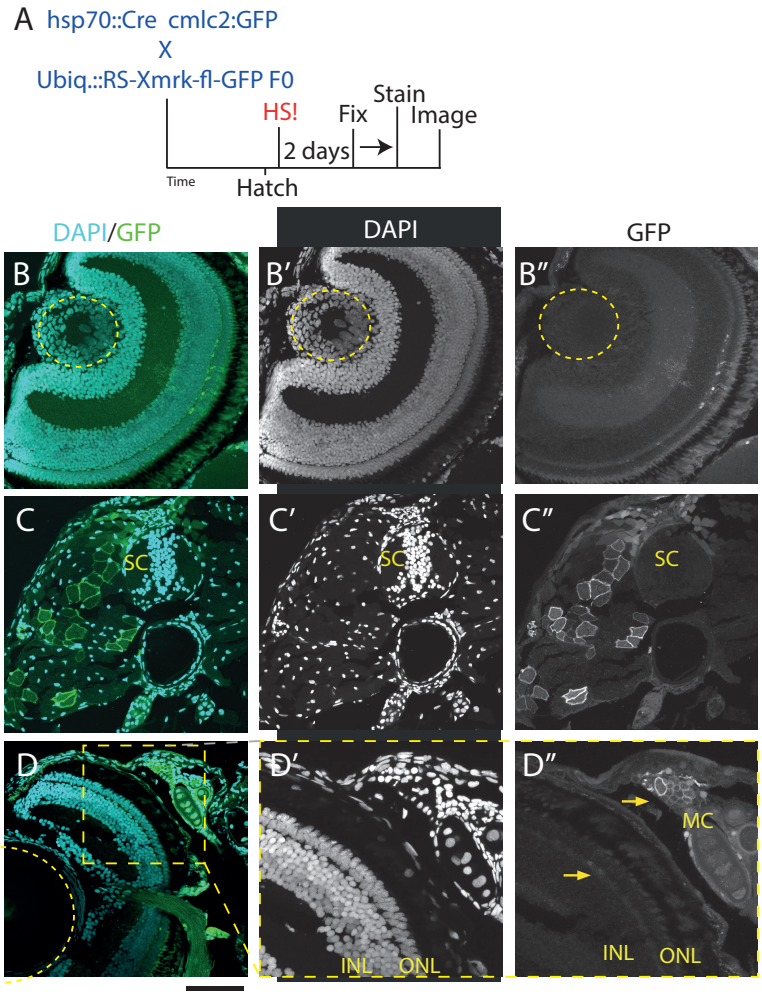

Figure 21: Heat-shock-induced recombination of RS-Xmrk-FL-GFP fish in the retina and somites. A. Experimental setup: Hsp70:Cre_cmlc2:GFP fish line was crossed to an F0 founder with a genomic insertion of Ubiq::RS-Xmrk-FL-GFP plasmid. Offspring was screened for ubiquitous mCherry expression and raised until hatch. A. Heat-shock was applied, and hatchlings were fixed, sectioned and stained with GFP and DAPI after that. B-D. Examples for recombination in the retina (B) and muscle cells of the tail (C). D. Section of recombined larvae in which head-muscle and retinal cells show different levels of GFP expression, D′ and D′′ are two times enlarged details of D. The dashed circle indicates the location of the lens. HS= heat shock SC= spinal cord, INL=inner nuclear layer, ONL=outer nuclear layer, MC= muscle cell. Scale bars are 50 µm.

To test if the oncogene lines can recombine in tissues other than somites we tested the F1 offspring directly. The *RSXmrk-FL-GFP* Line #1 founder was crossed to *Hsp70::Cre-NLS_cmlc2::GFP* fish, an HS was applied after hatch and larvae were fixed two days post-HS (experimental procedures see figure 21A.). Several fish showed recombination in the somites (figure 21D) as well as in the central part of the retina (21B), GFP expression in the retina was much weaker than the expression in muscle cells. Figure 21D shows a section of a larva in which recombined cells were found in the head muscle cells and the retina, the GFP signal in muscle fibers is however much

brighter than in retinal neurons. This staining revealed a critical drawback of the oncogene lines: the expression of GFP in the retina is weak and even after immunostaining barely detectable. When compared to the GaudiRSG lines in which recombined cells express H2B-GFP (Centanin et al. 2014), the membrane-localized GFP in neurons is considerably less prominent. Other than GFP localization, differences in plasmid copy number, tandem repeats and loci of integration could attribute to this variation in readout visibility. Another possibility might be the active downregulation of transgenes by epigenetic mechanisms which has been reported previously in grafted and cultured cells (Lundberg et al. 1996; Wolff et al. 1989) and *in vivo* in Zebrafish (Goll et al. 2009). Also, the activity of the Hsp70 promoter driving Cre has differential activity in somites and neural tissue, and therefore recombination in somites is more frequent than in other tissues.

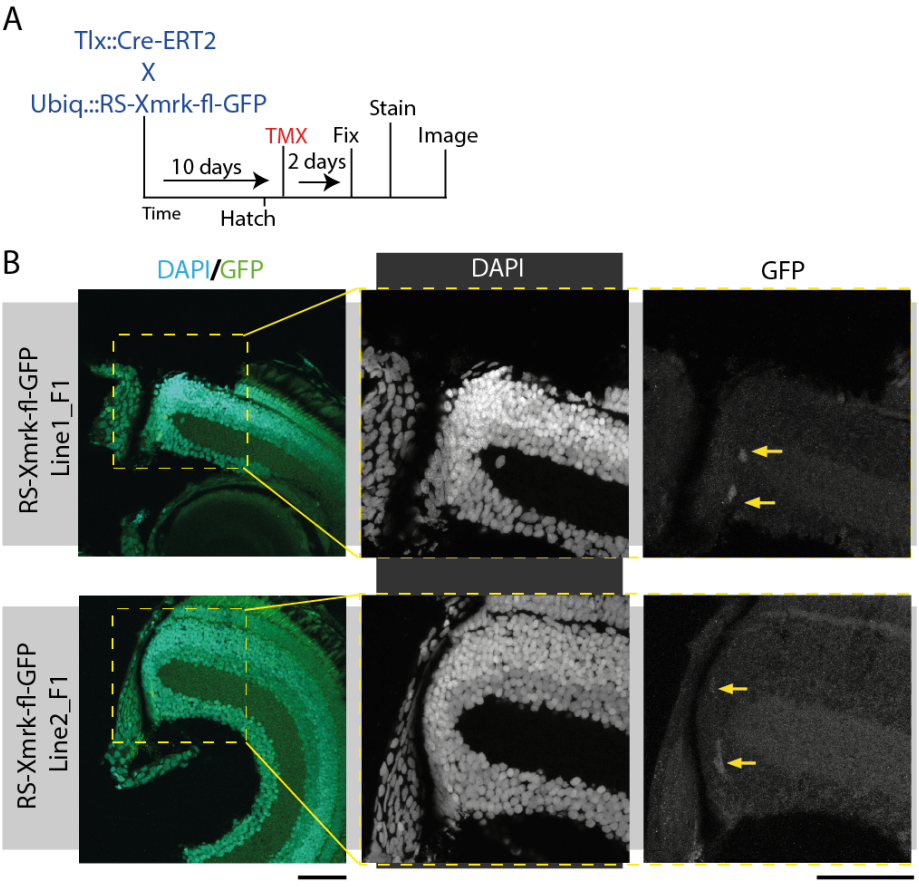

Figure 22: Recombination in the CMZ of *RSXmrk-fl-GFP_Tlx::Cre-ERT2* positive fish two days after TMX induction. A. Experimental setup: Tlx::Cre-ERT2 fish were crossed to RS-Xmrk-FL-GFP lines (F1) and raised until hatch. Upon hatch recombination in Tlx-positive cells was induced by TMX administration. Fish were fixed two days post induction and stained using antibodies directed against GFP. B. Examples of retinae derived from fish of two different RS-Xmrk-FL-GFP lines (L1 and L2) in which single recombined cells could be detected in the CMZ region of the retina. Expression of GFP was weak. Scale bars are 50 µm.

To investigate effects of Egfr-related oncogene expression specifically in the CMZ, I used Cre-driver lines that express the recombinase in specific cells in the CMZ. In a first short-term experiment, I wanted to know if shortly after recombination GFP-positive cells are detectable in the RSC zone. I crossed two *RSX-FL*-Xmrk lines with a *Tlx::Cre-ERT2_cmlc2::CFP* line. The tailless (tlx) promoter drives gene expression in the CMZ as well as proliferative zones in the brain. Recombination was induced two days post hatch (dph) and embryos were fixed two days later as described in figure 22A. In both lines, I could detect single, weakly GFP-positive, recombined cells in the CMZ where the Tlx promoter is active (figure 22B).

Since the before mentioned result showed that recombination events could be achieved at desired location and time in the CMZ, I set up crosses of various oncogene lines with either *Rx2::Cre-ERT2 cmlc2::CFP* fish or *Hsp70::Cre-NLS cmlc2::GFP* fish to perform long-term ArCoS assays. With this experiment, I aimed to address the effects of oncogene expression on the behavior of RSCs and their progeny. For that, I crossed F1 fish of the different oncogene lines (*RSXmrk-T2A-GFP, RSXmrk-FL-GFP,RSeGFP-K-RAS^{12V}* and *RSeGFP-myrAKT*) to before mentioned Cre lines and either treated larvae with five µM TMX after hatch or applied an HS and grew fish for several weeks (experimental setup demonstrated in figure 23A).

I could detect ArCoS formation only in the *RSeGFP-K-RAS^{12V}* line, which showed eGFP-K-RAS^{12V} expression in the retina (figure 23B) after heat-shock induced recombination. ArCoS were found in 2 out of 8 retinae starting at the induction ring, expressing GFP in the whole column of different retinal cell types and ending in the Rx2 expressing domain in the CMZ. The ArCoS therefore resembled WT ArCoS; an apparent effect of K-RAS^{12V} expression on RSCs could not be detected.

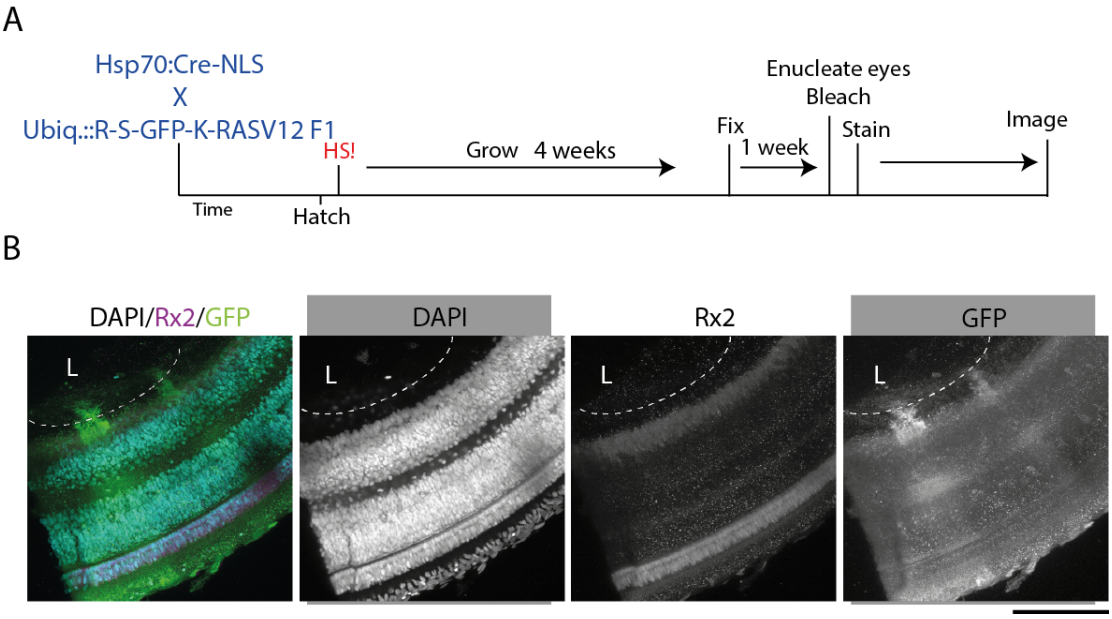

Figure 23: ArCoS observed in the *RS-eGFP-K-Ras_hsp70:Cre-NLS* line four weeks post heat-shock. A. Schematic setup for recombination experiment. F1 founders of *RS-eGFP-K-Ras* were crossed to *Hsp70:Cre-NLS* fish. After hatch fish were heat-shocked and raised for four weeks. Fish were then sacrificed, fixed and eyes were enucleated, bleached and stained for Rx2 and GFP. B. Example for one out of 4 retinae in which recombination could be detected as arched continuous stripes. ArCoS start in the Rx2 positive part of the CMZ along the lens and are marked here by yellow asterisks. The lower row shows an example ArCoS, a zoom-in from the retina represented in the upper row. Scale bars are 100 µm.

In total, I tested five different lines for Xmrk, two for K-RAS^{12V} and three for myrAKT (at least five hatchlings of each line) for the expression of the respective oncogene in single cells in the retina. Except for K-RAS^{12V}, I could never detect any ArCoS or recombined cells in the retina even though HS-induced recombination of muscle cells showed the functionality of the recombination in these cell types. The lack of effect of oncogenic K-RAS^{12V} expression is less surprising considering the survival function that the Ras/Mapk pathway has in neurons of the retina and the brain and the intense activity of the pathway in the INL and ONL as discussed in chapter 5.1.1. and 5.1.2. Although pErk was not detected in the Tlx expression zone (CMZ) (figure 9) *k-ras* is also expressed in the undifferentiated region of the retina (figure 8) but weaker than in amacrine cells.

Several technical difficulties can explain the lack of ArCoS formation in other oncogene lines. The inefficiency of TMX and HS-induced recombination in hatchlings, low expression levels of the GFP-fused oncogenes or silencing of the constructs in neuronal tissue could be reasons for the outcome of the experiments.

In the following generations of oncogene lines the intensity of GFP decreased even further so that in most lines even the somite expression of GFP after recombination became rather weak. For all oncogenes several lines were raised which are summed up in Table 1. To find out what happens to RSCs and RPCs directly after recombination, I performed several BrdU incorporation experiments and TUNEL stainings with TMX-induced RS-Oncogene hatchlings that I fixed two days post induction; I could however never detect any GFP signal in the retina.

Red-Switch Oncogene lines						
Oncogene	Stock # F1	Recombination somites	Recombination retina/brain	ArCoS assay performed	Outcome ArCoS assay	Stock # F3
Xmrk-fl-GFP L1	6603	Yes	Yes	Yes	None	7310
Xmrk-fl-GFP L2	6604	Yes	Yes	Yes	None	7311
Xmrk-fl-GFP L3	6610	Yes	No	Yes	None	7307
Xmrk-fl-GFP L4	6640	Yes	No	-	-	terminated
Xmrk-fl-GFP L5	6694	Yes	No	-	-	terminated
Xmrk-T2A-GFP L1	6641	Yes	No	Yes	None	7306
K-RAS-GFP L1	6642	Yes	No	Yes	None	7312
K-RAS-GFP L2	6643	Yes	Yes	Yes	ArCoS	7316
myr-AKT L1	6677	Yes	No	Yes	None	7314
myr-AKT L2	6689	Yes	No	Yes	None	terminated
myr-AKT L3	6755	Yes	No	-	-	terminated

Table 1: Generated RS-oncogene lines with previous and current stock numbers and summary of performed assays and findings.

Apart from the technical problems the absence of Xmrk- or myrAKT-ArCoS could be explained by the effect of these oncogenes on RSCs and RPCs. In the SVZ of mice, Egfr signaling regulates the balance between NSCs and NPCs together with Notch signaling. Enhanced Egfr signaling shifts the balance between symmetric and asymmetric divisions and the NPC pool expands while the NSCs are reduced (Aguirre, Rubio, and Gallo 2010). If the same would also happen to RSCs, a single RSC would divide into two progenitor cells that would proliferate and differentiate. Phenotypically this could be detected as a footprint of green neuronal cells on the level of the induction ring that are not connected to the CMZ. Another possibility is that RSCs exposed to enhanced growth signaling undergo apoptosis. Even though Egfr signaling usually has an anti-apoptotic effect, RSCs might have sensitive mechanisms that detect if cells are exposed to enhanced growth signaling and activate programmed cell death. The accumulation of activated Egfr on endosomes in cell culture, for example, can induce apoptosis (Högnason et al. 2001; Rush et al. 2012). RSCs and RPCs with enhanced growth signaling might also be rapidly detected and removed by

the immune system; immune cells were found to patrol the retina and CMZ actively. In a transgenic interleukin1::GFP line, Il1-positive immune cells were seen to localize in or at least near the CMZ (Katharina Lust, personal communication). Furthermore, it has been shown in Zebrafish that oncogene-transformed cells are rapidly detected by the immune system via H_2O_2 signaling. Even though the immune system was shown to have a positive effect on the growth of the transformed cells it could be that in the retina the immune system functions as a quality control system (Y. Feng et al. 2010).

3.3 Specific role of Egfra revealed by a CRISPR/Cas9 based knockout strategy

Teleosts retained two functional copies of the *egfr* gene, *egfr a* and *b* (Gómez et al. 2004), implicating that both receptors serve a vital function. The two receptors might be redundant for many functions since they show overlapping expression patterns in the CNS as demonstrated before. To unravel the particular role of Egfrs, I designed a CRISPR/Cas9 based knock-out (KO) strategy for *egfra* since it is more closely related to the mammalian *egfr*.

3.3.1 Experimental design of Egfra knock-out

A CRISPR/Cas9 based non-homologous end joining (NHEJ) approach was chosen to disrupt the ORF of the *egfra* gene by induction of double strand breaks (DSB). Three sgRNAs were designed using the *CCTop* prediction tool (Stemmer et al. 2015) to target the first exons of the *egfra* gene located on chromosome 17. I selected Exon #4 and #7 since they had the lowest probability of off-targets as predicted by *CCTop*. By choosing two target sites, I aimed to disrupt the extracellular domain of the receptor (Domain I and II).

Figure 24A shows a schematic representation of the Egfra-KO approach. Together with sgRNAs directed against the genomic locus I injected a plasmid coding for GFP lacking the start codon. An in-frame integration of the plasmid in exon 4 or 7 will result in a fusion protein of the Egfra N-terminus with GFP. The $eGFP^{var}$ plasmid is linearized by co-injection of a sgRNA directed against the T1 site immediately 5' of the GFP sequence; the same strategy was used for tagging of the *actin b* locus in (Stemmer et al. 2015).

First injections performed with all three Egfra-targeting sgRNAs (severe effects on injected embryos; more than 40 % died early after injection and several surviving embryos showed malformations or developmental delay (figure 24C). This observation is in line with the initial assumption that defective Egfr is lethal as it is the case in mammals. Genotyping pools of injected malformed embryos as well as phenotypically normal hatchlings showed high frequencies of Egfra mutations in exon 4 but not in exon 7 (data not shown), suggesting that only the sgRNA targeting exon 4

is functional and efficiently inducing DBS in the desired region. The probability of in-frame insertion of the GFP sequence is 1/6. GFP fluorescence could not be detected in the injected generation or any of the following, which is reported for several other cases of GFP insertion in first exons of an ORF in our lab.

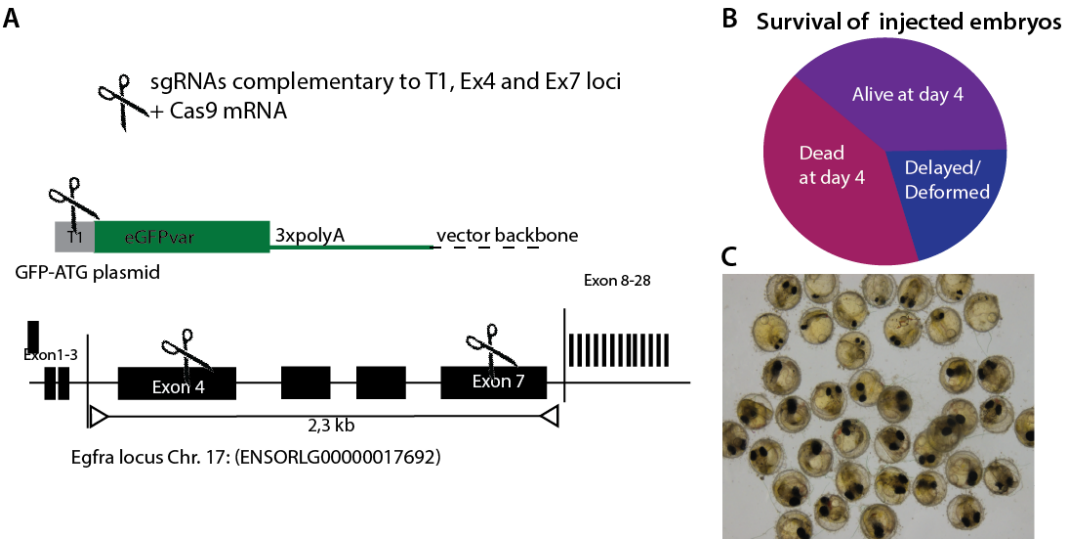

Figure 24: CRISPR/Cas9 based knockout strategy for NHEJ based insertion of an eGFP^{var} plasmid into the Egfra locus. A. Schematic representation of the GFP donor plasmid, which is linearized *in vivo* upstream of the eGFP^{var} at the CR13 site, and the target locus on Chr. 17 coding for the *O. latipes* Egfra gene. Two sgRNAs were designed to induce DSB in exon 4 and 7. B. Death rates after first injections with combined sgRNAs (Exon 4 and) were above 40%. One-third of surviving embryos showed severe malformations or growth delay four days post injection. C. An example of embryos injected with Egfra-targeting sgRNAs and Cas9 mRNA surviving until four days post injection.

Since the sgRNA targeting exon 4 was proven functional, I raised injected fish to adulthood. I then crossed them to WT cabs, and the offspring was screened for insertion of GFP, excision of the locus between exon 4 and 7 and INDEL mutation at the sites where the DSBs occur. Figure 25 illustrates the PCR and sequencing-based screening procedure for Egfra mutant fish. The PCR strategy for screening of F1 embryos and following generations is demonstrated in panel A. Most common were deletions of several base pairs. All identified mutations were deletions of triplets of bases ranging from 3 to 24, which do not cause a frame shift. Triplet deletions were observed for other cases of CRISPR/Cas9 mediated INDEL mutations in the lab. I identified two found fish and raised their offspring to adulthood. The first founder carried an insertion of the eGFP^{var} plasmid (Egfra$^{GFPins/+}$) at the double strand break (DSB) site in exon 4. The second founder had a deletion of 12bp at the same location (Egfra$^{12bpDEL/+}$). The four amino acids (glutamate (E), leucine (L), proline (P), and

methionine (M)) missing in the generated mutant version of Egfra are located in the extracellular domain 1 in which receptor-ligand binding takes place (Laisney et al. 2010). This mutation can thus disturb the ligand binding by inducing a conformational change in the binding pocket.

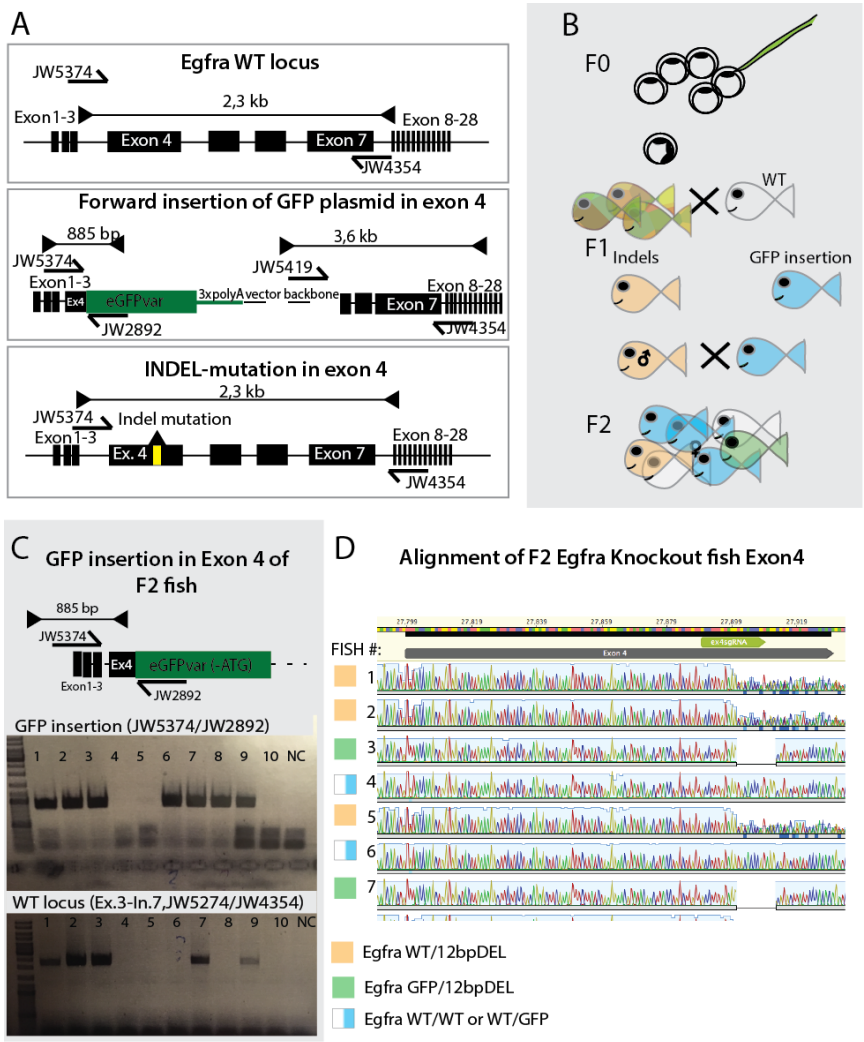

Figure 25: Experimental screening setup for detection of CRISPR/Cas9 mediated insertions and deletions in the *egfra* locus. A. Representation of the WT locus and primers used for amplification of the WT locus between exon 3 and intron 7 and two identified mutations identified in F1 (forward insertion of eGFP^{var} plasmid/INDEL mutation in Ex4). B. Injected generation was outcrossed to WT Cab fish. Positive founders were identified by genotyping pools of F1 embryos. Offspring of positively identified founders (GFP insertion or INDELS) were grown to adulthood. Female F1 fish harboring a GFP plasmid insertion in one allele (Egfra$^{GFPins/WT}$) were crossed to F1 males with a deletion in Exon 4. C. The F2 did not show any obvious phenotype and was grown to adulthood, fin-clipped and genotyped by PCR (GFP insertion). Sequencing of Exon 4 revealed that Egfra$^{-/-}$ are viable. - D. An example of sequencing results and assigned phenotypes of F2 fish, with responding genotype, please note that only the WT PCR bands (primers: JW5374/4354) were sequenced. The GFP plasmid containing alleles did not amplify with the used elongation time. Fish 1, 2, 5 amplified two different alleles (one with 12bp DEL and one WT), fish 3 and 7 only amplified a 12 bp DEL allele, the other allele must thus be GFP, since no two 12bp alleles can be present in the F2 (see crossing scheme in B).Fish 4 and 6 amplified one or two WT alleles, and their genotype is either GFP/WT or WT/WT.

Since all Egfra$^{GFPins/+}$ F1 fish were male and Egfra$^{12bpDEL/+}$ were female both lines were crossed to obtain homozygous mutants in the next generation. Figure 25B illustrates the crossing scheme used to raise homozygous Egfra mutant lines. Screening of the offspring revealed that homozygous Egfra mutants (Egfra$^{12bpDEL/GFPins}$) are viable and do not show distinct phenotypes as it is the case in knockout mice (Dackor, Caron, and Threadgill 2009; M Sibilia et al. 1998). This means that Egfra is either dispensable or the *egfra* transcripts deposited in the oocytes (Laisney et al. 2010) are sufficient to rescue its function in early development.

3.3.2 Offspring of Egfra$^{-/-}$ females is not viable due to polyspermy

Egfra knockout fish did not display a phenotype in the first two generations. However, offspring of homozygous Egfra$^{12bpDEL/GFPins}$ F2 females showed very early phenotypes. Oocytes and zygotes in one-cell-stage appear normal, but the first blastocyst cleavages are delayed and abnormal (see figure 26). In WT embryos the first cleavage furrow typically develops orthogonal to the axis of the micropyle (MP) and the second polar body (Iwamatsu 2004). In Egfra$^{-/-}$ however, multiple disoriented cleavage planes occur. Within the first two hpf, Egfra$^{GFPins/+}$ derived embryos have developed until four cell stage; at the same time 85% Egfra$^{-/-}$ show severe blastocyst cleavage defects and die (figure 26, panel B). Egfra$^{GFPins/12bpDEL}$ cells continue dividing in disordered fashion for several hours until they fail to gastrulate normally (28hpf). The same and even more pronounced phenotype could be observed in oocytes derived from Egfra$^{GFPins/GFPins}$ females where 98% of embryos show early cleavage defects. Some zygotes of Egfra$^{12bpDEL/GFPins}$ females develop normally which might be due to some retained function of the Egfra^{12bpDEL} variant. Both mutations thus lead to the same phenotype; therefore I assume that the insertion of the GFP plasmid or the 12bp DEL in exon 4 leads to a defective receptor unable to bind ligands. It still needs to be demonstrated that both Egfra mutant alleles are non-functional or hypomorph.

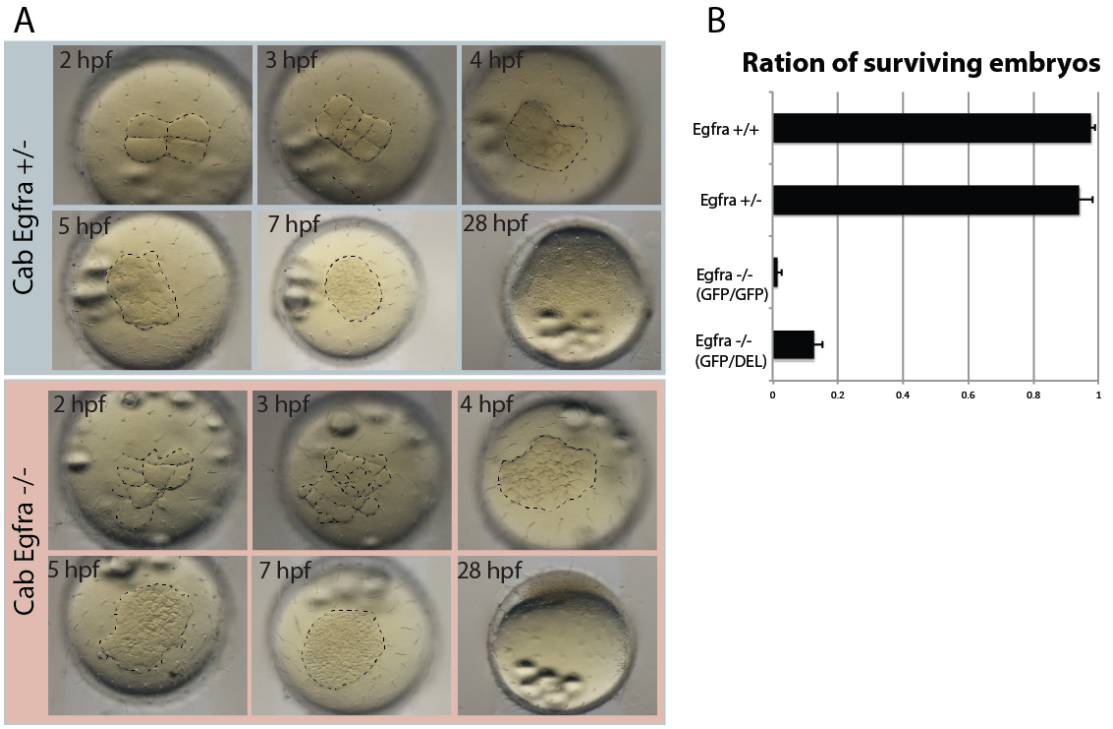

Figure 26: Phenotype of embryos derived from homozygous Egfra mutant females in comparison with heterozygous and WT females. A. An example of cleavage events of embryos 2 to 28 hpf (4-cell stage – end of gastrulation). WT embryos divide symmetrically in the first cleavages, 4-cell stage to 16-cell stage and have reached gastrulation 28 hpf (25°C). Embryos derived from homozygous mutant females already show abnormal first cleavages two hpf, asymmetric growth of blastula (7 hpf) and typically fail to reach gastrulation. B. The ratio of embryos that reach hatchling stage is above 95% in homozygous WT and heterozygous Egfra mutants. Almost no embryos derived from homozygous Egfra GFP insertion females ($Egfra^{GFPins/GFPins}$) manage to reach gastrulation. About 12% of the offspring of homozygous mutants with $Egfra^{GFPins/12bpDEL}$ genotype reach gastrulation and manage to hatch.

To determine the cause of the early cleavage phenotype and characterize the DNA replication dynamics I established a protocol that allows live imaging of chromatin dynamics in the forming zygote. The first striking feature that became evident in the time-lapse imaging (described later in figure 28) is the presence of multiple nuclei before the first cell division (30-40 mpf).

To address whether excess pronuclei are of paternal or maternal origin I collected unfertilized mature oocytes as well as fertilized oocytes at 2 and 25 mpf from $Egfra^{+/+}$ and $Egfra^{-/-}$ females to address the question if excess pronuclei are of male or female origin. Oocytes were stained with DAPI and γ-tubulin and imaged in collaboration with Daigo Inoue to check determine for chromosomal abnormalities and presence of centrosomes that are naturally of male origin in most species (Schatten 1994). Results of this stainings are presented in figure 27A.

The chromosomal content of mature unfertilized oocytes does not differ between Egfra$^{+/-}$ and Egfra-$^{/-}$ and all supernumerary pro-nuclei observed in the live imaging experiment must thus be of male origin (figure 27 A).

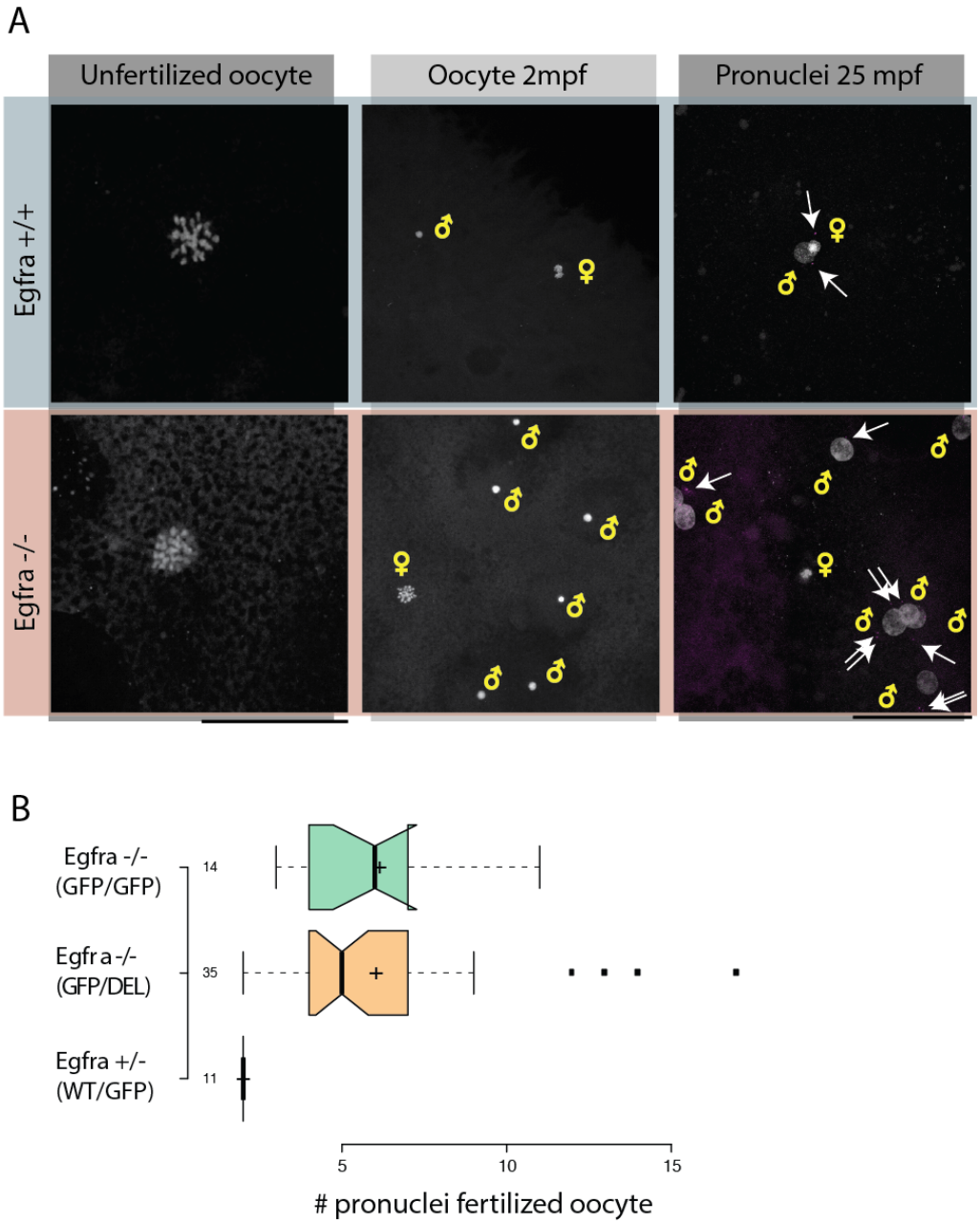

Figure 27: Oocytes derived from Egfra$^{-/-}$ females become fertilized by many sperms. A. Unfertilized oocytes of **Egfra$^{-/-}$** show regular metaphase-arrested pronuclei, upon fertilization multiple male pronuclei enter the oocyte: male pronuclei are highly condensed at first (2 mpf). In WT embryos the female pronucleus migrates towards the decondensed male pronucleus, and both start fusing 20 mpf. In multi-fertilized oocytes male pronuclei decondense and form aggregates. In fertilized embryos, the sperm brings one centrosome that divides before the first cell division (white arrows). In fertilized Egfra$^{-/-}$ oocytes multiple centrosomes are present (white arrows). B. Polyspermy only occurs in zygotes derived from homozygous Egfra mutant females, but not from heterozygous ones. The median number of pronuclei in fertilized mutant oocytes is 5 for Egfra$^{12bpDEL/GFPins}$ and 7 for Egfra$^{GFPins/GFPins}$ females. Scale bar is 25 µM for unfertilized oocytes and 50 µM for fertilized oocytes. mpf=minutes post fertilization, WT= wild type.

In WT embryos, male and female pro- nuclei can be distinguished by their size and dynamic. The male pronucleus is initially small (figure 27 A, 2mpf) but chromatin decondenses fast (figure 27 A, 25 mpf) and it becomes strikingly bigger than the female pronucleus. The female pronucleus remains in its metaphase confirmation and moves towards the male pronucleus along microtubules that are nucleated by the male centrosome (Schatten 1994).

Egfra$^{-/-}$ oocyte pronuclei appear indistinguishable from WT nuclei. I counted the number of pronuclei present after fertilization in Egfra$^{12bpDEL/GFPins}$, and Egfra$^{GFPins/GFPins}$ derived oocytes ranging between two (one male and one female) to 17 pro-nuclei that were visualized by DAPI staining of fertilized oocytes (2-15 mpf). The difference between Egfra$^{12bpDEL/GFPins}$ (median five pronuclei) and Egfra$^{GFPins/GFPins}$ (median is seven nuclei) might be due to the difference in the two mutant alleles where the 12bp DEL allele might be a hypomorph.

3.3.3 Polyspermy leads to uncoupling of DNA-replication and cell cleavage

To analyze the dynamics of polyspermy from, gamete fusion to later cleavages, I use fluorescent histone 1 (H1) to stain pro-nuclei before the first cell division. I imaged zygote formation and development *in* Egfra $^{-/-}$ female derived oocytes that were previously injected with H1 coupled to TexasRed under a confocal microscope as fast as possible ofter fertilization. Figure 28 shows several frames of two movies of a fertilized WT oocyte compared to a polyspermic Egfra$^{-/-}$ oocyte. The videos cover a time of about six hours in which the WT zygote manages to reach the 32-cell stage. The time frames shown in figure 28 represent the last moment in each cycle in which most condensed metaphase nuclei can be seen before chromosomes segregate and cells re-enter S-phase and lose H1-TexasRed signal.

The first frame (0:00) shows localization of male and female pronuclei at the beginning of recorded period (approximately 40 mpf, on ice); in the Egfr$^{-/-}$ oocyte at least nine male pronuclei can be distinguished. The second frame shows fused pro-nuclei in metaphase before the first mitotic chromosome segregation. In mutant oocytes, most male pronuclei form aggregates with the female pronucleus. After the first chromosomal segregation and cell division, one large DNA-aggregate and two independent nuclei appear. The two separate nuclei keep dividing normally but the

chromatin aggregate, formed by excess chromatin, replicates and is segregated incompletely. This is likely because the presence of several centrosomes brought along with each sperm and the formation of several sperm asters (Snook, Hosken, and Karr 2011).

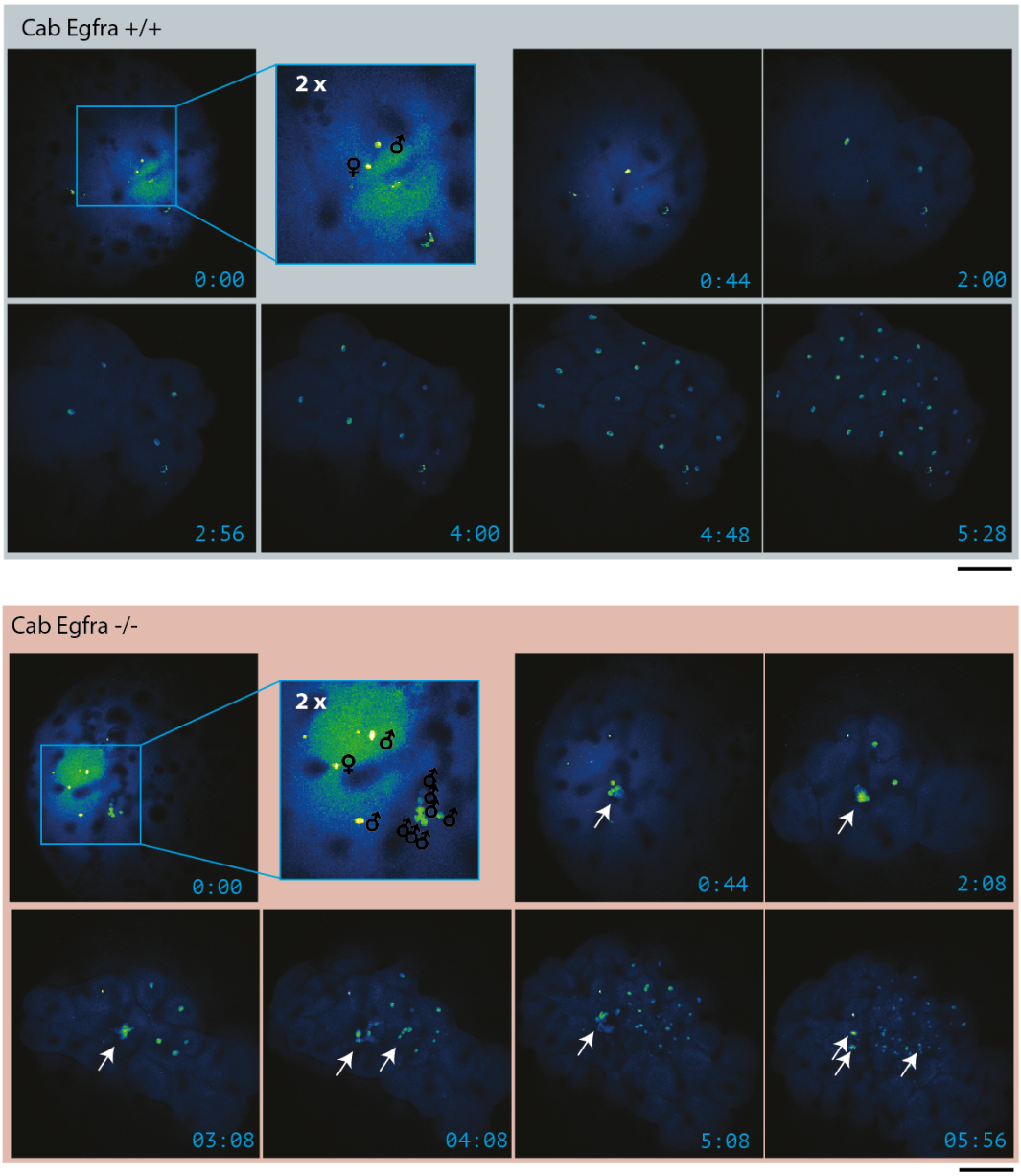

Figure 28: Time-lapse imaging of chromatin dynamics in early Egfra WT and homozygous Egfra mutant embryos reveal polyspermy as the cause for defective first cleavages. One-cell stage embryos were injected with H1-Texas red early after fertilization and imaged from about 40 mpf to 6hpf. Frames were chosen at time points of the highest number of metaphase nuclei. In Egfra WT-derived embryos male and female nuclei could be distinguished (frame 00:00) based on size and behavior. Egfra -/- derived embryos clearly have multiple male nuclei that aggregate, aggregates are highlighted by white arrows. Images are false colored, and the scale bar is 200 µm. mpf=minutes post fertilization.

Blastomeric cleavage seems to happen independently from proper chromatin segregation leading to the formation of multiple incompletely and non-nucleated subdivisions. The independence of blastomeric cleavage from DNA replication has been described before by Dekens et al. in the Zebrafish *futile cycle* (*fue)* mutant where cells cleave in the normal stereotypic way even though they are anucleate due to a chromosome segregation defects (Dekens et al. 2003). In the Egfra-/- these cleavages are not stereotypic probably due to microtubule organizing centers created around excess centrosomes.

Incompletely separated chromatin re-aggregates after each replication (Egfra$^{-/-}$, frame 2:08 and 3:08). The observed phenotype of Egfra$^{-/-}$ derived oocytes, and their failure to properly gastrulate is solely due to polyspermy since mutant embryos that are fertilized by only one sperm develop normally. In teleost oocytes, polyspermy does not occur naturally and cannot be compensated in most cases. Different cases of pathological polyspermy have been described, and species differ in how male and female nuclei interact. In sea urchin, two or more pronuclei can fuse with the female pronucleus while other male pronuclei do not interact. The multinuclear fusion leads to the occurrence of multipolar spindles and chromatin fragmentation (Laubichler and Davidson 2008). In Xenopus, all sperms that enter the oocyte form bipolar spindles and the number of cleavages corresponds to the number of sperm pronuclei (Snook, Hosken, and Karr 2011; E. B. Wilson 1897). Xenopus, sea urchin and also fish are thus unable to deal with excess centrosomes independent of how many male pronuclei fuse with the egg pronucleus.

In some species, as birds and newts, polyspermy occurs naturally and is necessary for proper oocyte activation and development of the oocyte (Snook, Hosken, and Karr 2011). In physiological polyspermy only one bipolar spindle forms around the egg pronucleus and one male pronucleus, the rest of the male pronuclei degenerate. In many bird species, it is necessary for proper karyogenesis that many sperms enter the egg. (Elinson and R P 1986; Rothschild 1954; Tarin and Cano 2000). For several species, it was reported that multiple sperms fertilize otherwise monospermic oocytes without having any adverse developmental effects (Rothschild 1954), this type of polyspermy is described as ‘compensable' polyspermy by Snook et al. (Snook, Hosken, and Karr 2011). Compensable polyspermy was observed in multiple taxa as insects,

newts and salamanders, reptiles, birds and cartilaginous fishes in all of these cases yolky eggs are externally fertilized, and no fast block of polyspermy exists.

3.3.4 Embryos have a rescue strategy for polyspermy

In Medaka polyspermy is pathogenic and in most cases leads to failure of gastrulation. While in other species polyspermy leads to developmental arrest when midblastula stage is reached Egfra$^{-/-}$ derived embryos develop until gastrulation in most cases and sometimes even manage to regain the normal developmental program and survive. Figure 29 shows a time-lapse series of pictures of three embryos collected from the same Egfra$^{12bpDEL/GFPins}$ female.

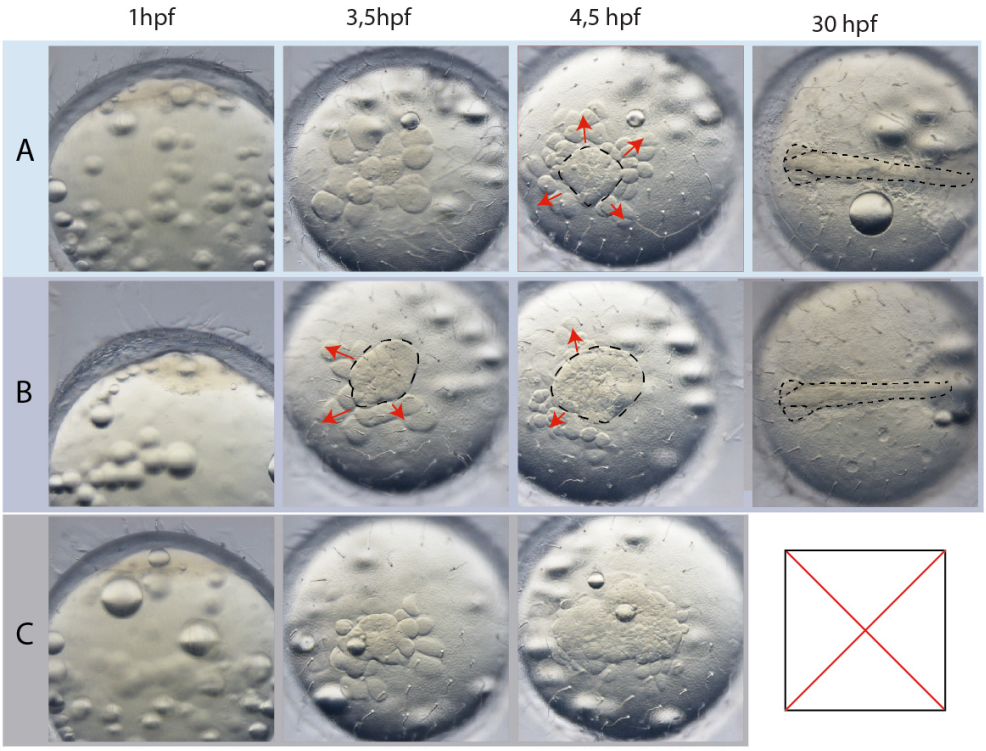

Figure 29: Survivors of polyspermy induced early cell division defect. Three examples of Egfra$^{12bpDEL/GFPins}$ derived zygotes with early cleavage defect due to polysemy. Polyspermic embryo A and B survived and formed viable embryos despite polyspermy. Embryos were followed for 30 hpf when embryos reach St 21, which is comparable to WT embryos.

In all three cases, one hpf embryos look similar to WT embryos of the same age. At 3,5 hpf (32-cell stage) all three zygotes had atypical cleavage patterns. Example A had approximately 15 large cells; Example B shows some separation between cells dividing in a contained space (dashed line) and cells that begin to migrate away from the animal pole. At 4,5 h the zygote A also showed a contained area which looked comparable to a WT embryo at stage 7-8 (32-64 cells) (Iwamatsu 2004). In embryo C

a comparably bigger area of the oocyte surface is covered by cells, and fewer cells are excluded from the conglomerate, suggesting that after 4,5 hpf the zygote is unable to form the dome-shaped blastoderm in early morula stages which typically comprises of three layers (Iwamatsu 2004). Embryo C finally failed to gastrulate and died at 30 hpf.

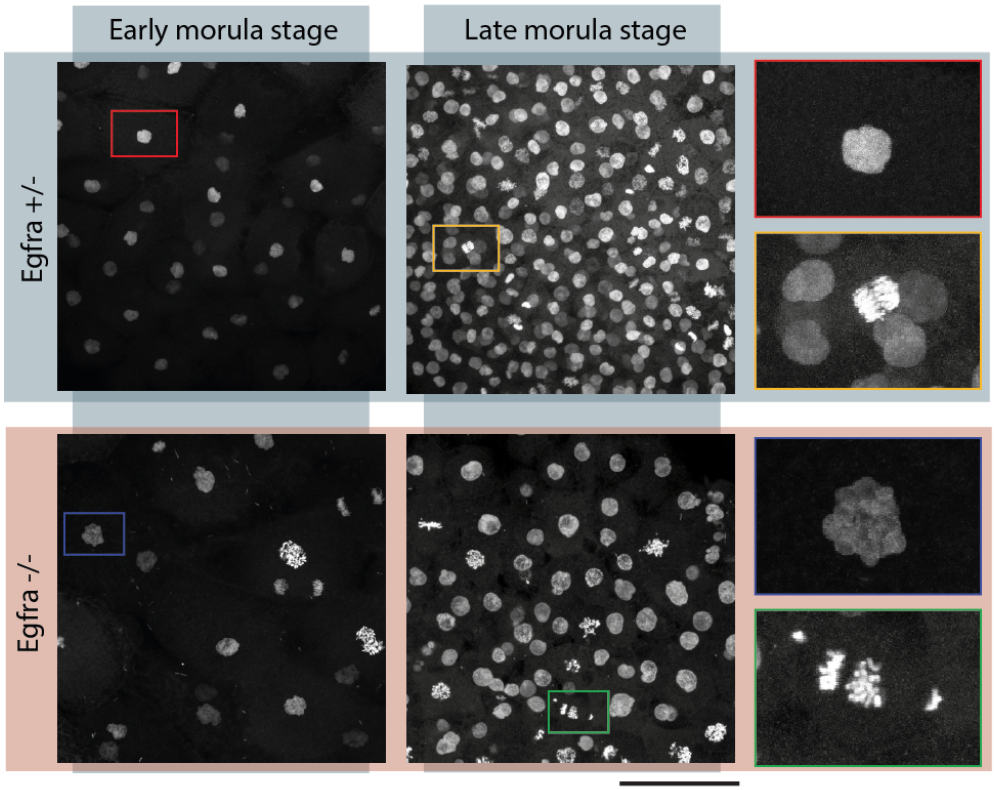

Figure 30: Appearance of chromatin in Egfra +/- and -/- embryos in early (stage 8) and late (stage 9) morula stage. Single nuclei are enlarged and depicted in colored frames. WT nuclei in stage 8 are mostly synchronous (here prophase) while in Stage 9 cells become increasingly asynchronous and chromatin can be found in different cell cycle stages (here anaphase along with prometaphase nuclei, yellow frame). In Egfra -/- embryos, cells divide asynchronously, and nuclei are mostly odd shaped due to aneuploidy (blue frame). Spindle separation is often imperfect with chromosomes leaking behind (green frame). Scale bar is 100 µm, color framed pictures are four times enlarged.

The described findings indicate that early *O.latipes* embryos have the ability to survive supernumerary pronuclei in rare cases. In polyspermic shark embryos (compensable polyspermy) supernumerary male nuclei undergo mitotic divisions synchronously with the synkaryon (fused male and female pronuclei) derived from one male and one female (the same can be observed here, figure 28). Supposable cells from the synkaryon occupy the central part of the germinal disc and push the supernumerary sperm containing cells to the periphery. The male pronuclei even display superficial cleavage sites (Ginzburg 1968). Similar mechanisms seem to operate in example A

and B indicating that in some circumstances polyspermic embryos manage to rescue themselves if the synkaryon derived cells manage to displace supernumerary pronuclei.

To obtain insights into the reactions of embryos to an abnormal DNA content I performed DAPI stainings of Egfra $^{-/-}$ and WT embryos in early and late morula stage (figure 30). In the early morula stages of WT embryos, the cell cycle is still synchronized, and all nuclei can be found in a similar stage of cell cycle. In Egfra$^{-/-}$ embryos nuclei with abnormal shapes can be seen (figure 30, blue frame), and the cells cycle asynchronously (condensed metaphase and decondensed S-phase chromosomes). Furthermore, most polyspermic embryos did not manage to separate male pronuclei from the synkaryon and become aneupleudic (chromatin aggregated, blue frame). In late morula stage WT cells start to cycle increasingly asynchronous, nuclei show typical rounded shapes and mitotic figures are symmetric (figure 30, yellow frame). Metaphase chromosomes of Egfra$^{-/-}$ embryos often look abnormal and fail to segregate (figure 30, green frame) which leads to less but bigger, uneven shaped nuclei with high chromatin content when compared to a WT embryo of the same stage. Interestingly, cells continue to divide even after midblastula transition, and the zygote manages to develop into a mostly irregular cell mass and in most cases only fails at gastrulation stage and dies (figure 26).

To check for the presence and appearance of metaphase chromatin and mitotic spindles, we (together with Daigo Inoue) performed phospho-Histone 3 (pH3) and α-tubulin and stainings of embryos at four hpf. The results revealed additional abnormalities in polyspermic Egfra$^{-/-}$ embryos demonstrated in three examples in figure 31 (B-D).

In heterozygous Egfra mutant as in WT embryos, all spindles, visualized by α-tubulin staining, are symmetric and always exist in two fold (fig. 31.A''). Metaphase chromosomes as revealed by pH3 staining are always located along a line between two spindles (dashed line in A'''). In Egfra$^{-/-}$ embryos division defects resulting from the presence of multiple spindles becomes apparent. Differently shaped chromosomal aggregates stain positive for the metaphase marker pH3 (B'') and are connected to at least two, but often more, spindles. The large chromatin aggregates are clear indications for aneuploidy (B'), which is a standard feature in polyspermic embryos

resembling phenotypes that can be found in cancer cells (Snook, Hosken, and Karr 2011).

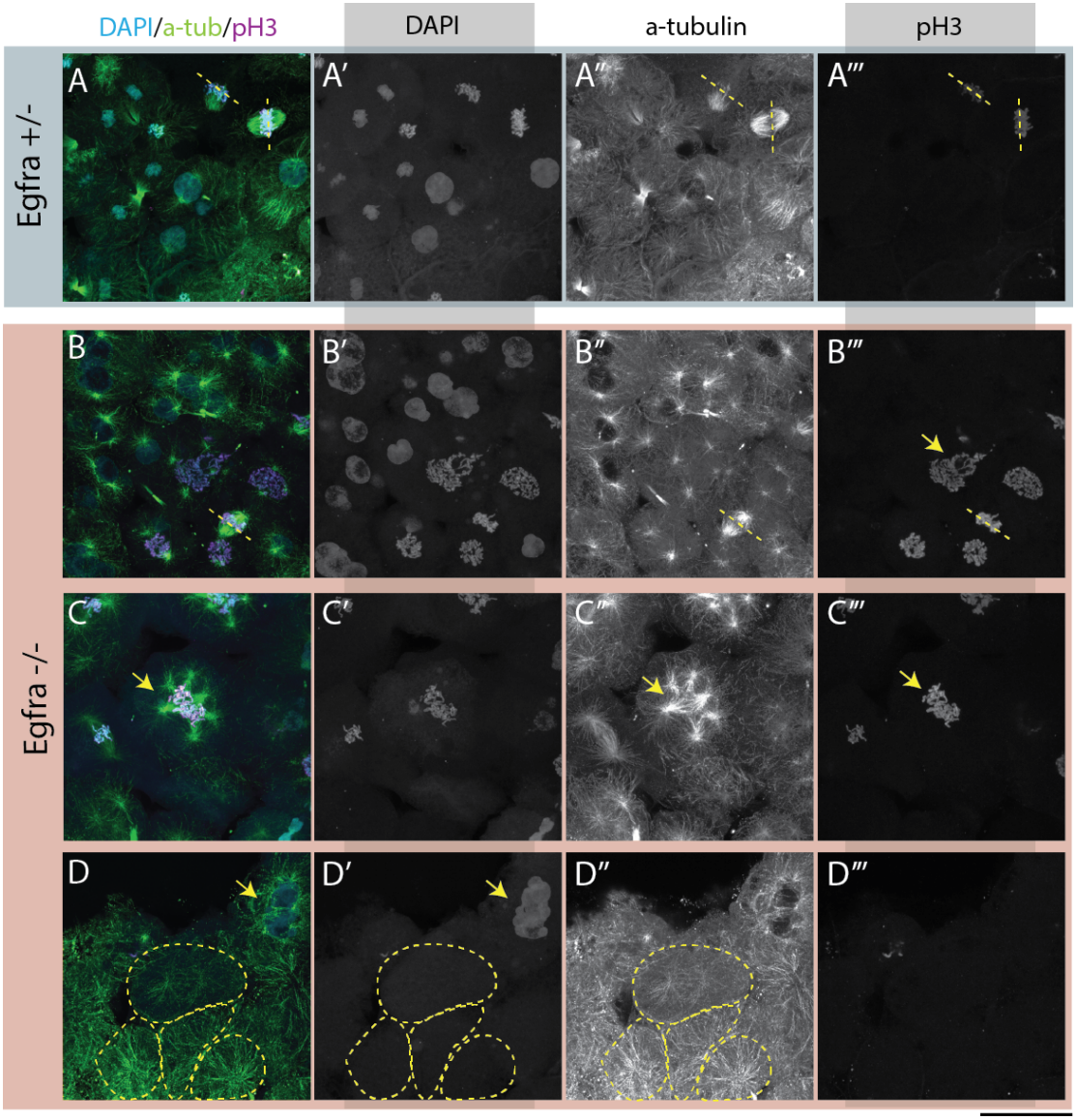

Figure 31: Phenotypes of early cell cleavage and cell division in polyspermy embryos (offspring Egfra -/-) in comparison with heterozygous embryos (Egfra +/-). Embryos were fixed four hpf and stained for a-tubulin (green), phosphorylated H3 (magenta) and DAPI (cyan). A. In normally fertilized embryos, metaphase chromosomes (division plain indicated by dashed line in A''') are always pulled by two spindles and chromosomes are divided evenly (A'') with each cleavage. B-D. Examples of unusual events caused by abnormal chromosome content of polyspermy embryos derived from Egfra -/- females. B. Mitotic figures (pH3 associated chromatin) have irregular shapes (arrow B'''), and chromatin is divided unequally between cells. C. Up to six spindles (C'', arrow) were found to be associated with one metaphase (C''') chromatin aggregate (arrow in C'''). D. Cell division (cleavage) can take place independently of DNA replication. Some blastomeres defined by tubulin distribution (approximate location of cell borders marked by dashed lines) (D'') lack chromosome content, large chromatin aggregates appear (D', arrow). Scale bar is 50 µm.

In one extreme example, we saw up to six spindles pulling on one chromosomal set (C'') that fails to organize itself properly along one axis (C'''). Even chromosomes only pulled by two spindles often fail to organize themselves along the equatorial axis

between spindles (figure B, arrow in B'''). Furthermore, polyspermic *O.latipes* embryos have the ability to cleave and form newly separated cell space, independent of DNA replication (fig. 31D), which I observed in the live imaging as well (figure 28).
No cases of naturally occurring polyspermy in teleost species have been reported so far thus the polyspermic block, which in fish is mainly mediated by the egg shell works very efficient. The only describe cases of polyspermy in teleosts are described for denuded eggs of various species (Ginzburg 1968; Sakai 1961).

3.3.5 Polyspermy in Egfra$^{-/-}$ embryos is due to multiple and abnormal shaped micropyles

Polyspermy in teleost fish is prevented by a mechanical blockage of sperm entry through the protective eggshell (chorion) (Ginzburg 1968; Murata 2003). In this chorion only one point of sperm entry, the micropyle (MP), is present.
In Egfra heterozygous and WT embryos only a single MP channel was found (figure 32A). The chorions of Egfra$^{12bpDEL/GFPins}$ and Egfra$^{GFPins/GFPins}$ female derived zygotes displayed multiple MP channels (indicated by violet asterisks in fig. 32A). The Egfr$^{-/-}$ MPs are distributed around the animal pole of the chorion, which can be identified as the site opposite of the long attaching filaments on the vegetal pole of the egg. Besides the multiple MPs and the more "curly" filaments around the MP area the chorion of Egfra$^{-/-}$ mutants look normal.
The shape of the micropyle is essential for the described way of polyspermy block in Medaka. WT MPs always displayed a characteristic funnel shape, becoming narrower from the surface towards the oocyte (Iwamatsu et al. 1991; Nakashima, S; Iwamatsu 1989) (Fig. A, lower picture). In Egfra $^{-/-}$ mutants the micropyles are often odd-shaped and do not have the characteristic funnel shape of WT MPs (fig. 32A, lower picture). Mutant micropyles display straight channel walls probably allowing access to multiple sperms.
Egfra$^{12bpDEL/GFPins}$ mutants had a broader range of MP numbers compared to Egfra$^{GFPins/GFPins}$ mutants and in average have more MPs per oocyte even though Egfra$^{GFPins/GFPins}$ oocytes in average have more pronuclei after fertilization (Figure 32 B). The variance of MP numbers in Egfra$^{12bpDEL/GFPins}$ oocytes is bigger, indicating a less predictable outcome in which sometimes only very few MPs are found accounting for

the percentage of monospermic fertilizations. Monospermy was never observed in Egfra$^{GFPins/GFPins}$ derived oocytes. The higher number of MPs in Egfra$^{12bpDEL/GFPins}$ oocytes might be related to the age of the females, which were bigger and older at times of oocyte collection. The MP numbers of both Egfra mutant genotypes together with the data acquired for survival rates of offspring imply that there is some residual function of the Egfra12bpDEL variant which leads to a broader range of phenotypes.

In the following, I also correlated the number of MPs and pro-nuclei by counting both in the same embryo (Egfra$^{12bpDEL/GFPins}$ and Egfra$^{GFPins/GFPins}$ taken together). No direct correlation could be identified (R^2=0.064) between the two factors as shown in figure 32 panel C, indicating that besides the number of MPs also the shape of the channels contributes to the failure of the polyspermy block in Egfra mutant oocytes.

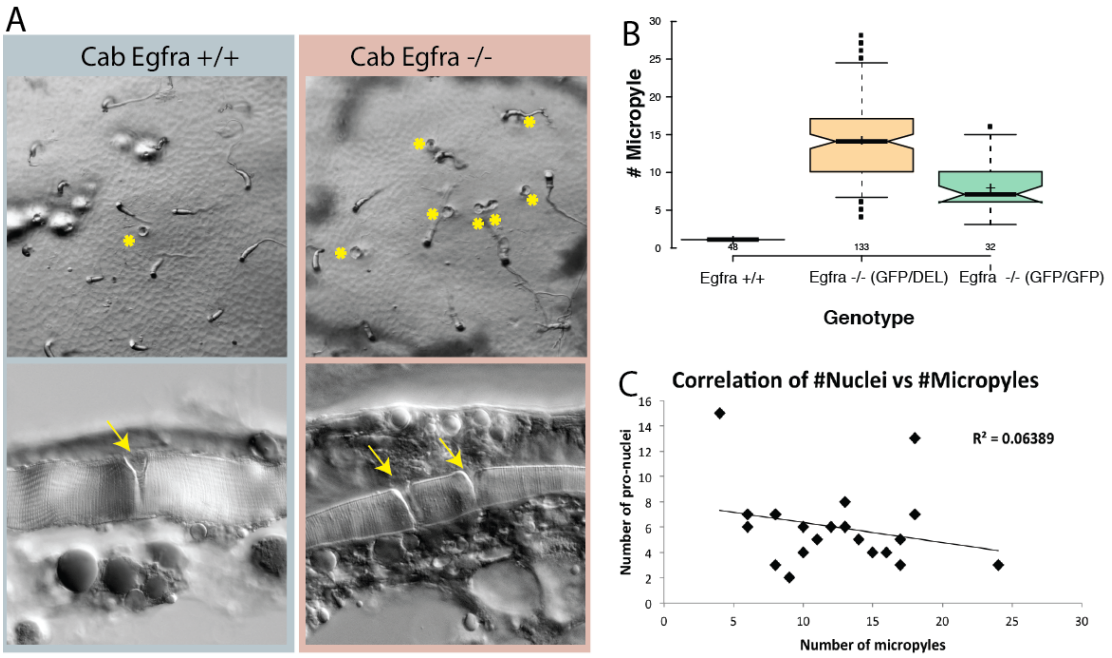

Figure 32: Egfra mutant females produce oocytes with multiple micropylar channels. A. The surface of a Cab and an Egfra-mutant chorion. Egfra $^{-/-}$ derived oocytes have many MPs at the animal pole of the oocytes. MP are marked by asterisks. Micropyles in mature oocytes (yellow arrows) differ in number and shape. B. Box plot for numbers of MP channels found in Egfra mutants. Only one MP channel was present in 48 observed Cab oocytes. Egfra mutants always had many MPs with an average of 15 MPs for Egfra$^{GFPins/12bpDEL}$ and 8 for Egfra$^{GFPins/GFPins}$ genotype. C. No correlation could exist between the number of micropyles and the number of male pronuclei in Egfra mutants (R=0,064).

The occurrence of multiple micropyles was so far not described for teleost; they typically have one micropyle. In acipenserid fish (primitive sturgeon species), which are not considered teleosts, the occurrence of multiple micropyles was described and visualized by electron microscopy (Clark 1982). The perforation of the white sturgeon complex egg-envelop by multiple channels (around 10) is thought to increase the

probability of fertilization in spawning grounds of low sperm density (Clark 1982; Ginsburg 1961). It is possible that the block to polyspermy that consists of the blocking of MP channels with vitelline fluid to generate a fertilization cone takes place faster in sturgeon eggs. Since fertilization in Medaka takes place very localized with high sperm density, the existence of multiple MPs inevitably leads to polyspermy.

3.3.6 Egfrs and ligand expression in mature ovaries

Egfrs are key players of interaction between the follicle cells and the oocytes(FregosoLomas et al. 2013; Hsieh, Thao, and Conti 2011; Jamnongjit, Gill, and Hammes 2005; Park 2004). The before mentioned results show that in Medaka, the Egfra is important in guaranteeing that only one MP is formed through which the sperm can penetrate the mature oocyte. To gain insights into the role of Egfr-signaling and expression of both receptors in the oocytes, we (with the help of Narges Aghaallaei) performed in situ hybridization (ISH) on sections of adult ovaries. Figure 33 shows the expression of *egfra* and *b* (fig 33A) as well as of three Egfr ligands: *egf*, *hb-egf*, and *tgf-a* at different stages of oogenesis as well is an example of a vitellogenic oocyte (150-300 μm). Due to the enormous size of the gametes compared to surrounding follicle cells and the signal that becomes trapped in the hairs surrounding the vitellogenic oocytes, expression profiles are hard to interpret. Also, no difference between expression in granulosa and follicular cell layer can be seen because of lack of resolution.

Egfra and *egfrb* are expressed in previtellogenic oocytes as well as in follicle cells around vitellogenic oocytes. At least *egfra* appears to be expressed to a higher extend in follicle cells at the animal pole. The egfr ligand *egf* and *tgf-a* are expressed in some previtellogenic and *egf* also in vitellogenic oocytes of medium size. *Hb-egf* seems to be transcribed in some cells of the follicles are interspersed support tissue as well as in the epithelial layer surrounding the ovary.

Egfrs, as well as the ligands *tgf-a* and *egf*, are also present in the ovaries of birds and mammals (Fukumatsu, Katabuchi, and Okamura 1995; Göritz, Jewgenowyer, and Meyer 1996; Maruo et al. 1993; Scurry et al. 1994). Both cell types of the follicle layer, granulosa, and thecal cells express *tgf-a* (Kudlow et al. 1987; Yeh, Lee, and Aanderson 1993) and the production of this ligand is stimulated by FSH (Kudlow et al. 1987).

Egf has an activating effect on oocyte maturation in mammals (Brucker et al. 1991; S Coskun and Lin 1995; Serdar Coskun and Lin 1994; Dekel and Sherizly 1985) and Zebrafish and Goldfish in which Tgf-a has the same effect (Pang and Ge 2002; Pati et al. 1996). Although follicle cells have been identified as the most probable site for egf activity (Procházka et al. 2000), it might also act directly on the oocytes since it was shown that it also exerts and effect on denuded bovine oocytes (Lonergan et al. 1996).

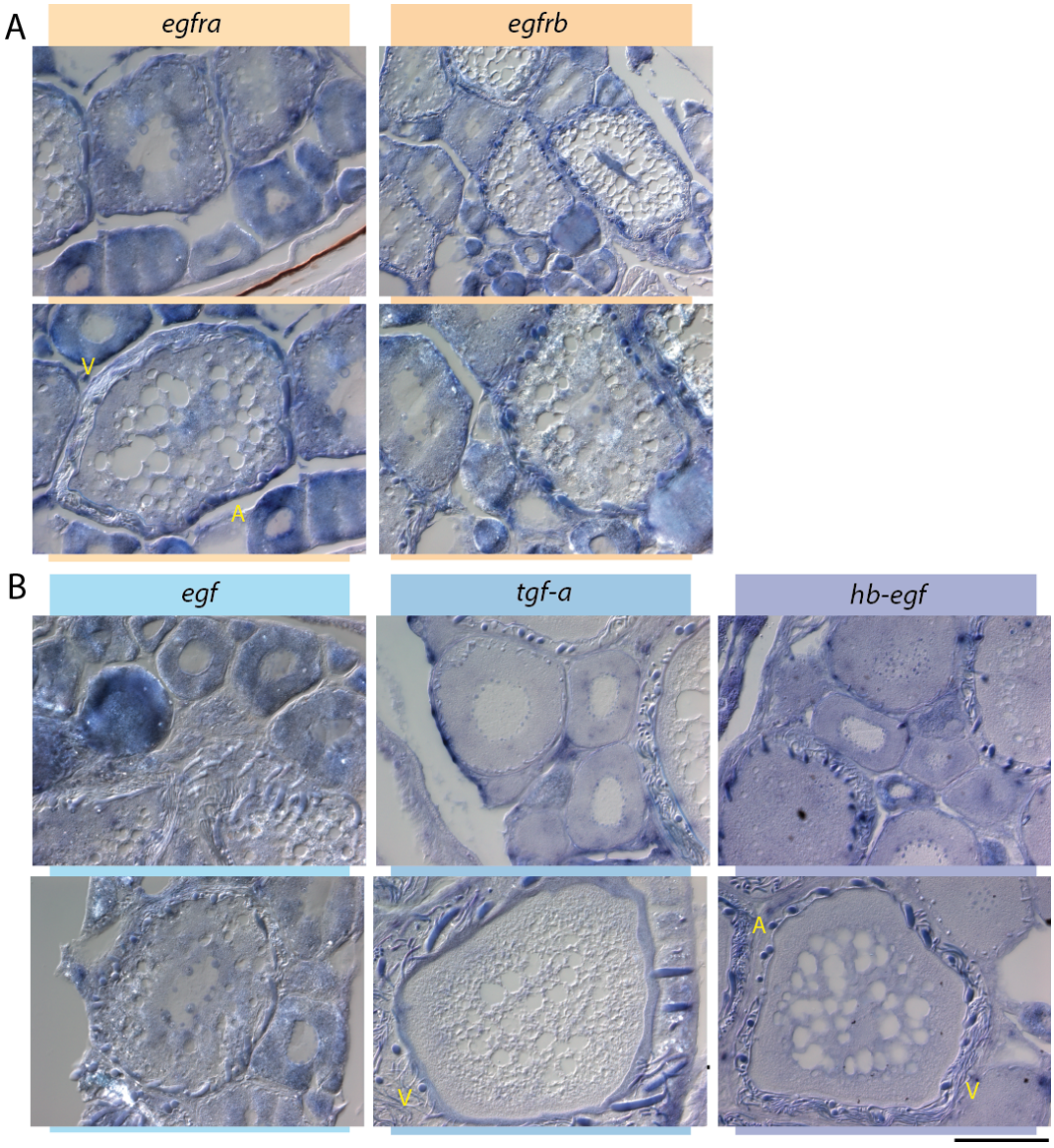

Figure 33: Expression pattern of *egfra* and *egfrb*, egfr ligands *egf*, *hb-egf*, and *tgf-a* in adult ovaries. Two pictures are displayed for each staining; one is showing different stages of previtellogenic oocytes (no filaments and no yolk vesicles) and the other displaying a vitellogenic oocyte (surrounded by chorion with attached filaments) in which a follicular layer can be distinguished. Filaments stain with trapped signal. Both Egfrs are expressed in previtellogenic oocytes and follicle cells surrounding vitellogenic oocytes. Expression patterns of ligands are difficult to discern. *Hb-egf* and *tgf-a* seem to be expressed by single follicular cells and epithelial lining of the ovary as well as in individual previtellogenic oocytes as is egf. If identifiable the vegetal pole of vitellogenic oocytes is marked with V and the animal pole with A. Scale bar is 100 µm.

There is plenty of egfr-dependent crosstalk between follicles and oocytes reported in various species (Park 2004; Pati et al. 1996; Wayne et al. 2007). The formation of a micropyle is an essential step in oocyte maturation in the teleost, and it is therefore not surprising that Egfr-signaling functions in the communication of the granulosa cell layer with the oocyte about the existence of one channel. Since all steps of oogenesis except for the formation of the micropyle seem to be normal in Egfra$^{-/-}$the only defect lies in the induction of several granulosa cells to differentiate into micropyle cells (MCs) in which signaling through Egfra appears to be specific. The ISH studies of WT ovaries shows that both receptors are expressed in the ovary in primary oocytes and the follicle layer and might be redundant for most of their functions.

3.3.7 Activity of Ras/MAPK/Erk pathways in WT and Egfra mutant ovaries

As previously described the MP is formed by a single granulosa cell (GC) that gradually adapts a particular cell shape and forms a channel by pushing of microtubule and tonofilament bundles through the chorion towards the oocyte. The micropylar cell (MC) loses contact to surrounding GCs and stays connected to the oocyte to the moment of follicular rupture (Nakashima, S; Iwamatsu 1989). I first addressed the question if the multiple MPs observed in Egfra $^{-/-}$oocytes are due to the occurrence of multiple MC or to the fact that one MC forms several channels. For this, I stained whole mount or sectioned ovaries of adult reproducing Egfra WT and mutant females for DAPI, α-tubulin and phospho- p42/44 Erk (pErk) (figure 34). Although the Erk/MAPK signaling pathways are widely used by other growth related receptors (e.g. the IGF-receptors) the comparison between WT and Egfra mutant allowed to narrow down the site of egfr-signaling deregulation.

Active pErk was detected in primary oocytes of WT and Egfra $^{-/-}$, in levels decreasing with oocyte growth, and in GC directly adjacent to the MC. In mutant oocytes, multiple MCs are among the GCs around the animal pole of vitellogenic mutant oocytes all of which are surrounded by pErk-positive GCs (figure 34 A, B, D & E).

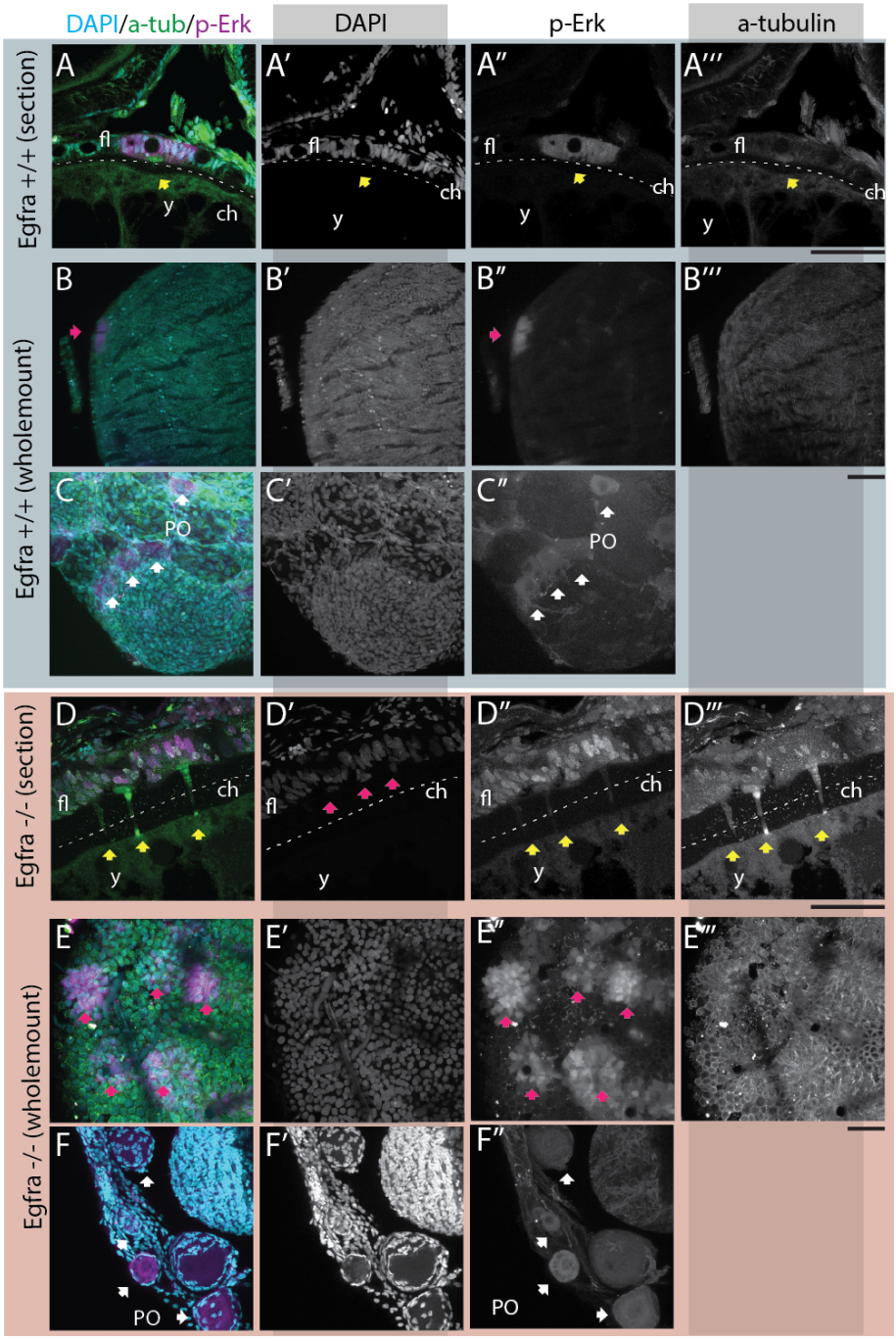

Figure 34: Active Erk signaling in WT and Egfra$^{-/-}$ovaries. A-C WT ovaries: A. Section of the MP region of a vitellogenic WT oocyte. A yellow arrow indicates the location of the micropylar channel where it meets the oocyte cytoplasm. Follicular cells immediately adjacent to the micropylar cell are positive for phospho-Erk (p-Erk) (A''). B. Whole mount staining of a vitellogenic WT oocyte with a region of cells positive for p-Erk on the animal pole (B''). C. Oocytes of different stages, primary oocytes stain positive for p-Erk (white arrows). D-F Egfra$^{-/-}$ ovaries: D. Section through an MP region of an Egfra $^{-/-}$ oocyte. Multiple MP channels, deriving from different MC in a thickened part of the chorion (dashed line), can be distinguished by a tubulin staining (D'''). Nuclei of micropylar cells are located below nuclei of the follicular layer (D', indicated by red arrows). Follicular cells are surrounding the MP region stain positive for pErk (D''). E. Whole mount staining of the follicular layer at the animal pole of a vitellogenic oocyte. Multiple pErk-positive areas can be distinguished (red errors in E & E'') around the MPs (holes in y-tub staining E'''). F. PO in Egfra$^{-/-}$ stain positive for pErk (white arrows). Scale bar is 50 µm. Ch=Chorion, fl=follicular layer, y=yolk, PO= primary oocyte.

An example of an MP region in WT (MP marked by yellow arrows) and $Egfra^{GFPins/GFPins}$ mutant can be seen in figure 34. In the chosen section plane of the Egfra mutant oocyte, three MP channels are visible in the a-tubulin channel (D'''), all three nuclei can be distinguished from the GC nuclei and are marked with red arrows in the DAPI channel (D'). The MC nucleus can be distinguished from nuclei of surrounding GCs by its flat shape. GC nuclei usually have nuclei that are elongated on the axis perpendicular to the oocyte (see in figure 34, D'). The MC is considerably bigger than other GCs, judging from the space that is formed around the MP nucleus. Around the MC, GC nuclei appear less elongated, and the whole MP area is protruding (fig. 34A). In the $Egfra^{12bpDEL/GFPins}$ oocytes the granulosa layer is more disorganized in the MP region (fig 34D). In whole mount stainings, it becomes evident that each MC forms a focus point around which pErk-positive GCs and microtubules organize (E''').

These results indicate that Ras/Mapk/Erk signaling is not active in the MC itself since it never stains positive for pErk. So far nothing has been reported about the mechanisms through which a GCs differentiates into an MC and how this is maintained. Whether the differentiation of a single GC into an MC is a result of the localized upregulation of pErk or if the cells around the MC upregulate Erk signaling as a response to the MC still needs to be elucidated. However, there seems to be more to a micropyle than a single cell.

Egfra mutant embryos apparently fail to signal the animal pole surrounding GC that an MC has successfully formed an MP and that no more are needed. Instead, more than one MC differentiates. Cells in the MP domain appear very disorganized whenever many MPs are present within close proximity as depicted in figure 35B'.

Figure 35 shows false colored sections of micropylar and non-MP regions of WT (fig.35A) and Egfra mutant (fig.35B) oocytes. Nuclei positive for pERK are colored violet in the DAPI channel, and the nucleus of the MC is colored yellow. No difference can be seen in the appearance of GCs (gray) and follicle cells (green) in any other region of the oocytes of WT and Egfra mutant oocytes. pErk-positive nuclei around the MC are organized to fit around the MC. In the broad pErk-positive "mutipyle" region of Egfra mutant oocytes, granulosa and follicular layer are thickened (B') and nuclei have a rounder shape. If an MC in an Egfra-/- follicle is not

near another MC (Fig.35B''), the surrounding GC layer looks comparable to WT. Follicle irregularities originate thus from the presence of densely placed MCs that have difficulties to gather supporting pErk-positive granulosa cells and therefore hinder themselves which could cause the occurrence of odd-shaped MP channels in Egfra$^{-/-}$ mutants. The Ras/Mapk/Erk was found to be critical for the differentiation of rat granulosa cells and is stimulated by FSH in Egfr dependent manner (Buratini and Caixeta 2012; Wayne et al. 2007).

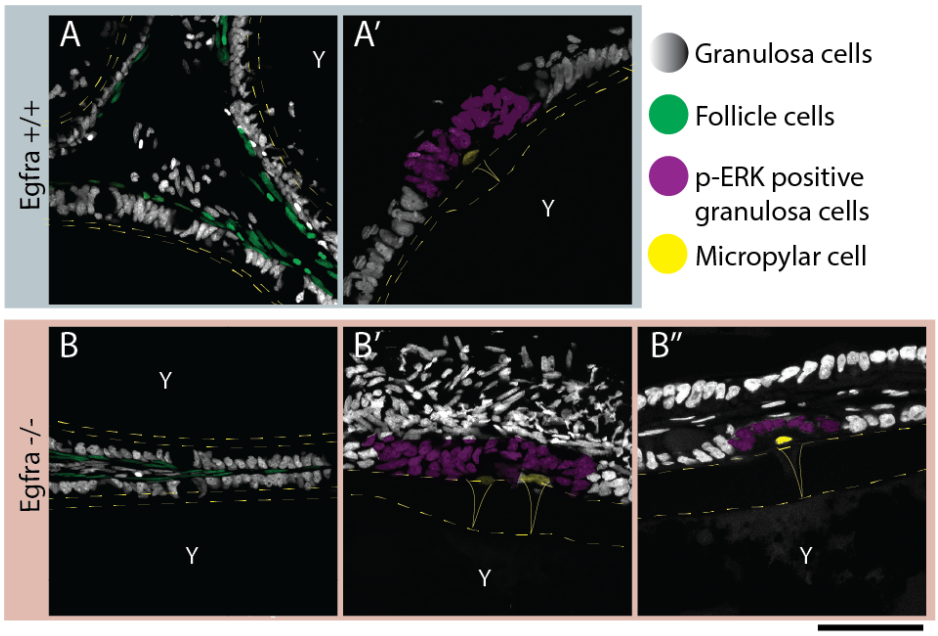

Figure 35: The appearance of the follicular layer outside of the micropyle region is indistinguishable between WT and Egfra mutant oocytes. False-colored images of sections of WT and Egfra mutant ovaries stained for p-Erk. A. Appearance nuclei of the follicular layer around chorions (dashed lines) of different oocytes at non-micropylar (A) and micropylar region (A'). Oocytes are surrounded by the granulosa layer (gray nuclei) and a follicular layer (green flattened nuclei). Nuclei of cells positively stained for pErk are indicated in purple and appear elongated. The nuclei of micropylar cells are colored in green. B. On the vegetal side Egfra-/- follicles are indistinguishable from WT follicles. In the animal region several micropylar cells can be found (B') and surrounding granulosa cells form a cluster of pErk-positive cells B.' The thickness of the chorion varies between non-micropylar and micropylar region. Whenever there is only one micropylar cell present, the follicular layer appears indistinguishable from the WT follicle. Scale bar is 50 µm. Y=yolk.

The only other reported case of multiple micropyles in teleosts is the Zebrafish mutant bucky ball (*buc*). Buc is essential for the assembly of the balbiani body and the localization of animal and vegetal transcripts in primary oocytes. The failure to establish the animal-vegetal axis in *buc* mutants also leads to the formation of micropyles all around the chorion (Marlow and Mullins 2008). In the Egfra mutant, however, all micropyles are concentrated around the animal pole, and the animal-vegetal axis is not disturbed. In mammals, follicle formation is initially similar to

teleosts, but then follicle cells divide faster to form multiple follicular layers. In the secondary follicle (antral follicle) an asymmetric cavity forms and upon oocyte-derived stimuli, a distinct population of follicle cells is generated, the mural and cumulus cells (Diaz, Wigglesworth, and Eppig 2007; Eppig 2001). It remains to be determined if there is any relationship between differentiation of the MP cell in teleosts and the formation of the granulosa cell types in the antral cavity of mammals. With Egfra we identified another important player in the crosstalk between follicle and oocytes that lead to the differentiation of specialized GCs.

4. Conclusion

Fish are an ideal model to study the role of growth factor receptors since they increase in size throughout their lives and develop externally. The characterization of Egfr signaling in the CNS of Medaka embryos and hatchlings showed that both Egfrs are expressed overlapping. The difference between stem cell zones of the retina and the brain lies in the expression of different ligands. Especially Egf is strongly upregulated only in the SVZ of fish but not of mammals (Novak, Walker, and Kaye 2001) (Vaughn et al. 1991) and might form a gradient to regulate proliferation of NSCs and their progenitors.

Only very few studies address Egfr-signaling in the teleost, and it is still unclear why fish retained two copies of the receptor (Laisney et al. 2010). The results of the Egfra knockout indicate that most functions of Egfra can be rescued by Egfrb. If Egfra can compensate the loss of Egfrb needs to be shown by another KO line which is being generated at the moment. The injection of sgRNAs against Egfrb did not cause lethality in the injected generation supporting the hypothesis of a general redundancy of the receptors. If the loss of one receptor leads to the upregulation of the other can be demonstrated by WISH on mutant embryos.

The specification of a single micropyle at the animal pole of oocytes seems to be the only function that cannot be rescued by Egfrb. We identified a connection of Egfr signaling with the MC by showing Ras/MAPK/Erk signaling activity in MC surrounding cells at several spots at the animal pole of mutant oocytes. The lack of one Egfra might lead to an over-compensation by Egfrb that fails to restrict the signal to one particular MC. Based on the literature we assume that GCs, as well as the oocytes, express Egfr. To confirm that, more ISH studies are necessary to differentiate the expression between follicular layers and oocyte. Another possibility is that Egfra expressed in follicular cells is required to prevent several GC from differentiating into an MC in response an Egfr ligand send by the oocyte. The oocyte itself could also need Egfrs signaling to sense the presence of the MP. The two Egfrs have a different binding affinity for the ligands (Gómez et al. 2004), and it is possible that the specification of the MC is dependent on the interaction of Egfra with a particular ligand that does not bind Egfrb.

So far this is the only report showing that not only the MC specifies the animal pole of the follicle but also MC-surrounding granulosa cells.

It is probably the oocyte that provides the signal for differentiation of the MC since this process is particular to the animal pole which is specified by the oocyte (Marlow and Mullins 2008), it is thus the oocyte that has to initiate the formation of animal pole specific structures. It would also be interesting to compare the process and the genetics of MC formation between Medaka, as an example of single MP, and the multiple MPs in Sturgeons. The sturgeon micropyles look very similar concerning number and localization (Clark 1982) when compared to the Egfra mutant, but sturgeons have a large polyploid genome that might have even more copies for the egfr.

The single micropyle strategy as a block for polyspermy is so effective that no cases of naturally occurring polyspermy are reported in teleosts (Ginzburg 1968; Snook, Hosken, and Karr 2011) except for the *buc* Zebrafish mutant that fails to develop the animal-vegetal axis (Marlow and Mullins 2008). The Egfra mutant generated in this work provides a new and so far the only genetic model for polyspermy in teleost fish. Using this mutant will allow studying fertilization and zygote formation without disturbing animal development by denuding or injecting fragile unfertilized oocytes. Polyspermic embryos share some characteristic with fast dividing cancer cells as aneuploidy, the presence of multiple centrosomes and fast replication and division cycle. Therefore, the easy-to-image polyspermic embryo can also serve as a disease model to study centrosome and chromatin dynamics in degenerated cells.

In contrast to *Chondrichthyes* (cartilaginous fish) where polyspermy occurs frequently and can be compensated (Ginzburg 1968; Snook, Hosken, and Karr 2011), it is pathogenic in teleosts and zygotes usually die. Here we report several instances in which Medaka zygotes can survive with supernumerary sperm. The way in which this is achieved resembles the mechanism in which shark zygotes dispose of excess male pronuclei (Rothschild 1954). The Egfra$^{-/-}$ mutant is, therefore, interesting to study from an evolutionary point of view. By fertilizing embryos with

By creating the toolbox for the expression of Xmrk, oncogenic K-Ras, and myrAKT in single cells or cell types we observed that cell types react differently to the expression of oncogenes. Xmrk, very potent in stimulating melanomas also caused over-

proliferation of somites but so far did not show a noticeable effect on neural cells. Even though many lines were tested for the ubiquitous expression and induction of oncogenes, it was rare to find oncogene-expressing cells in neural tissues. The shape and growth of the retina in teleost fish is very robust, and the growth of a tumor derived from an adult retina has so far not been observed. For studying the effect of oncogenes in the CMZ, detailed proliferation and apoptosis assays have to be performed. It is probable that RSCs have efficient regulatory mechanisms to avoid excess growth that act early to keep cells with enhanced growth signaling under control. One of the biggest obstacles encountered when creating the oncogene lines was the lack of a defined locus that allows high and ubiquitous expression of oncogenes as the Rosa-26 locus in mice (Zambrowicz et al. 1997). It would thus be of great importance to invest in the identification of this ubiquitously accessible locus in Medaka. This could be done by sequencing of existing ubiquitous lines and subsequent targeting locus by CRISPR/Cas9 approaches. Creating a genetic toolbox with stable expression of different oncogenes would highly improve the application of Medaka as a model for cancer.

5. Appendix

5.1 Transparent QuiH fish are suitable for *in vivo* imaging

One of the major advantages of fish model systems compared to mammalian models is the extra-uterine development that allows following development of embryos from the first cell division on. In later stages of development the appearance of autofluorescent pigments interferes with the imaging of deeper or highly pigmented tissues as the brain or the eye. A possible solution for this problem is the use of pigment-free fish lines. The QuiH fish line has several mutations in pigmentation-related genes (up to seven). The line originates from a cross of the albino line Heino (Loosli et al. 2000) with the Quintet line mentioned in (Kuroyanagi et al. 2010). In line was inbred for at least 15 generations and has some important features. Figure 36 shows bright field pictures of a QuiH larva (A) compared to a WT hatchling at ten dpf. QuiH fish are completely transparent and have no pigmentation and are therefore free of autofluorescence (A''). These features make the line optimal for *in vivo* imaging in fluorescence microscopy.

There is, however, a shiny layer around the eyes that becomes more pronounced with the age of the fish. The intensity of this layer is strongly enhanced when fish are grown in Hatch medium containing methylene blue and can vary between offspring of different females. We (together with Katharina Lust) compared hatchlings of two lines with retinal GFP expression for the feasibility of *in vivo* imaging using a two-photon laser in a Leica SP5 confocal microscope. These lines were: the Fu_mitfb::GFP QuiH line (C) and the Tlx::GFP Cab (C') line. Cab embryos were treated with 5xPTU to suppress pigmentation and observed considerable differences in image quality. In Cab fish, the autofluorescent choroid layer hampered the imaging of a big part of the retina while in QuiH we could discern different retinal layers easily.

The lack of pigmentation and therefore autofluorescence in QuiH fish is not caused by the absence of pigment cells as was shown by injecting a plasmid leading to melanocyte-specific GFP expression (Ol_mitf::GFP) as shown in transient in figure 36D.

When crossing different QuiH females to Cab based WT and transgenic lines, I observed that every once in a while some fish in the F1 lacked pigmentation in the eyes and had reduced auto-fluorescence. Several crosses were set up to fathom this phenomenon, and three successful cases are reported so far.

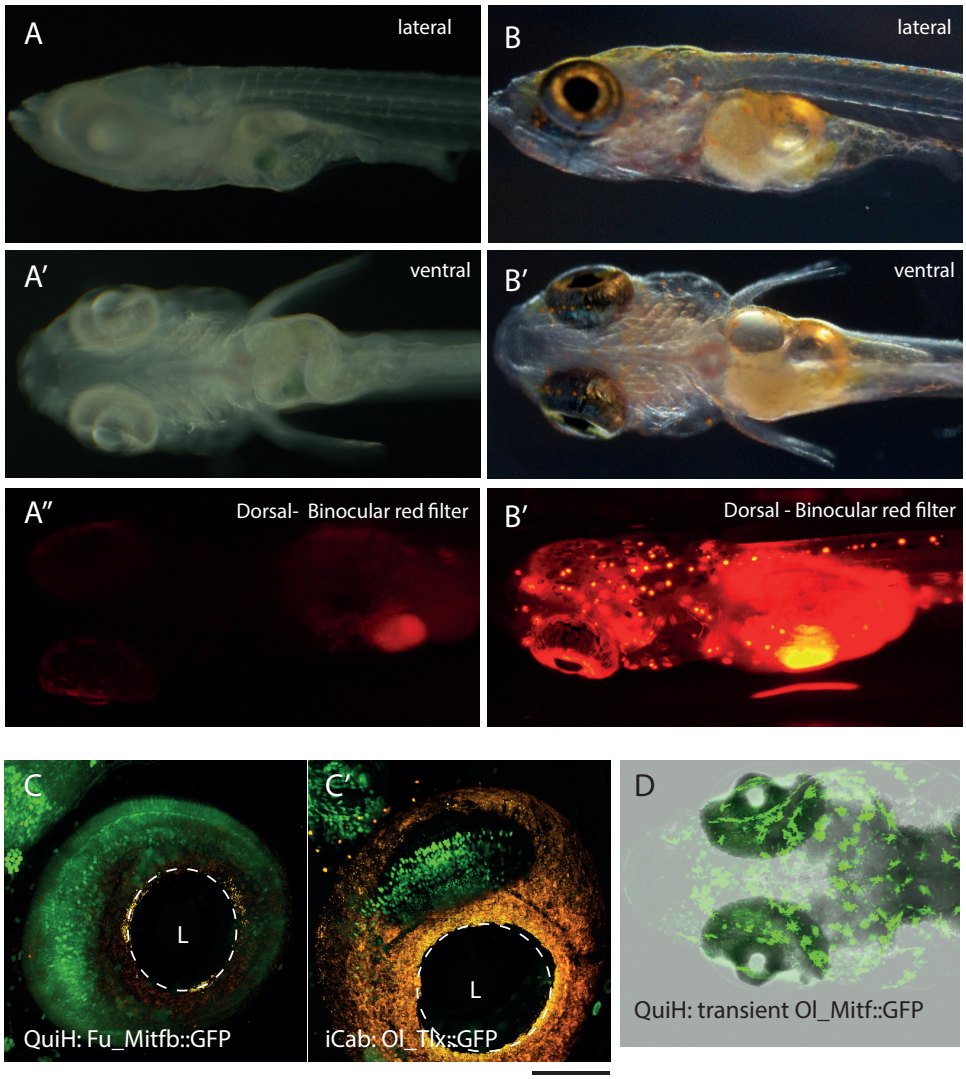

Figure 36: The pigment-free QuiH line allows *in vivo* imaging undisturbed by auto-fluorescence. A. The appearance of QuiH hatchling under a bright field microscope, lateral (A) and ventral (A') view and dorsal view under filtered red light to show auto-fluorescence (A''). B. The appearance of WT hatchling under a bright field microscope, lateral (B) and ventral (B′) view and dorsal view under filtered red light to show auto-fluorescence (A''). C. Comparison of the imaging conditions under confocal imaging of hatchling eyes expressing GFP in the retina. C. QuiH line is expressing GFP under the Fu_Mitfb promoter in neurons. C′. Cab expressing GFP under the tlx promoter in neural proliferative zones. D. Expression of GFP in pigment-free melanocytes in hatchlings injected with the Ol_Mitf::GFP plasmid.

The direct generation of pigment-free fish only worked when female QuiHs were crossed out, it worked only with some females and also only with some lines. From this crosses, we were unable to devise a theory. The findings hint towards a dominant

factor suppressing pigmentation that is present only present in some females and dependent on the genetic background as well as environmental factors.

A transgenic fish line that was created by injecting a plasmid containing the promoter element of the microphthalmia-associated transcription factor B (mitf) of fugu and a GFP sequence illustrates the image-advantages of QuiH fish. Against expectations, the fu_mitfb element did not drive expression of GFP in the pigment cells but in most neurons of the fish. Figure 37A shows an embryo of the fu_mitfb::GFP QUiH line were all neuronal tissues (brain, retina and spinal cord) are clearly visible without being disturbed by pigments. We used hatchlings of the line for live imaging with the two-photon laser and were able to distinguish single cells in the optic tectum and the retina (B) and the spinal cord (C). Neuromasts (C), as well as skin innervating neurons and single axons in the spinal cord, are nicely visible in this line. In the retina, the expression pattern of GFP was analyzed in more detail. Almost all neurons express GFP but with varying intensity, MGCs, RPCs and RSCs do not show any expression indicating that in Medaka the promoter is activated only in differentiated neurons. A sharp border marked by GFP expressing cells can be observed between the CMZ and the differentiated part of the retina.

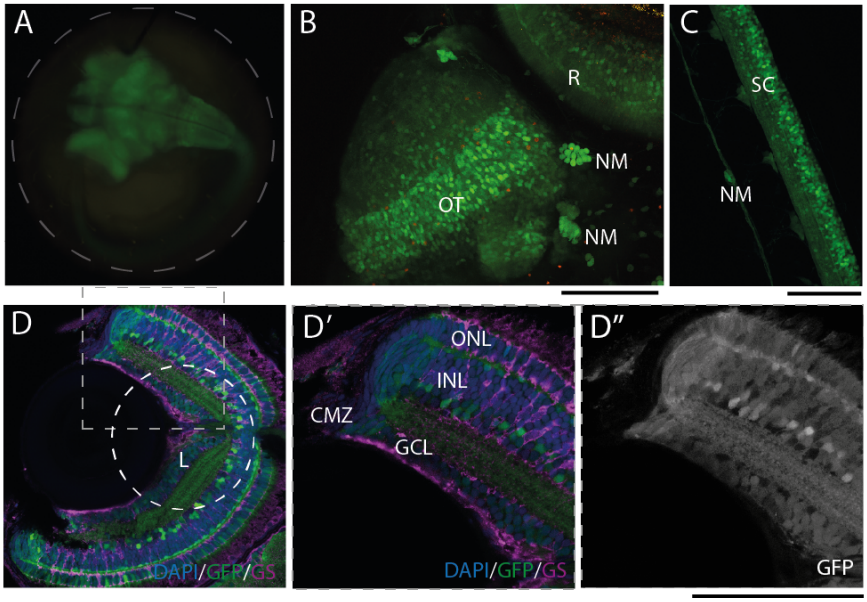

Figure 37: A Fugu mitfB promoter element is activated in most neurons of the CNS in Medaka. A stable transgenic QuiH line with an integration of the Fu_mitfb::GFP plasmid displays GFP expression in most neurons of the central nervous system. A. An embryo of the Fu_mitfb::GFP QuiH lines showing expression in neuronal tissue without auto-fluorescence, the chorion is represented by a dashed line. B & C. Live imaging in a Fu_mitfb::GFP hatchling in optic tectum and retina (B) and spinal cord (C). D expression of GFP in the retina of the Fu_mitfb::GFP, GFP is expressed in most differentiated neurons of the retina but not in the CMZ. The GS staining of MGCs (magenta) shows that GFP is not expressed in these cells. The scale bars are 100 µm.

1.1.3 Endogenous Tlx translational reporter

In the course of my PhD, I also worked on a strategy for endogenous tagging of factors specifically expressed in the CMZ with fluorescent proteins and transactivators to analyse the effect of oncogene expression in this specific cell types. One fish line that was generated in the course of these experiments is a Tlx-T2A-GFP fusion line. In this line, the endogenous Tlx (tailles) locus was tagged on its 3'end by a CRISPR/Cas9 mediated homology-directed repair strategy demonstrated in figure 38A. For the induction of a DSB two sgRNA were chosen next to the Stop codon using CCTop (Stemmer et al. 2015).

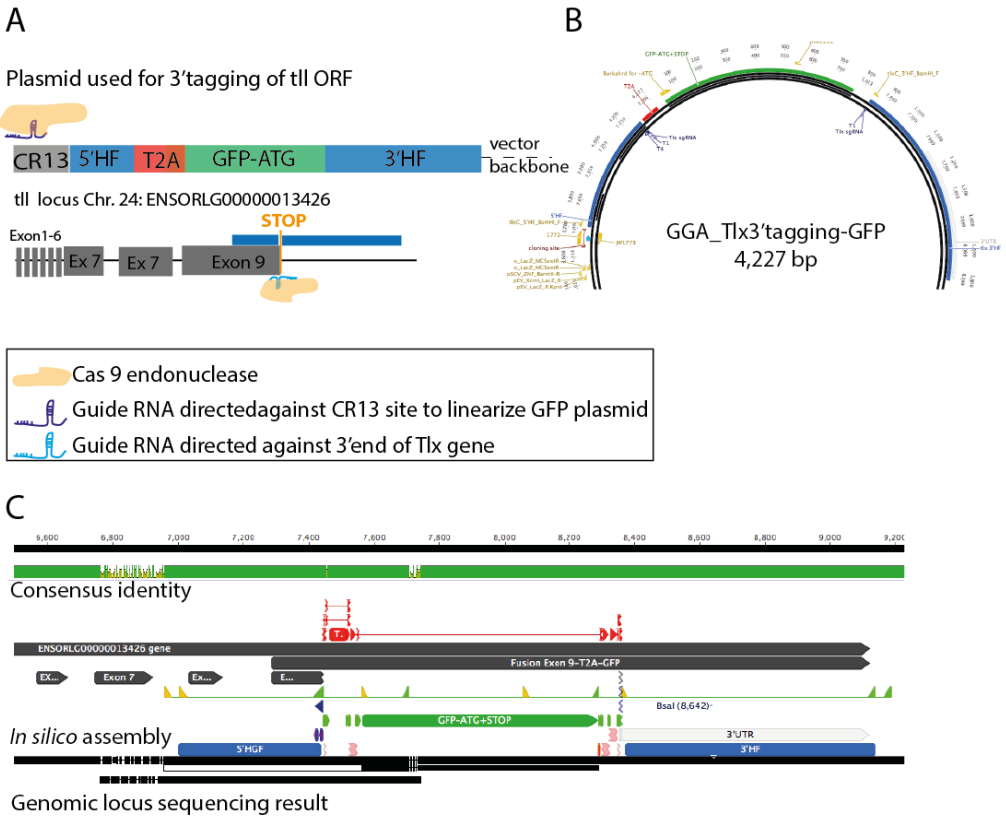

Figure 38: CRISPR/Cas9 based endogenous 3'tagging of the tlx locus by homology-directed repair. A. Schematic representation of the plasmid containing a CR13 site for linearization, 5' and 3'HF consisting of the sequences upstream and downstream of the stop codon and a T2A-GFP sequence between HFs. B. in silico assembled plasmid used for endogenous tagging. C. Alignment of sequencing result showing successful integration by homology-directed repair on the 5'end.

A plasmid was cloned in which two homology flanks (HFs) 440 bp upstream (5'HF) and 760 bp downstream (3'HF) of the stop codon are placed left and right of a T2A-GFP sequence lacking a start codon (figure 38B). The 3'HF contained the entire 3' end untranslated region (3'UTR). The plasmid was injected with sgRNAs, and Cas9 mRNA and one founder was selected that displayed distinct GFP expression in the

brain and early retina. The proper fusion of T2A-GFP with the ORF of endogenous Tlx was confirmed by sequencing of GFP positive offspring (figure 38C). We only confirmed the in frame integration on the 5'end and did not check for tandem integrations.

Since we included the entire 3'UTR and the expression pattern is similar to what was observed in the Tlx::GFP line we are confident that multiple integrations do not influence the expression pattern of the endogenous gene significantly.

By tagging of the endogenous locus, we created a translational reporter for the Tlx transcription factor. Figure 39 shows the expression pattern of the line in the brain and the retina, Tlx-T2A-GFP is expressed in the proliferative zones in the brain (A) as well as in the CMZ (B) in the retina. The expression observed here is consistend with the transcriptional reporter line published by Robert Reinhardt et al. (Reinhardt et al. 2015). Additionally, Tlx protein is present in glial cells which was confirmed by GS staining (A''' and B'''). The staining reveals that GFP is localized in the cytoplasm rather than in the nucleus, indicating that the T2A linker is efficiently causing separation of the two peptides.

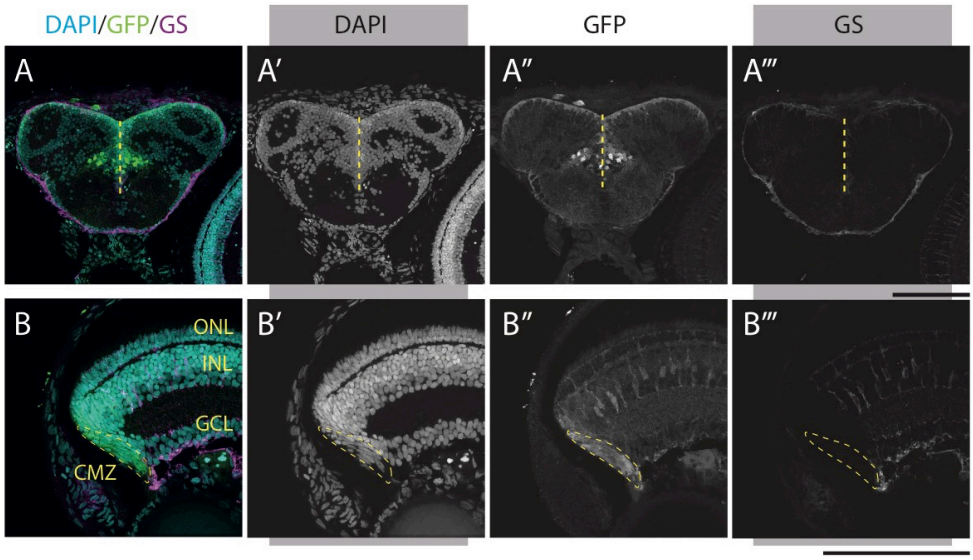

Figure 39: Localization of GFP in an endogenously tagged Tlx-T2A-GFP translational reporter line. A. In the brain, Tlx is translated in the subventricular zone (ventricle marked by dashed line) and glia cells around the telencephalon, GS (A''') staining overlaps with GFP staining (A''). B. In the retina Tlx-T2A-GFP is RSCs and progenitor cells in the CMZ (marked by dahsed outline) (B'') and MGCss (B'''). Scale bars are 100 µm.

6. Materials & Methods

6.1 Materials

6.1.1 Fish lines

- Cab F61-F65: Inbred strain was used as wild type (wt) Medaka (*Oryzias latipes).*
- QuiH2 F12-F15: Pigment free inbred strain, cross of Heino and Quintet pigment mutant lines
- Heino F26-F27: Albino Medaka line used for ISH experiments with hatchlings and later developmental stages.
- Ubi::loxPmCherryloxP_Xmrk-FL-GFP F0-F2: Lines expressing Xmrk tagged to eGFP after Cre-mediated recombination. Several lines were raised (see table 1 in results) Stock numbers: F0:
- Ubi::loxPmCherryloxP_Xmrk-T2A-GFP F0-F2: line expressing Xmrk tagged with GFP via T2A linker
- Ubi::loxPmCherryloxP_GFP-K-RAS^{12V} F0-F2: Line expressing EGFP tagged K-RAS after Cre-mediated excision of stop cassette
- Ubi::loxPDsRedloxP_GFP-myrAKT F0-F2: Line expressing EGFP tagged myrAKT after Cre-mediated excision of stop cassette
- Dual Tet::Xmrk/H2B-GFP_Hsp70::tTA_cmlc2::GFP) F0 (#5956)-F2 (#6365)
- DualTetRE::H2BGFP/mCherry_ Hsp70::tTA_cmlc2)F0-F1: bidirectional heat-shock inducible expression of H2B-GFP and mCherry
- DualTetRE::H2BGFP/Xmrk-FL-CFP_ Hsp70::tTA_cmlc2)F0: bidirectional heat-shock inducible expression of H2B-GFP and Xmrk-FL- CFP
- DualRTetRE::H2BGFP/Xmrk-T2A-CFP _ Hsp70::tTA_cmlc2)F0: bidirectional heat-shock inducible expression of H2B-GFP and Xmrk-T2A-CFP
- DualRTetRE::H2BGFP/ GFP-K-Ras^{12V} _ Hsp70::tTA_cmlc2 F0: bidirectional heat-shock inducible expression of H2B-GFP and GFP-K-Ras^{12V}

- DualRTetRE::H2BGFP/ GFP-myrAKT _ Hsp70::tTA_cmlc2 F0: bidirectional heat-shock inducible expression of H2B-GFP and myrAKT
- Fu_Mitf::eGFP F0-F5: fugu promoter driving GFP, expression in Neurons
- Tlx-T2A-GFP F0- F3: endogenous Tlx locus fused 3' to GFP via T2A expressing GFP in CMZ, SVZ and glia cells
- Egfra $^{-/-}$ F0: injected fish for CRISPR/Cas9 based induction of DSB in Exon4 and 7, 3 sgRNAS injected
- Egfra $^{12bpDEL/WT}$ F1: Female founders having a 12bp deletion in Exon four of one Egfra allele
- Egfra $^{GFPins/WT}$ F1: Male founders having a GFP plasmid insertion in one Egfra allele
- Egfra $^{12bpDEL/GFPins}$ F1-F2: Homozygous Egfra mutants with one 12bp deletion and one GFP plasmid insertion allele
- Egfra $^{GFPins/GFPins}$: F1 Homozygous Egfra mutants with two GFP plasmid insertion alleles

6.1.2 Plasmids

Table 2: pGEM-T easy vectors

Plasmid	Primers used (JW)	Stock number	Cloned by
pGEM-T_egfra insitu probe (770 bp)	4215/4140	4415	EH
pGEM-T_egfrb insitu probe (650 bp)	4295/4139	4593	EH
pGEM-T_hb-egf insitu probe (690 bp)	3652/4144	4417	CEPB/EH
pGEM-T_stat5b_insituprobe (700 bp)	5516/5517	4710	CEPB/EH
pGEM-T_akt1_insituprobe (700 bp)	5506/5507	4730	CEPB/EH
pGEM-T_akt2_insituprobe (700 bp)	5504/5505	4732	CEPB/EH
pGEM-T_stat5a_insituprobe (790 bp)	5514/5515	4740	CEPB/EH
pGEM-T_egf_insituprobe (678 bp)	3560/4145	4741	CEPB/EH
pGEM-T_tgfa_insituprobe (433 bp)	5508/5509	4742	CEPB/EH
pGEM-T_K-RAS_insituprobe (500 bp)	5510/5511	4743	CEPB/EH
pGEM-T_stat3_insituprobe (770 bp)	5518/5519	4798	CEPB/EH

Table 3: sgRNA oligos cloned into DR274 sgRNA expression vector

Plasmid	Stock number	Oligos (JW)	Cloned by
DR274_Tlx_stop_sgRNA_T1	4597	3525/3526	EH
DR274_Tlx_stop_sgRNA_T4	4598	3527/3528	EH
DR274_Egfra_Ex4_sgRNA	4599	4345/4346	EH
DR274_Egfra_Ex4_sgRNA	4600	4347/4348	EH
DR274_Egfrb_Ex2_sgRNA_T3	4684	4326/4328	EH
DR274_Egfrb_Ex2_sgRNA_T6	4685	5330/5331	EH
DR274_Egfrb_Ex5_sgRNA_T2	4686	5332/5333	EH

Table 4: Entry vectors used for Golden Gate Assemblies described in this work

Name entry vector	Internal stock number	Cloned by
pGGEV_6_Linker	2818	KL
pGGEV_3_loxP	2829	KL
pGGEV_5_loxP	2832	KL
pGGEV_7_linker	2849	KL
pGGEV2_+(H2B-EGfpinv)+_-1_PCR	3789	LC
pGGEV_8_-(ISCeI_3')-_+/-1_PCR	3793	LC
pGGEV_1_-(ISCeI_5')-_+/-1_PCR	3794	LC
pGGEV_5_-(3xpolyA)-_+1_BK	3901	MS
pGGEV2_-(ubi_3.4kb)-_+1_PCR	4018	TTT
pGGEV4(dsRed_3xpolyA)+_+1_BK	4019	TTT
pGGEV6_(cmlc2 promoter)-_-1_BK	4023	EH
pGGEV7(H2A mCherry_3xpolyA)+_+1_BK	4027	EH
pGGEV7_-(3xpolyA)-_+1_BK	4120	TTT
pGGEV2_(Tlx3'end tagging 5'HF (416bp))-_+1_PCR	4319	EH
pGGEV8_(Tlx3'end tagging 3'HF (763bp))-_+1_PCR	4321	EH
pGGEV6(old)_+(CFPwCR13_3pA)+_+1_BK	4329	EH
pGGEV6_-(Xmrk)_+1_GG	4334	CB
pGGEV5_(flexilinker)-_+1_OA	4353	EH/CB
pGGEV6_(eGFPmyrAKT)+_+1_BK	4419	CB/EH
pGGEV4_(eGFP-myrAKT)+_+1_BK	4420	CB/EH
pGGEV6_+(CFPwCR13_3pA)+_+1_BK	4422	CB/EH
pGGEV4_(eGFP-K-RAS12V)+_+1_BK	4424	CB/EH
pGGEV6_(eGFP-K-RAS12V)+_+1_BK	4425	CB/EH
pGGEV2_(Egfrb_Ex2_5'HF)-_+1_PCR	4687	EH

Table 5: GG Assemblies performed in course of this work. All assemblies were performed in pre-digested DV #3900.

Assembly	Stock number	Entry vectors used in DV #3900
SC(DualTet::Xmrk/H2B-GFP)	3944	3794, 3789, 3191, 3901,2818, 3192, 3793 and Xmrk PCR product
SC(DualTet::Xmrk-fl-CFP/H2B-GFP)	4437	3794, 3789, 3791, 4317, 4353, 4422, 4120, 3793
SC(DualTet::Xmrk-T2A-CFP/H2B-GFP)	4434	3794, 3789, 3791, 4317, 4122, 4422, 4120, 3793
SC(DualTet::DsRed/H2B-GFP)	4433	3794, 3789, 3791, 4019, 3901, 4023, 4028, 3793
SC(DualTet::eGFP-myrAKT/H2B-GFP_cmlc2:DsRed)	4440	3794, 3789, 3791, 4420, 3901, 4023, 4028, 3793
SC(DualTet::eGFP-K-RAS/H2B-GFP_cmlc2:DsRed)	4441	3794, 3789, 3791, 4424, 3901, 4023, 4028, 3793
Sc(Ubiq::loxPDsRedloxPXmrk)	4335	3794, 4018, 2829, 4019, 2832, 4334, 4120, 3793
Sc(Ubiq::loxPDsRedloxPXmrk-fl-GFP)	4405	4335 mutated with JW4079/4080 primers and assembled with 3885 and 3961
Sc(Ubiq::loxPDsRedloxPXmrk-T2A-GFP)	4390	4335 mutated with JW4079/4080 primers and assembled with 3885 and 4121
Sc(Ubiq::loxPDsRedloxPeGFP-K-RAS)	4443	3794, 4018, 2829, 4019, 2832, 4425, 4120, 3793
Sc(Ubiq::loxPDsRedloxPeGFP-myrAKT)	4442	3794, 4018, 2829, 4019, 2832, 4419, 4120, 3793
CR13_tlx3'end-T2A-GFP tagging	4418	3776, 4315, 4373, 2801, 3885, 2822, 2849, 4321
pGGDestSC_Cr13_egfrb_ex2_5'HF_-GFP+_3xpolyA	4688	3776, 4687, 4681, 4044, 3190

Table 6: Other plasmids

Plasmid	Stock number	Cloning strategy	Cloned by
SC(Fu_Mitf::GFP)	1120	PCR/ Restriction digest	Martinez Morales
SC(Ol_Mitfa::eGFP)	3352	unknown	Schartle Lab
pDest_SC(hsp70::tTA_cmlc2::GFP)	4007	Gateway cloning	EH

6.1.3 Primer and other oligonucleotides

Table 7: Primer used for PCRs and sequencing of plasmids

Number	Name	Sequence
JW2352	Ev4overhangXmrkfor	CAGGGTCTCGACTAATGGAGTTTCTGCGCGGAGGAG
JW2353	Ev4 overhang Xmrk rev	CAGGGTCTCGGCAGCTAGCGGACAGGAGTGTACAGTGC
JW2848	XmrkEv6 new OH for	CAGGGTCTCGAACTCTAGCGGACAGGAGTGTACAGTGC
JW3415	EGFRa in situ f	GCAACCGTTTAAACCTGCTAGG
JW3416	EGFR a in situ rev T7	CCAAGCTTCTAATACGACTCACTATAGGGAGAGCAGTTCTTTACACAGGTGGC
JW3417	EGFRb in situ f	ATCTGTGTGTGTTTCAGTATGCC
JW3418	EGFR b in situ r T7	CCAAGCTTCTAATACGACTCACTATAGGGAGACCTGCTGGCTTTTGTGGTTA
JW3444	TlxC_5'HF f	GCCGGATCCTTGTTAAAAAGTAATGTGTGTTTTGCA
JW3445	TlxC_5'HF_KpnI	GCCGGTACCTATATCGCTCGACTTGTACATGTCCGAGAGGAG
JW3446	TlxC_3'HF_BamHI_f	GCCGGATCCACCCTTTCCCAAACCGTCCG
JW3447	TlxC_3'HF_KpnI_r	GCCGGTACCCCAGATAATGTGACAGCTGGATTT
JW3448	TlxC_seq_f	TTGAGGAAACAGGAGGAGAAATGT
JW3449	TlxC_seq_r	CAAGGTTGCTCAAGGAGAAAACAA
JW3560	EGF in situ_f	GAAGGGGGAGGTACGGAGAA
JW3561	EGF_in situ_Rev_T7	CCAAGCTTCTAATACGACTCACTATAGGGAGAACCGAGAGAGCAGCCGT
JW3562	hbegfa in situ_f	AAGAGGAATATGACGATGAAGCCT
JW3563	hbegfa_rev_T7	CCAAGCTTCTAATACGACTCACTATAGGGAGAGGACAGGCCGGTCTTCTTC
JW3848	Xmrk4H-Stop rev	CAGGGTCTCGGCAGGCGGACAGGAGTGTACAGTGC
JW3922	MCS Xmrk II	CCAAGGCCGTTTAAACTAGTTAATTAAGGCGCGCCGC
JW3923	MCS Xmrk II rev	GGCCGGTTCCGGCAAATTTGATCAATTAATTCCGCGCGGCGCCGG
JW4139	egfrb in situ rev	CCTGCTGGCTTTTGTGGTTA
JW4140	egfra in situ rev	CAGTTCTTTACACAGGTGGC
JW4142	egfrb in situ rev	GCTTGCATTTTCGTCCACATTGG
JW4143	egfrb in situ f new	GGCCTCATGCGCTACGATC
JW4144	Hbegfa in situ rev	GGACAGGCCGGTCTTCTTC
JW4145	EGF in situ rev	ACCGAGAGAGCAGCCGTg

JW4295	egfrb in situ fwd	CGTACACTCTGGAAAACCAGG
JW4353	egfra f 1	TGAGAGCAAACAGGCATGTGTGG
JW4354	egfr rev 1	CCCAACACTGTCATTGTCAAACAGT
JW4355	egfra seq f 2	TGTTACCCGAAGTCATCAACTGTT
JW4356	egfra seq r 2	AAAGTCCATTCAGTCGGTGACA
JW4357	egfra seq f 3	TCCTGGAGGGGTAAAAGCCATCC
JW4479	Xmrktag_mut PCR for	ggtctcatcagAGTTGCGGATCCACCATC
JW4480	Xmrktag_mutPCR rev	ggtctcttagtGCGGACAGGAGTGTACAG
JW5335	egfrb ex2 5'HF rev kpnI	GACTGGTACCATTGACCAGCGGGACGGTC
JW5336	egfrb ex2 5'HF for BglII	AGTCAGATCTCTGCTGAAGTCAGACTCTTTC
JW5355	egfraa simp KO seq fwd	AGACCTGCCACTCCCTGCTG
JW5356	egfra simp KO seq rev	GCAAGTCAGCCTCCATCAGCA
JW5374	egfra ex4 KO seq fwd	ATCTGCGCATCATCCGGGGT
JW5375	egfrb ex4 KO rev	CGACAGGCCTGCAGCACAAA
JW5376	egfrb seq ex2 rev	CAACGATGTCCCACCACTG
JW5377	egfrb Ex5 seq fwd	ACTCCTTCCCCATGAGCGCA
JW5378	egfrb Ex5 seq	AACAGCTGCGTGCCTCACAG
JW5379	egfrb 5'HF rev wob	ATTGACCAGCGGGACTGTCG
JW5440	egfrb seq primers 5'of ex2	GCCACCCTTCCCCTTCTC
JW5504	akt2 fwd	AGACAGGGCGCGGTTTTACG
JW5505	akt2 rev	TCATTCCCGAATGCTGGCGC
JW5506	akt1 fwd	CCACGTGGAGACCCCTGAGG
JW5507	akt1 rev	GCGGCCGTAGTCGTTGTCTT
JW5508	tgf-a fwd	GTGGCTGCAGCTGTTCGGTC
JW5509	tgf-a rev	CAAAGGTTTGTGGGCCACAC
JW5510	k-ras fwd	TTGGCAAGAGCGCGCTTACC
JW5511	k-ras rev	AGGTTGACACAGCGTGGAGTCT
JW5514	Stat5a	CAACTGGCAGGCAATGGGGG
JW5515	Stat5a rev	CGGTTGCTCTGCACCTCTGC
JW5516	Stat5b fwd	AAGTTTGCAGCCACGGTCCG
JW5517	Stat5b rev	GCTCCACCACGCCATCGAAC
JW5518	Stat3 fwd	TGGTTCAGCAGCCCATCCCA
JW5519	Stat3 rev	TGACCCTCGAATGGCAGCCA

6.1.4 sgRNA oligos

Table 8: Oligonucleotides used for the generation of sgRNAs, annealed and cloned in DR274 plasmid.

Number	Name	Sequence
JW3525	Tlx sgRNA T1 f	TAGGAAAGGGTTCATATATCGC
JW3526	Tlx sgRNA T1 r	AAACGCGATATATGAACCCTTT
JW3527	Tlx sgRNA T4 f	TAggCGCTGGACTTGTACATGT
JW3528	Tlx sgRNA T4 r	AAACACATGTACAAGTCCAGCG
JW4343	egfra ex5 sgRNA T1 f	TAgGCCAAAGATGGAGCTCCCGA
JW4344	egfra ex5 sgRNA T1 rev	AAACTCGGGAGCTCCATCTTTGG
JW4345	egfraa ex4 sgRNA T6 f	TAgGTTAATTCTGATAAAGGAAC
JW4346	egfr ex4 sgRNA T6 rev	AAACGTTCCTTTATCAGAATTAA
JW4347	egfra ex7 sgRNA T1 f	TAggCCTTACACACCCCGTCGTCT
JW4348	egfra ex7 sgRNA T1 r	AAACAGACGACGGGGTGTGTAAGG
JW5326	egfrb sgRNA Ex2 T3 fwd	TAggCCGTCCCGCTGGTCAATCTA
JW5328	egfrb sgRNA ex2 T3 rev	AAACTAGATTGACCAGCGGGACGG
JW5330	egfrb sgRNA Ex2 T6 for	TAgGTCAATCTAAGGCTGATCCG
JW5331	egfrb sgRNA Ex2 T6 rev	AAACCGGATCAGCCTTAGATTGA
JW5332	Egfrb sgRNA Ex5 T2 fwd	TAggCTGCTCAGCACACACTAGCT
JW5333	egfrb sgRNA Ex5 T2 rev	AAACAGCTAGTGTGTGCTGAGCAG

6.1.5 Antibodies

Primary antibodies

Antibody directed against	Species	Producer/Catalog number	Dilutions
a-Tubulin	mouse	Sigma Aldrich / T9026	1:200
Phospho-p44/42 MAPK (Erk1/2)	Rabbit	NEB cellsignaling / 4370	1:200
PhosphoH3(Ser10)	rabbit	Millipore/ 06-570	1:200
y-Tubulin	mouse	Sigma / T6557	1:200
anti EGFP IgY	Chicken	life technologies / A10262	1:200 whole mounts, 1:500 sections
Rx2	Rabbit	Lab made (Reinhardt et al. 2015)	1:200 whole mounts, 1:500 sections
BrdU BU1/75 (ICR1)	Rat	AbD Serotec / OBT0030G	1:750
Glutamine Synthetase (GS)	mouse	Chemicon / MAB302	1:500 sections
Anti-Digoxigenin-AP, Fab fragments	sheep	Roche	1:2000 WISH, 1:1000 section ISH

Secondary Antibodies

Alexa Fluor® 647 anti-Rabbit IgG (H+L) *2 mg/mL*	Goat	Life Technologies / A21245	1:500
Alexa Fluor 488 anti-mouse IgG (H+L) 2mg/ml	Goat	Life Technologies / A11029	1:500
AlexaFluor 633 anti-rat IgG (H+L)	Goat	Life Technologies	1:500
DyLight549 anti Rat IgG ML	Goat	Jackson	1:500
AlexaFluor 633 phalloidin		Life Technologies	1:200 / 1:50
Alexa Fluor 488-AffiniPure Anti-Chicken IgY (IgG) (H+L)	Donkey	Jackson / 703-545-155	1:500

6.1.6 Chemicals, reagents and bacteria

Chemical/Reagent	Supplier
4',6-Diamidino-2-phenylindole (DAPI)	Roth
10% Sodium dodecyl sulfate (SDS)	Roth
10xPBS (section ISH)	
20 % Sodium dodecyl sulfate (SDS)	Roth
5-Bromo-4-chloro-3-indoxylphosphate (BCIP)	Roche
6x DNA loading dye, blue	Thermo Scientific
Adenosine triphosphate (ATP)	Thermo Scientific
Agar	Sigma
Agarose	Sigma
Ampicillin	Roche
Blocking reagent	Roche
Blocking reagent	
BM purple	Sigma Aldrich
Bovine Serum Albumin (BSA)	Sigma
Deoxyadenosine triphosphate (dATP)	Thermo Scientific
Deoxynucleotide Triphosphates Set (dNTPs)	Life Technologies
Digoxigenin-dUTP (10 mM)	Roche
Dimethyl sulfoxide (DMSO)	Roth
Dithiothreitol (DTT)	Sigma
dNTP Mix (10mM)	Sigma
Ethanol	Sigma
Ethidium Bromide (EtBr)	Sigma
Ethylene-diamine-tetra-acetic acid (EDTA)	AppliChem
Ethylenediaminetetraacetic acid (EDTA)	Roth
Ficoll	
Formamide	Sigma
Formamide	Sigma
Gelatine	Sigma

GeneRuler DNA Ladder Mix	Thermo Scientific
Glacial acetic acid	Merck
Glutaraldehyde Solution	Fluka
Glycerol	Merck
Glycine	Sigma
Heparin	Sigma
HEPES	Roth
Hydrochlorid acid	Merck
Isopropanol	Sigma
Kanamycin	Roth
Mach1TM T1 phage resistant chemically competent E. coli	Lab made
Magnesium chloride	Merck
Magnesium sulphate heptahydrate	Grüssing
Methanol	Roth
Methylene blue	Sigma
Mowiol 4-88	Roth
Nitro blue tetrazolium (NBT)	Roche
Normal goat Serum (NGS)	Gibco
Paraformaldehyde (PFA)	Sigma
Phenol:Chlorophorm:Isoamyl (25:24:1)	Roth
Potassium acetate	Sigma
Potassium chloride (KCl)	Applichem
Potassium dihydrogen phosphate (KH2PO4)	Merck
Proteinase K	Merck
Ribolock	Thermo Scientific
Ribonucleoside Triphosphate Set	Roche
Roti Aqua-P/C/I	Roth
Sheep Serum	Sigma
Sodium chlorid dihydrate	Sigma
Sodium chloride (NaCl)	Sigma
Sodium citrate	Merck
Sodium hydrogen phosphate (Na2HPO4)	Applichem
Sodium hydroxide (NaOH)	Merck
Sucrose	Sigma
Torula RNA	Sigma
Tricaine mesylate	Sigma
TRIS-Hydrochloride (TRIS-HCl)	Sigma
Triton X100	Sigma
Tryptone	Sigma
Tween20	Sigma
Water (H_2O)	Sigma
X-gal (5-Bromo-4-Chloro-3-Indolyl-β-D-Galactopyranoside)	Roth
Yeast Extract	Roth

6.1.7 Buffers and media

Buffer/medium	Composition
100x Denhardts solution	5 g Ficoll, 5 g BSA 5g Polyvinylpyrrolidone in 250 ml RNAse free water
10x Blocking reagent	Blocking reagent powder (10%) was diluted in MAB buffer under heating.
10x PBS pH 7,3	1,2 M Sodium chloride, 0,35M Sodium hydrogen phosphate, 25mM Potassium dihydrogen phosphate
10x Yamamoto	171 mM Sodium Chloride, 4 mM potassium chloride, 2.7 mM calcium chloride dihydrate, 4.9 mM magnesium chloride hexahydrate,24 mM sodium hydrogen carbonate, pH 7.3
1x Medaka hatch solution	0,1 % (w/v) Sodium chloride, 0,003% (w/v) Potassium chloride,0,004% Sodium chloride dihydrate(w/v), 0,016% (w/v) Magnesium sulphate, heptahydrate,0.00002% (w/v) Methylene blue
1xPTW	1x PBS, 0,4% tween20
20xSSC	3 M Sodium chloride, 0,3 M Trisodium citrate dihydrate adjusted to pH 7
4xSSCT	2x SSC, 0,1 % Tween20
Annealing buffer	10mM Tris pH 7.5 - 8, 30mM NaCl
ERM	17 mM NaCl, 0.4 mM KCl, 0.27 mM CaCl2, 0.66 mM Magnesium Sulphate Heptahydrate, pH7
Fin-Clip buffer	2 M Tris pH8, 0.5 EDTA pH8, 15 M NaCl, 20% SDS
Gelatine/Albumin	0,49 g gelatine disssolved in 100 ml 1xPBS upon heating, 30 gBSA , 20 g Sucrose added after cooled down, store at -20°C
Hybridization Mix	50% Formamide, 5x SS, 50 µg/ml Heparin, 0,1% Tween20, 5mg/µl Torula RNA
LB	10 g/l bacto-tryptone, 5 g/l yeast extract, 10 g/l sodium chloride
LB-plates	10 g/l bacto-tryptone, 5 g/l yeast extract, 10 g/l sodium chloride, 18g/l Agar-Agar
MAB	100 nN Maleinsäure, 150 mM NaCl, 2mM Levamisol, 0,1% Tween 20, PH adjusted to 7,5 with NaOH pellets
NTMT	100 mM Tris pH 9,5, 50 mM MgCl2, 100 mM NaCl, 2mM levamisol 0,1% Tween20 in RNAse free H_2O
P1	50 mM glucose, 25 mM Tris-HCl, 10mM EDTA, 100 µg/ml RNAse A, pH8
P2	0.2 N NaOH, 1% SDS
P3	5 M Potassium acetate
TAE	242 g/l Tris-base, 5.71% glacial acetic acid, 50 mM EDTA, pH8,5
TB Medium	12 g/l bacto-tryptone, 24 g/l yeast extract, 0.4% glycerol,2.13 g/l potassium hydrogen phosphatepotassium dihydrogen phosphate, 12.54 g/l
TE Buffer	10 mM Tris-HCl, 1mM EDTA pH 8.0

6.1.8 Antibiotics

Kit Name	Stock concentration	Working concentration	Producer
Ampiciline	50 mg/ml	50 µg/ml	Sigma
Kanamycine	100mg/ml	100 µg/ml	Roth

6.1.9 Enzymes and Buffers

Enzyme	Buffer	
BamHI HF	Cutsmart	NEB
KpnI HF	Cutsmart	NEB
BsaI/Eco31I FD	Fast digest	Thermo Scientific
PmeI	Cutsmart	NEB
HpaI	Cutsmart	NEB
SpeI HF	Cutsmart	NEB
NcoI Fast digest	Fast Digest Green	Thermo Scientific
EcoRI HF	Cutsmart	NEB
Sac II	Buffer B	Thermo Scientific
DraI HF	Cutsmart	NEB
T4 Ligase	Ligase Buffer	Promega
Taq Roboklon	Buffer B	Promega
Proteinase K		Roche
20 U/µl Sp6 RNA polyerase	10x Transcription Buffer	Roche
20 U/µl T7 RNA polyerase	10x Transcription Buffer	Roche

6.1.10 Kits

Kit Name	Company	Used for
RNeasy MinElute Cleanup Kit	Quiagen	RNA cleanup used for sgRNA production
innPREPPCR pure Kit	Analytic Jena	PCR clean up
innuPREPGel Extraction Kit	Analytic Jena	DNA cleanup after gel electrophoresis
Plasmid Midi Kit	Quiagen	Plasmid preparation
QIAquick PCR Purification Kit	Quiagen	Cleanup of DNA fragments
Q5 site directed mutagenesis	NEB	Xmrk tagging in oncogene plasmids
pGEM®-T Easy Vector System	Promega	TA-cloning of in situ probes
MEGAshortscript™ T7 Transcription Kit	Applied Biosystems/	sgRNA transcription
Gateway cloning Kit	Invitrogen/Thermo	Gateway assembly of

6.1.11 Miscellaneous material

Material	Source
6xDNA loading dye, purple	NEB
6x DNA loading dye, blue	Thermo Scientific
Borosilicate glass capillaries GC 100T	ClarcElectromedical Instruments
GeneRuler DNA Ladder Mix	Thermo Scientific
Jung Tissue Freezing Medium	Leica
Glass bottom dishes	MatTEC
Slides and coverslips	Roth
Slides for cryosetions: Superfrost Plus	Thermos Scientific

6.1.12 Software

Geneious R8: Planning and testing of cloning strategies *In silico* assembly of constructs. Alignments and plasmid database

CCTop: Online tool for target and off-target prediction of sgRNAs http://crispr.cos.uni-heidelberg.de/

Fiji Image J: Image processing, quantification

Adobe Illustrator: Graphs and Figures

Adobe Photoshop: Image processing

Statistics: BoxPlotR: http://shiny.chemgrid.org/boxplotr/

Pearson Correlation: http://www.socscistatistics.com/tests/pearson/

NEB TM calculator: http://tmcalculator.neb.com/#!/

6.1.13 Equipment

Equipment	Source
"Insitu Pro" robot	intravis AG bioanalytical Instruments
Axio Imager M1 microscope	Zeiss
Bacterial Shaker INNOVA 44	New Brunswick scientific
Centrifuge 5417C	Eppendorf
Centrifuge 5430 R	Eppendorf
Centrifuge 5810 R	Eppendorf
Cryostat CM 3050S	Leica
Digital sight DS-U3	Nikon
Embryo incubators	Heraeus instruments and RuMed
FemtoYet express or Microinjector 5242	Eppendorf
InjectMan NI2	Eppendorf
Leica TCS SPE	Leica
Leica TCS SP5	Leica
Microwave	Sharp
Mini-centrifuge	Starstedt
Multipette	Eppendorf
NanoDrop 2000C Spectrophotometer	Thermo Scientific
Needle puller P-30	Sutter Instrument Co USA
Pipettes 10 µl & 200 µl	Eppendorf
Pipettes 20 µl, 1 mL	Gilson
Power supply Power-PAC Basic	Bio RAD
Shaker Innova44	Eppendorf
SMZ18 stereomicroscope	Nikon
Stereomicroscope Olympus SZX7	Olympus
Stereomicroscope Zeiss Stemi 2000	Zeiss
Thermocycler	Bio RAD
Thermomixer 5436	UV-Gel-cutting Table
Vibratom VT1000S	Leica

6.2 Methods

6.2.1 Fish maintenance and embryo collection

All used fish used in this work were of the species *Oryzias latipes*. The WT strain from which most lines were generated is Cab. Fish were maintained under standard aquaculture conditions with water recirculation. The day/night cycle was 14/10 h. For embryo collection the fertilized eggs were carefully removed from the ventral part of the female using a net and a metal hook. Embryos were freed from sticky filaments by rolling or forceps and placed in plastic dishes containing 1xERM or 1xHatch solution. Embryos were incubated at either 18°C, RT of 28°C dependent on desired rate of development. Embryos that need to be screened were kept in 1xERM to prevent autofluorescence caused by methylene blue in hatch solution.

6.2.2 Mating and microinjection

For mating of fish males were separated from females over night and placed back to female tanks the next day. 15 to 25 min after spawning fertilized oocytes were collected from each female and placed in RT or ice cold 1x ERM. Embryos were freed of filaments and either placed in pre-cooled injection molds (1,5% agarose/$_{d}H_2O$ in a petri dish) or fixed at desired stage.

For injection, embryos in one cell stage were sorted in molds and orientated in a way that they could be injected using a fine glass needle attached to an automatic injection device. Glass needle were made of borsilicate glass capillaries pulled with a P-30 needle puller. The needle was loaded with injection mix from the back using Micro-loader tips. Approximately 10% of the visually estimated zygote volume was injected using a Microinjector and InjectMan N12. For details see (Porazinski, Wang, and Furutani-Seiki 2010). After injection embryos were taken out of the molds and placed in dishes with 1xERM at 28°C or RT.

For generation of transgenic lines by random genome insertion using a meganuclease based approach as described in (Thermes et al. 2002) was used. Injection mix contained 10 ng/µl Plasmid, 1xYamamoto buffer, 1xI-SceI buffer, 1 µl I-SceI meganuclease in dH_2O.

For CRISPR/Cas9 based genetic manipulation I used 150 ng/µl Cas9 mRNA, 15 ng/µl of each sgRNA and 10 ng/µl of plasmid.

Cre-mRNA mRNA was injected in a concentration of 10 ng/µl.

H1-Texas red protein eluate kindly provided by the Lemke Lab was injected undiluted.

6.2.3 PCR

PCRs for amplification of genomic loci, cDNA sequences (in situ probes), and sequences form plasmid and genotyping of CRISPR/Cas9 manipulated lines were performed using Q5 polymerase with following conditions.

Component	50 µl mix	25 µm mix	15 µm mix
5x Q5 Reaction buffer	10 µl	5 µl	3
10 mM dNTPs	1 µl	0,5 µl	0,3
10 µm fwd primer	2,5/1 µl	1, 25 µl	0,4
10 µm rev primer	2,5/1µl	1, 25 µl	0,4
gDNA/cDNA/plasmid	2 µl/1µl/<10 ng	1µl/0,5µl/-	1 µl
Q5 High-Fidelity DNA polymerase	0,5/0,3 µl	0,2 µl	0,05 µl
Nuclease-free H_2O	Ad 50 µl	Ad 25 µl	Ad 15 µl

We decreased the amount of Q5 polymerase recommended by the manufacturer. Desalted primers were ordered at MWG. PCRs were run in thermo cyclers using following conditions adapted to melting temperature of primers and length of amplified fragment.

Step:	Temperature	Time
1	98 °C	2 min
2	98 °C	20 sec
3	TM	20 sec
4	72°C	30 sec/kb
5	go to 2.	30-35 times
6	72°C	5 min
7	10 °C	10 min

PCR fragments were purified either from the gel or directly using the innuPREP DNA purification kit.

6.2.4 Agarose gel electrophoresis DNA

Gel electrophoresis was carried out for PCR amplificates and restriction digests. Usually 1% Agarose/TAE gels were used in TAE filled champers. DNA samples were mixed with 6x purple loading dye and loaded on gels together with a Generuler 1kb ladder (thermo scientific). A voltage between 120 and 140 V was applied for 30 to 50 minutes. Gels were stained in a TAE bath containing 2 µg/µl ethidiumbromide (10-20 min). EtBr stained DNA was detected using a UV-based gel documentation system.

6.2.5 Agarose gel electrophoresis RNA

For RNA gels, chambers, combs and ridges were cleaned by incubating in 0,1 M NaOH for 20 min. 1x TAE was diluted from the stock using Millipore water and 1%-1,5% agarose gels were prepared freshly. 2 µl RNA aliquots were mixed with 3 µl RNAse free water and 5 µl 2x RNA loading dye. RNA was denatured by heating to 80 °C for 10 min and the gel was pre-run at 120 V for 10 min. EtBr bath was prepared freshly and gels were stained for 10 min. Filter tips and gloves were used at all times. Detection was done as for DNA gels.

6.2.6 Gel extraction of DNA fragments

DNA fragments as PCR products and or restriction digests that were used for subsequent cloning or send for sequencing were run on 1% agraose gels. PCR fragments were cut out from stained gels using a fresh scalpel and cleaned up with the innuPREP Gel Extraction Kit from Analytic Jena according to the manufacturers instructions. Instead of elution buffer we used pure water to elute DNA fragments from the column.

6.2.7 Finclipping

For genotyping we use finclips of juvenile and adult fish. For that fish were anaesthetized in 1x Tricane and placed in a plastic spoon. The tailfin was placed in a way that it hung over the edge of the spoon. The tip of the fin was cut of with a sharp scissor and placed in a 1,5 ml tube containg 100 µl finclip-buffer and 5 µl Proteinase

K. Finclipped fish were placed in individual numbered tanks containing 1/3 hatch medium and 2/3 fish water.

6.2.8 Genomic DNA extraction

Genomic DNA (gDNA) was extracted either from clipped fins or single or pools of embryos. Finclips and embryos were placed in 100µl finclip-buffer containing 5 µl proteinase K. Embryos were homogenized using a pestle. Emerged tissue and homogenized embryos were incubated at 60 °C over night. The next day 200 µl of H_2O were added and proteinase K was deactivated by boiling for 10 min at 95°C. gDNA dilutions were then centrifuged for 20 min at 10.000 rpm, 4°C. 2 µl of gDNA dilution was used in 50 µl PCR mix.

6.2.9 A-tailing and TA-cloning in pGEM-T easy vector

PCR fragments that were amplified with Q5 proofreading-polymerase were A-tailed for TA cloning into pGEM-T-easy vector. For that cleaned up PCR product was incubated with 3 U Taq polymerase (Robokon) and 2 mM dATP, 1x standard polymerase buffer B for 25 min at 72°C.

Cloning into pGEM-T easy vector (Promega) was done with half the amount of vector as recommended by manufacturer. 3,5 µl of A-tailed PCR or Taq PCR product was used for a ligation with 0,5 µl pGEM-T easy vector in 2x ligation Buffer, using either the T4 DNA ligase provided by the kit or the common lab T4 DNA ligase (5U). the ligation-mix was incubated for at least 1 hour at RT. Transformation was performed after standard protocol in 50 µl of chemically competent DH5α cells. For blue-white selection ampicillin plates were coated with 50 µl X-Gal using glass beads prior to plating of transformed bacteria.

6.2.10 Design and Cloning of sgRNAs

Target sites for sgRNAs were identified using the CCTop online tool (Stemmer et al. 2015). Sequences of first exons of *egfra* and *egfrb* were entered and sequences with least off-targets were selected as target. For tagging of the *tlx* locus I selected the region 20 bp upstream and downstream of the stop codon and selected target sequence with least off-targets.

Oligo Annealing

Two complement DNA oligonucleotides were ordered at MWG, oligos were diluted to 100 µM. 1 µl of each oligo was mixed with 18 µl H_2O and 20 µl annealing buffer and incubated in thermal cycler: 5 min at 95°C, ramped down (0,1°C/s) to 70 °C, hold for 10 min and ramped down to 65 °C (0,1°C/s) hold for 10 min, ramped down (0.1°C/s) to 60°C, hold for 10 min, ramped down (0.1°C/s) to 10°C. The oligo-solution was diluted 1:3 and ligated with 0,025 pmol BsaI predigested sgRNA vector (DR273; addgene #42250).

sgRNA plasmid generation

Bacterial transformation was performed after standard protocol and plated on ampicillin-plates. Up to five colonies were prepared for test-digest with BsaI. Non-digested plasmids were confirmed for oligo-insertion by sequencing and Midipreps were performed to amplify correct sgRNA containing plasmids.

6.2.11 Generation of plasmids

Constructs listed in 6.1.2 were assembled as described in chapter 6.2.12 (GG assembly). Plasmids with internal stock numbers 4405 and 4390 (see table 5) were cloned via Q5 site directed mutagenesis PCR (NEB Kit) from plasmid 4335 with primers JW4079 and JW4080 (Table 5). The mutagenesis PCR removed the Xmrk Stop-codon and inserted an Eco31I restriction site that upon digest will generate EV4 and EV5 overhangs. The mutated plasmids was thus used in a GG Assembly together with plasmids #4121 and 3885 for generation of plasmid 4390 and vectors 3961 and 3885 for plasmid #4405.

6.2.12 Cloning of entry vectors

Inserts for entry vectors were either sub-cloned from other entry vectors or amplified from the genome (homology flanks, HF) or other plasmids (Xmrk, HRAS, myrAKT) via PCR. Most entry vectors were cloned into the BamHI/KpnI digested site of Entry vectors, PCR products were amplified using BamHI/BglII and KpnI restriction site containing primers. Some inserts were cloned into other restriction sites in multiple cloning site (MCS) containing entry vectors. Entry vectors 4419 and 4420 were cloned

via BamHi/KpnI release of insert from vector 4414 and ligated in EVs 4 and 6 (3240 and 4274) at same restriction sites. Entry vector

6.2.13 GG-Assemblies of oncogene constructs

Assembly of oncogene containing plasmids (except entry vectors) was based on (Kirchmaier, Lust, and Wittbrodt 2013). 20 fmol of each entry vector (1-8) and 50 ng BsaI pre-digested destination vector were mixed with 1 µl FD Buffer, 1 µl T4 Ligation buffer, 1µl 10 mM ATP, 0.6 µl Eco31I FD enzyme and 0,6 µl 30U/µl T4 ligase. The volume was added up with dH_20 to 20 µl. The reactions were incubated in the thermo cycler for 10 repeats of 30 min at 37°C (digest) and 20 min at 15 °C (ligation). Enzymes were inactivated by 10 min incubation an 85°C and then cooled down to 10 °C. Since in most assemblies there was at least one insert with internal BsaI restriction sites another 30-60 min ligation step was performed adding 1 µl of ligase and 1 µl 10mM dATP and incubating at RT. 3-5 µl of the assembly were transformed in 50 µl bacteria after standard transformation protocol and bacteria were plated on Kan-LB-plates previously treated with X-Gal. In case of plasmid 3944 (DualTet::Xmrk/H2B-GFP) Xmrk was amplified by PCR using primers JW2352 and JW2353, that generated EV4 overhangs upon digestion, cleaned up after gel electrophoresis and used directly in the assembly with other EVs and DV as indicated in table 5 (chapter 6.1.2.). NOTE: GG assembly of Xmrk did not work when internal Eco21I sites were mutated; the cloning of Xmrk is extremely facilitated when cloned in a multi-factor ligation.
Whenever an insert did not fill a space in the assembly we used EVs containing linkers. When the assembly was shorter we used STOP EVs that upon Eco31I digest have DV compatible overhangs.

6.2.14 Standard transformation procedure

Ligations were transformed in chemically competent DH5α bacterial cells (prepared by the lab). For that 3 to 5 µl of ligation were incubated for 15-45 min with 50 µl competent cells that were thawed on ice in a 1,5 ml tube. A 42 °C 45s heat shock was then applied and cells were stored on ice for 2-3 min. Cells were then provided with 250 µl TB and incubated for 1 hour at 37°C in the shacking incubator (200 rpm). Using glass beads bacteria were then plated on agar plates with desired antibiotic

(ampicillin for standard ligations and pGEM-T easy TA cloning and kanamycin for golden gate assemblies). We usually plated 100 µl of transformed cells. Plates with transformed bacteria were incubated over night at 37°C.

6.2.15 Bacterial cultures and plasmid preparation

Mini prep

For small-scale plasmid preparations (Mini prep) 2-5 ml LB medium containing the respective antibiotic were inoculated with a single colony (white colonies when blue-white selection was applied) from the overnight plate using an autoclaved toothpick. 2 ml cultures were grown for 4-5 h at 37°C and 200 rpm, 5 ml cultures were grown o/n. 2 ml of cultures were transferred in 2 ml tubes and spun down for 1 min at 14000 rpm. Supernatant was discarded and the pellet resuspended in 250 µl P1 (10°C). Lysis was done by adding 250 µl P2 at room temperature and mixing by inverting the tube. Immediately afterwards, 250 µl P3 were added for neutralization. The tube was mixed by inverting and the mix then centrifuged for 10 min at 14000 rpm at 10°C. The supernatant was transferred to a fresh 1,5 ml tube and plasmid DNA was precipitated by adding 500 µl isopropanol and shacking. Precipitated plasmid were pelleted by centrifugation (15 min, 4°C and 14000 rpm). The supernatant was discarded and the pellet washed with 500 µl 70% ethanol. After centrifugation (5 min at 14000 rpm) ethanol was removed and the pellet dried at 60°C. Subsequently the DNA-pellet was resuspended in 30 µl H_2O. Plasmids were then tested for proper ligation by restriction digest and successful cloning was confirmed by sequencing.

Midi prep

For large-scale clean plasmid preparation of cloned constructs 80-100 ml LB medium containing either amp or kan were inoculated by adding a drop of positively identified mini-culture. Midi-cultures were grown o/n in 37°C shacking incubator and filled in 50 ml the next day. Cells were pelleted by centrifugation (4000 rpm, 1h at 4°C). Plasmid purification was performed with the QIAGEN Plasmid Midi Kit widely according to the manufacturers instructions. Following changes have been made to the protocol due to equipment limitation. After P3 buffer was added the solution was filtered using QBT equilibrated filter paper that was installed in a funnel on the column directly.

Following centrifugation steps (pelleting plasmid DNA and washing pellet) were performed at 4000 rpm for 45 min each at 4°C. After pellet was dried the plasmid DNA was resuspended in 80 µl TE and DNA concentration was measured using the NanoDrop. DNA was diluted to a concentration of 1 µg/µl with TE whenever possible and stored at -20 °C.

6.2.16 Restriction digest

Restriction digests were performed to test for linearization of plasmids, excise DNA fragments from plasmids for subsequent cloning and to check for successful ligations of inserts in plasmids.

Screening for positive ligation

Whenever possible restriction digests were set up with either FastDigest enzymes (Thermo Scientific) or High Fildelity (HF, NEB) enzymes. For digestion of 5 µl mini-prep 0,1 µl enzyme and 1 µl FD or CutSmart buffer were used in 10 µl volume. The digest was incubated at 37°C for 20 min up to several hours.

6.2.17 Linearizing plasmids for mRNA

For *in situ* probe generation we digested 10 µg of clean plasmid with 1-2 µl of restriction enzyme in 50 µl volume o/n at 37 °C. Following enzymes and buffers were used:

Template	Enzyme	Enzyme volume	Buffer	Promoter for transcription
ISH probe pGEMT easy	SpeI HF (NEB)	1	CutSmart	T7
ISH probe pGEMT easy	NcoI (NEB)	1	CutSmart	SP6
ISH probe pGEMT easy	SacII (Thermo	2	Buffer B (thermo)	Sp6

An aliquot of linearized plasmids were then run on gel, cleaned with the InnuPREP Kit (Analytic Jena) and used for mRNA transcription.

6.2.18 In Situ RNA probe transcription

10 µg of digested plasmid were cleaned up with InnuprepPCRpure Kit or the QIAquick PCR Purification Kit according to the instructions. Elution was carried out with 22 µl RNase free H_2O. The concentration of purified plasmid was determined and 1 µg used for in vitro transcription. Following transcription mix was pipetted on ice, using filter tips:

Component	Volume	Final concentation
Linearized Plasmid	1 µg	50 ng/µl
100 mM DTT	2 µl	10 mM
NTP-Mix	1,3 µl	0,77 mM ATP, CTP, GTP 0,5 mM UTP
10 mM Dig-UTP	0,3 µl	0,35 mM
RiboLock (40 U/µl)	0,5 µl	1 U/µl
10x Transcription Buffer	2 µl	1x
RNase free H_2O	Ad 18 µl	-
RNA-Polymerase (SP6/T7)	2µl	2/U µl

Polymerase was added last, after the rest of the transcription mix was mixed gently. Sp6 polymerase was used for NcoI and SacII digested template vectors and T7 polymerase was used for transcription from SpeI digested plasmids. The reaction mix was incubated fir 3 h at 37°C and then placed on ice. 1 µl TurboDNas (2U/µl) was added and the mix was incubated again at 37°C for 15 minutes. mRNA was then immediately purified using the RNeasy MiniElute Cleanup Kit according to the instructions. RNA was eluted by applying 25 µl H_2O two times. A 2 µl aliquot was used on a RNA gel to test mRNA quality and relative quantity. 150 µm of Hybridization-Mix was added to the rest of the mRNA ISH-probe which was then stored at -80°C.

6.2.19 SgRNA production

Transcription

For production of sgRNAs 12 µg of sgRNA sequence containing DR274 plasmids were digested with 2µl FD-DraI (Thermo Scientific) in 50 µl o/n at 37°C. The digest of was run on a freshly prepared RNAse free agarose gel and the 300 bp band was cut out and purified using the InnuPrep gel purification Kit or the MinElute Kit from Quiagen. 15 µl of H_2O were used for elution and concentration has been measured. 300 ng of DNA were then used for the transcription reaction when possible otherwise

the maximum amount that could be obtained in 6,5 µl. Transcriptions of sgRNAs was done with the MEGAshortscript™ T7 Transcription Kit from Life Technologies according to the manufacturers instructions. After minimum 3 h of incubation at 37°C the, 1 µl of TurboDNase was added to the transcription reaction and incubated for another 15 min at 37°C. The reaction was placed on ice and the clean up was started immediately.

Chloroform extraction and alcohol precipitation

The 20 µl of Megashort-sample were mixed thoroughly with 250 µl of H_2O and Ammonium Acetate Stop (provided with the MEGAshortscript™ T7 Transcription Kit) to stop DNAse digest.

Under the fumehood 300 µl of Roti Aqua-P/C/I (Phenol-Chloroform-Isoamylalkohol 25:24:1, pH 4,5-5) was added, mixed thoroughly and incubated for 5 min at RT. Phases were separated by centrifugation (13.000 rpm at 4°C for 5 min). The upper aqueous phase was transferred to a new tube and same volume of chloroform was added. After thorough mixing and 5 min incubation at RT the mix was centrifuged again at 13.000 rpm and 4°C for 5 min. After centrifugation the upper aqueous phase was transferred to a new tube, 2 vol 100 % EtOH was added and well mixed. For optimal precipitation EtOH RNA mix was incubated at -20 °C for one hour and then centrifuged at 14.000 rpm for 8 min. Supernatant was removed carefully and 500 µl of ice-cold 75% EtOh were added to wash DNA pellet by another 8 min centrifugation at 14.000 rpm and 4°C. The wash step was repeated one time after which the supernatant was removed and the pellet dried for maximum 5 minutes. The pellets were typically diluted in 50 µl of RNAse free H_2O. The RNA concentration was measured and the sgRNA was diluted to 150 ng/µl. The working concentration for all sgRNAs used was 15 ng/µl. The quality of produced sgRNAs (ca. 200 bs) was confirmed by gel-electrophoresis.

6.2.20 Induction of recombination by heat shock

Embryos younger than stage 36 were heat shocked by 1h incubation at 39°C (heating block in tubes) after which they were transferred back to 28°C. Older Embryos and hatchlings were heat shocked by replacing the RT ERM to 42°C warm ERM and

incubating the dish for 2 hours at 37°C. Afterwards hatchlings were kept at RT on the bench until screened the next day.

6.2.21 Induction of recombination by tamoxifen

Hatched embryos of the oncogenes lines crossed to Cre-ERT2 lines were treated with tamoxifen in order to induce recombination. For that hatchlings were placed in six-well plates and fed with arthemia prior to o/n treatment. Tamoxifen was diluted to a concentration of 5 µM in ERM and hatchlings were incubated o/n in the dark. Hatchlings were washed several times the next day and screened for recombination in muscle cells and/or retina. Positive fish were fixed after 2-3 days or placed in the fish room for ArCoS assays.

6.2.22 Cryo-sectioning

For sectioning of hatchlings, adult fish and organs (ovaries, brain) fixed tissue was dehydrated by incubating in 30 % Sucrose at least o/n on 4°C. 30 % Sucrose was then replaced by a 1:1 mix of 30% sucrose and tissue freezing medium and tissues/fish were incubated for several days (minimum 3). Prior to sectioning, fish or tissues were placed in cryomolds, covered with tissue freeze medium, oriented and deep-frozen in liquid nitrogen. When the block was frozen thoroughly it was either placed in the cryostat directly or stored at -80°C. After mounting and orientating the frozen block, sections were cut 16-25 µm thick and collected on specifically coated clean glass slides. Sections were then dried either at RT for at least 4 h or o/n up to three days at 4°C.

6.2.23 Immuno-stainings of cryosections

For staining of sections from 16 to 25 µm the slides were placed in tight plastic containers. Dry sections were rehydrated for 20 min with 1xPTW and blocked for 2 h with 10% NGS/PTW. After rinsing 2x with PTW the 1.AB in 1%NGS/PTW was applied and slides were covered with parafilm, incubation was o/n at 4°C. The next day the slides were washed 3x 10 min with PTW and the 2.AB in 1%NGS/PTW with 1:1000 diluted DAPI was applied and slides were covered with parafilm. The 2.AB was incubated for 2h at 37°C and then washed off 3x 10 min. After washing slides were

dried using a tissue. 60 µl of 60% glycerol was pipetted on stained section and a cover slip was put and sealed with nail polish.

6.2.24 BrdU staining of tissue-cryoscetions

For BrdU stained sections a special treatment was applied on sections previously stained with other antibodies as described in 6.2.23. After 2.AB incubation and wash steps the sections were fixed in 4%PFA for 30 min at RT and washed again 3x10 min with 1xPTW. Sections were then treated for 60 min at 37°C with 2N HCl 0,5%/ TritonX in PTW for antigen retrieval and washed again 3x 10min with PTW. The pH was recovered by applying a 2:3 dilution of saturated Borax in PTW for 15 min. Slides were washed again, blocked for 2 h with 10% NGS /PTW, rinsed with PTW and incubated o/n at 4°C with 1.AB (1:750 a-BrdU (rat) in 1% NGS/PTW). After six 10 min washes with PTW the 2. AB was applied 1:750 in 1%NGS/PTW for 2 h at 37°C. After final washing steps (3x10 min with PTW) the slides were mounted as described in 6.2.23.

6.2.25 Whole mount immunostainings (no heating)

The whole mount staining was used to stain young embryos and hatchlings as well as adult ovaries and brains. Fixed embryos were washed in PTW at least 3x 5min and dechorionated using two forceps. PTW was then removed and replaced by pre-chilled acetone (-20°C). Samples were incubated for 20 min at -20°C. Acetone was removed and samples washed 3x 5 min with PTW. Samples were blocked for 2-3 h with blocking buffer (10% SS or NGS, 1% BSA and 0,8% TritonX100 in PTW). 1. ABs were diluted 1:200 in (1% SS/NGS, 0,8% TritonX100, 1%BSA)/PTW and samples were incubated with 1.AB for two days on turning wheel at 4°C. Samples where then washed 2x 30 min with PBS-TS (1% TritonX100, 1% SS/NGS in 1x PBS) and then 1h with PBST (1%TritonX100 in PBS). After washing secondary AB was diluted in the same way together with 1:500 DAPI and samples were incubated again for 2 days at 4°C in the dark on a turning wheel. Washing steps after 2.AB were the same as for the first AB. Samples were then mounted for imaging in methyl-cellulose or 1% low melting agarose/dH_2O.

6.2.26 Whole mount immuo-staining (heating method)

The whole mount immuno-stainings with the heating method were performed for embryos and hatchlings and organs when the phospho-pErk1/2 antibody was used. The staining protocol was similar as in 6.2.25 except for the heating step before acetone treatment. Samples were placed in 100 mM Tris-HCl (pH 8.0) for 15 min at 70°C (in 1,5 ml tubes on heat block). Samples were then allowed to cool down and washed with PTW 3x 5 min before proceeding to Acetone treatment.

6.2.27 DAPI staining of fertilized oocytes

The staining of fertilized oocytes, which were fixed 2 min to 40 mpf, was performed after fixing for several days with 4%PFA. The oocytes were first dechorionated and then stained o/n in 1:500 DAPI/PTW.

6.2.28 Fixation, dissection and staining of adult retinae

Adult fish were sacrificed by 20x tricane treatment and fixed in 4%PFA/2XPTW for at least one week. Fish were washed for several hours with PTW replacing it at least five times. Heads of fish were cut using a scalpel and bleached in 3%H_2O_2, 0,5% KOH in H_2O in six-well plates shacking. After 1-2 hours fish-heads were washed with PTW and retinae were dissected carefully using two sharp forceps, the lens was removed. Retinae were bleached again in described ways until all pigmentation disapeared. The retinae were rinsed in PTW two times and incubated in pre-cooled acetone at -20°C for 15 min. Retinae were again rinsed with PTW, then washed 2x 5 min in PTW on the shaker and blocked in 1 ml blocking buffer (4% SS, 1% BSA, 1% DMSO in 1xPTW) o/n rotating at 4°C. A 1:200 dilution of the 1. AB in blocking buffer was prepared the next day and retinae were incubated for at least two o/n at 4°C on a rotor. After 1.AB incubation retinae were washed in 10 cm petri dishes on shaker at least 5 times for 30 min. The 2.AB was diluted 1:200 in blocking buffer together with 1:500 DAPI and retinae were incubated in it o/n rotating at 4°C in the dark.

6.2.29 Fixation, dissection of adult ovaries

For dissection of ovaries and other organs from WT and Egfra mutants, fish were treated with 20x tricane. When fish were dead the tail was removed with a razor blade and the belly was opened with a forceps to extract ovaries and other organs. Ovaries and other organs were then fixed separately in 4%PFA/PTW for several days or frozen in liquid nitrogen for protein and mRNA extraction.
Adult ovaries were stained as described in chapter 6.2.25 and 6.2.26 for phosphorylated-pErk1/2 and a-tubulin.

6.2.30 Preparation of hatchlings for in vivo imaging

Hatchlings were anaesthetized in 1x tricane and mounted in 1% low melting agarose (LMA) in ERM in a glass bottom dish (MaTEC-dish). For that hatchlings were transferred to the agarose tube and from there pipetted onto the glass bottom of the dish with 160 µl of LMA. Fish were oriented for imaging and agarose was allowed to solidify before overlaying the agarose with 1xtricane/ERM. In vivo imaging was mostly carried out under the Leica TCS SPE and in some cases (fu_Mitf::GFP line) under the Leica TCS SP5 using the two-photon setup.
Embryos injected with H1-texasred were mounted the same way (but no tricane) and embryos were imaged under the Leica TCS SPE for several hours.

6.2.31 Preparation of fixed tissue for imaging

Fixed tissue or whole mount embryos were mounted with 3% methyl-cellulose in MaTeC glass bottom dishes in order to be able to reorient the specimen faster.

6.2.32 Screening and imaging

General screening for phenotypes of FP expression was performed using the Nikon AZ100 Multizoom macrofluorescence binocular. Hatched fish were anaesthetized in 1xTricane/ERM before screening.

6.2.33 Whole mount *in situ* hybridization (WISH)

Embryo preparation

Embryos for ISH were collected for stage 18 and 24 from Cab and for later stages and hatchlings from Heinos. Embryos were grown until desired stage and fixed with 4% PFA for several days at 4°C. Hatchlings were grown until hatch, euthanized with 20x tricane and fixed in 4% PFA at least o/n.

After fixation all embryos and hatchlings were washed at least 5 times for 5 min with PTW and embryos were dechorionized using two forceps. Embryos were then stored in 100% MeOH at -20 °C for at least one week.

Proteinase digestion and postfixation

All steps were performed in a 6 well culture dish with a standard volume of 5 ml.

Embryos were rehydrated by incubation in a serial section of 75, 50 and 25 MeOH/PTW for five minutes each on a shaker. Embryos were then rinsed two times five minutes in PTW (on shaker) and digested with 1 µg/ml proteinase K dependent on the developmental stage of the embryo:

Embryonic stage	Time of proteinase digest
18	5 min
24	7 min
32	45 min
Hatchling	2 hours

After proteinase K digest embryos were rinsed two times shortly with freshly prepared 2 mg/ml glycine/PTW after which they were fixed in 4% PFA/PTW for 20 min. Fixation was followed by five times washing for five min with PTW.

Hybridization

Hybridization mix was defrosted and warmed up to RT. Embryos were transferred to 2 ml tubes and 1 ml of RT warm Hyb-mix was added. After embryos sank to the bottom of the tube it was placed in a 65°C water bath for pre-hybridization (2 hours). RNA ISH probes were natured in 200 µl Hyb mix by heating for 10 min to 80°C. We used between 2-5 µl probe per 100 µl Hyb-Mix. When probe was denatured, Hyb-mix

was taken off the embryos and probe-mix was applied. Embryos were incubated for hyrbridization o/n at 65°C.

Washes

The next day washing solutions were all pre heated to 65°C and wash steps were performed at the same temperature. Embryos were washed two times for 30 min with 2 ml 50%Formamide/4xSSCT, then two times for 15 min with 2 ml 2xSSCT and finally two times 30 min with 2ml 0,2xSSCT. After the last wash step embryos were brought back to RT.

Detection

Embryos were blocked for 1-2 h with 5% SS/PTW at RT on a turning wheel. Embryos were then incubated with anti-Dig-AP Fab Fragments (1:2000) in 400 µl PTW/5%SS o/n at 4°C on a turning wheel.

The next day staining buffer (SB) was prepared freshly. Embryos were transferred to 6-well plates and washed 6x for 10 min while shaking in PTW at RT. Embryos were equilibrated in SB 2x for 5 minutes while shaking. 4,5 µl NBT (finale concentration: 337,5 µg/ml) and 3,5 µl BCIP (final 175 µg/ml) per 1 ml SB were dissolved and applied to embryos in 12-well plates. Embryos were stained up to 24 hrs and then washed 3x 5min in PTW and destained using a serial dilution series of EtOH (50, 75, 100 % EtOH) and incubating for 1 hour shacking. Embryos were then rehydrated and fixed for 20 min in 4%PFA/PTW. For imaging of embryos they were then stored in 87% glycerol for several day before they were mounted and imaged with the Zeiss microscope.

For preparation of vibratome sections from hatchlings and embryos they were stored in PTW after fixation until they were mounted in gelatin.

6.2.34 WHISH of Medaka embryos using the in situ robot

For developmental stage 24, 28 and 32 WISH where performed with the in situ robot. Rehydration, Proteinase K treatment and post fixation where done as described in previous chapter. Per stage and probe a minimum of five embryos were transferred from 1xPTW in small nets that where then mounted in the device. The bufferes A, B, C, D, E, F, G, L and M were prepared in assigned tubes and placed in the machine.

The machine can hold up to 30 samples and all volumes given in the table are based on the maximum number of samples.

Buffer	Component	Volume
A	1xPTW	150 ml
	20% Tween 20	750 µl
B	Hybridization mix	15 ml
C	4xSSCT	15 ml
	100% Formamide	15 ml
D	2x SSCT	30 ml
E	0,2xSSCT	30 ml
F	TRIS-HCL pH 7,5	2,5 ml
	NaCl	500 µl
	20%Tween20	125 µl
	water	ad 25 ml
L	2x Malate-Buffer pH 7,5	10 ml
	10%Blocking Reagent	4 ml
	20% Tween20	100 µl
	Water	ad 20 ml
M	Blocking Buffer L	9 ml
	Anti-Dig AB Fab-Fragment	4,5 µl

The Blocking solution L was allowed to settle and only the supernatant was used to not block the robots pump device.

All probes were repared in 0,5 ml tubes by diluting them 1/50 to 1/20 in hybridization mix. The probes were denatured by heating for 10 minutes at 80 °C and placed in the machine according to pre-determined order. When everything but buffer G (staining buffer, as previously described) was placed in the machine the machines program was started. The next day buffer G was freshly prepared (see protocol staining buffer in WISH protocol) and placed in the robot. The robot then finished the protocol and samples were removed from the nets and placed in 24-wellplates to start the staining procedure. Staining was performed as described before for 3-5 h in the dark. Embryos were then washed, destained with EtOH and post-fixed in 4%PFA. Embryos were placed in 87% glycerol for imaging of kept in PTW at 4°C for vibratome sectioning.

Sections and whole embryos were imaged using an Axio Imager ZEISS upright microscope with DIC filters.

6.2.35 Vibratome sectioning of WISH embryos and mounting

For vibratome sectioning of hatchlings and stage 32 embryos, 3 cm wide plastic dishes were filled with 2,5 ml gelatin/albumnin and 1-3 embryos were oriented in the gelatin. For polymerization 200 µl of glutaraldehyde solution was added and mixed by pipetting with blue tips. Embryos were re-oriented quickly before polymerization was completed. A small gelatin block, around the embryo to be sectioned, was cut out using a scalpel and glued on a metal block that was mounted in the vibratome. The gelatin was then submerged in a water-bath and cut in 25 µm thick sections. Single sections were collected using two fine brushes and placed in 64 well plates filled with water. The single sections were then moved to a glass slide and water was removed as good as possible. 60 µl moviol was used to mount the sections under a cover slip.

6.2.36 In situ hybridizationon paraffin sections

For the detection of mRNA of *egfrs* and ligand in ovaries together with Narges Aghaallaei we performed ISH on paraffin sections of adult WT IdU treated fish (kindly provided by Narges Aghaallaei). Slides with paraffin sections were kept at 4°C and dried in the incubator at 37°C for 20 minutes after being placed in an RNAse free Coblin jar. Sections were dewaxed by 15 min incubation in Xylol and washed afterwards with 100% EtOH for 5 min. Sections were then rehydrated by incubating for 2 min each in 95%, 90%, 70% and 30 % EtOH. After washing 5 min with PBS sections were fixed in 4% PFA/PBS for 20 min and washed again 2x for 5 min with PBS. Sectioned tissue was then digested with 10 µg/ml Proteinase K/0,1M Tris pH7,5 for 10 min at 37°C. The digest was stopped by incubating slides for 10 min in 0,2% Glycine/PBS (freshly prepared). After a 2x 5 min wash with PBS sections were washed with 0,2 N HCl for 15 min and again 2x 5 min with PBS. Then sections were incubated in 0,1 M Triethanolamin pH 8,0/0,25% Acetic-anhydride (freshly prepared) under strong stirring. This step was followed by a 5 min wash in PBS and 5 min wash in H_2O.

Pre-hybridization was performed after an 5 min incubation in RNAse free water (MilliQ). 150 ml of Pre-hybridization buffer were prepared as following.

Pre-hybridization Buffer Component	Volume for 150 ml
100 % Formamide	75 ml
20 SSC pH7,5	37,5 ml
100x Denhardt's solution	1,5 ml
20x Tween20	0,75 ml
H_2O	35, 25 ml

Slides were incubated in pre-hybridization buffer for 2 hours at 70°C.
5 µl of each probe placed in one PCR (100 µl) tube and heated up to 70°C for 10 min. In parallel 1:200 tRNA was heated up to 70°C and 5 µl were added to 1 ml pre-hybridization buffer to make the hybridization buffer. 60 µl of hybridization buffer was added to each probe and incubated for another couple of minutes at 70°C. Probe was then applied to the sections and a cover slip was placed atop. The hybridizing slides were then placed in an air-proof humid container at 65°C o/n.
The next day following solutions were prepared:

Solution	Component	Volume for 200 ml
1	Formamide	100 ml
	20xSSC pH 4,5	50 ml
	20% SDS	10 ml
	Water	30 ml
2	Formamide	100 ml
	20xSSC pH 4,5	20 ml
	20% SDS	4 ml
	Water	76 ml

Solution 1 and 2 were warmed up to 65°C before cover slides were removed from hybridized section. Slides were then placed in a Coblin jar containing pre-warmed solution 1 in which they were incubated 3x 30 min at 65°C. Solution 1 was then replaced with solution 2 and incubated 2x 30 min at 60°C. Slides were then washed 3x 5 min in MAB at RT and blocked for 3 h in MAB/1%Blocking Reagent. The slides where then covered with 100 µl AB-solution (1:4000 anti-Dig fab Fragment AB in

MAB/1%Blocking Reagent) and a cover slip and incubated o/n at 4°C in a humid chamber.

The next day cover slips were removed and slides were rinsed with MAB. Then slides were washed 3x 10 min and 3x 30 min with MAB and 3x 10 min with NTNT. Sections were then stained with BM Purple/2mM Levamisol in plastic containers by placing the sections upside down on the staining solution. Sections were then stained in the dark for three days at 4°C. The plastic container was kept from drying by closing container with parafilm. Since no obvious staining could be detected after three days the AB incubation was repeated. Sections where thus washed in water, blocked again, then and incubated o/n with 1:1000 anti-Dig fab fragments AB. From then on all steps were repeated as described before. After staining the straining solution was washed with pure water and sections were left to dry a bit and mounted with moviol.

6.2.37 IR-lego

For the local induction of heat-responsive elements in vivo we used an laser-evoked gene operator system as published in (Deguchi et al. 2009; Kamei et al. 2009).

HSindX_H2B-GFP embryos were kept in heat-stable conditions until hatch and then anesthetized and mounted with methylcellulose (to prevent heat shock by warmed up agaraose) in glass bottom dishes. The dishes were mounted onto an inverse spinning disc microscope coupled to an infrared (IR) later (1480nm). Fish were mounted in a way that regions of interest were closest to the objective to reduce energy loss (figure 16A). The target region was then selected using the bright field channel and applied laser pulses with an energy of 60-100 mw for 1 to 3 seconds until we could see twitching of cells. The region of IR-Lego activity was determined before by testing the bleaching of Flourescin by laser exposure. This experiment was conducted with the help of Jan-Felix Evers and Franz Kuchling.

III. Contributions

Clara Baader clones several in situ probes and most of the bench work for the WISH screen for Egfr-signaling components during her Bachelor thesis. She also helped with screening the F2 of Egfra mutant fish.

Clara Becker did most of the cloning work for the oncogene lines (mostly Golden Gate assemblies of final constructs) and injected and performed initial tests of the Oncogene lines (Figures 17-19) during her Master Thesis.

Dr. Narges Aghaallaei did the injections and took the picture for double clonal expression of oncogenes in figure 20 and helped with the ISHs on ovary sections for which she also provided the material.

Daigo Ioune did the staining of unfertilized oocytes and the a-tub, pH3 stainings of Egfra-/-embryos 4hpf (figure 31).

Katharina Lust did the immuno-stainings of the Fu_Mitf::GFP line in figure 37 D.

IV. Abbreviation list

A	Anterior
AB	Antibody
ADAM	A disintegrin And metalloprotease
AKT (PKB)	Protein Kinase B
AP	Alkaline Phosphatase
ArCoS	Arched COntinuous Stripe
AREG	Amphiregulin
ath5	Atonal bHLH transcription factor 7
BCIP	5-Bromo-4-chloro-3-indolyl phosphate
bp	base pair
BSA	Bovine Serum Albumin
BTC	Betacellulin
cDNA	Complementary DNA
CFP	Cyan fluorescent protein
CMZ	Ciliary Marginal Zone
CNS	Central Nervous System
Cre	Cyclization recombinase
CTP	Cytidine triphosphate
D	Dorsal
DNA	Deoxyribonucleic Acid
DAPI	4',6-diamidino-2-phenylindole
DIG	Digoxigenin
DMSO	Dimethyl sulfoxide
dNTP	2'deoxy-nucleotide-tri-phosphate
dpf	Days post fertilization
DTT	Dithiothreitol
E.coli	Escherichia coli
eCFP	Enhanced cyan fluorescent protein
EDTA	Ethylenediamine-tetraacetic acid
EGF	Epidermal growth factor
eGFP	Enhanced green fluorescent protein
EGFR	Epidermal growth factor receptor
egfra	Epidermal growth factor receptor a
egfrb	Epidermal growth factor receptor b
EPGN	Epigen
ErbB	Erb-B receptor tyrosine kinase
EREG	Epiregulin
Erk	Extracellular signal-regulated kinase
ERM	Embryo rearing medium
EtBr	Ethidium bromide
EtOH	Ethanol
FGF	Fibroblast growth factor
FGFR	Fibroblast growth factor receptor
FL	Flexible linker

FP	Fluorescent protein
fwd	Forward
GCL	Ganglion cell layer
gDNA	Genomic deoxyribonucleic acid
GFP	Green fluorescent protein
Grb2	Growth factor receptor-bound protein 2
GTP	Guanosine triphosphate
h	Hour
H_2O	Water
H_2O_2	Hydrogen peroxide
Hb-egf	Heparin-binding EGF-like growth factor
hpf	Hour post fertilization
IGF	Insulin-like growth factor
IGFR	Insulin-like growth factor receptor
INL	Inner nuclear layer
ISH	In situ hybridisation
K-RAS	Kirsten rat sarcoma viral oncogene homolog
LB	Lisogeny broth
MAPK	Mitogen-activated protein kinase
MC	Micropylear cell
MeOH	Methanol
MGC	Müller glia cell
MP	Micropyle
MCS	Multiple cloning site
MEK	Mitogen-activated protein kinase kinase
min	Minute
mpf	Minutes post fertilization
mRNA	Messenger ribonucleic acid
myrAKT	Myristoylated protein kinase B
NaCl	Sodium chloride
NaOH	Sodium hydroxide
NBT	Sodium bismuth titanate
NFκB	Nuclear factor 'kappa-light-chain-enhancer' of activated B-cells
NGS	Normal goat serum
NLS	Nuclear localization signal
NPC	Neural progenitor cell
NR	Neural retina
NSC	Neural stem cell
ONL	Outer nuclear layer
ORF	Open reading frame
OT	Optic tectum
P	Posterior
PBS	Phosphate buffered saline
PCR	Polymerase chain reaction
pErk	Phospho-p44/42 MAPK (Erk1/2) (Thr202/Tyr204)
PFA	Paraformaldehyde
PI3K	Phosphoinositide-3 kinase
PKB	Protein kinase B
PKC	Protein kinase C

PLCγ	Phosoholipase Cγ
PTW	Phosphate buffered saline + tween-20
qRT-PCR	Quantitative reverse transcription PCR
RAS	Rat sarcoma
rev	Reverse
RNA	Ribonucleic acid
RPC	Retinal progenitor cell
RPE	Retinal pigment epithelium
RSAKT	Red switch myrAKT
RSC	Retinal stem cell
RSG	Red switch green
RSK-RAS	Red switch K-RAS
RSX	Red switch Xmrk
RSXFLGFP	Red switch Xmrk flexible linker GFP
RSXT2AGFP	Red switch Xmrk T2A GFP
RT	Room temperature
RT-PCR	Reverse transcripase-PCR
RTK	Receptor tyrosine kinase
Rx2	Retinal homeobox gene 2
SB	Staining buffer
SC	Rtem cell
SDS	Sodium dodecyl sulfate
sgRNA	Single guide RNA
SOS	Son of Sevenless
SS	Sheep serum
STAT	Signal transducer and activator of transcription
SVZ	Sub ventricular zone
TAE	Tris-acetate EDTA buffer
TGF-β	transforming growth factor β
TGFα	transforming growth factor α
tlx	T-cell leukemia
Tris	2-amino-2-hydroxymethylpropane-1,3-diol
tTA	Tetracycline transactivator
ubi	Ubiquitin promoter
UTP	Uridine triphosphate
V	Ventral
wa-2	Waved-2
WISH	Whole mount in situ hybridization
wpf	Weeks post fertilization
WT	Wild type
X-gal	5-bromo-4-chloro-3-indolyl-β-D-galactopyranoside
Xmrk	Xiphophorus Melanoma Receptor Kinase

V. References

Abe, Gembu, Maximilliano L. Suster, and Koichi Kawakami. 2011. 104 Methods in Cell Biology *Tol2-Mediated Transgenesis, Gene Trapping, Enhancer Trapping, and the Gal4-UAS System*. Third Edit.

Aguirre, Adan, Maria E. Rubio, and Vittorio Gallo. 2010. "Notch and EGFR Pathway Interaction Regulates Neural Stem Cell Number and Self-Renewal Adan." *Nature* 467(7313): 323–27.

Ahuja, M.R., and F. Anders. 1976. "A Genetic Concept of the Origin of Cancer, Based in Part upon Studies of Neoplasms in Fishes." *Prog Exp Tumor Res* 20: 380–97.

Alghisi, E et al. 2013. "Targeting Oncogene Expression to Endothelial Cells Induces Proliferation of the Myelo-Erythroid Lineage by Repressing the Notch Pathway." *Leukemia* 27(11): 2229–41.

Alunni, Alessandro et al. 2010. "Evidence for Neural Stem Cells in the Medaka Optic Tectum Proliferation Zones." *Developmental neurobiology* 70(10): 693–713.

Amato, Marcos a, Emilie Arnault, and Muriel Perron. 2004. "Retinal Stem Cells in Vertebrates: Parallels and Divergences." *The International journal of developmental biology* 48(8–9): 993–1001.

Angénieux, Brigitte, Daniel F Schorderet, and Yvan Arsenijevic. 2006. "Epidermal Growth Factor Is a Neuronal Differentiation Factor for Retinal Stem Cells in Vitro." *Stem cells (Dayton, Ohio)* 24(3): 696–706.

Arai, R et al. 2001. "Design of the Linkers Which Effectively Separate Domains of a Bifunctional Fusion Protein." *Protein engineering* 14(8): 529–32.

Aroian, Raffi V et al. 1990. "The Let-23 Gene Necessary for Caenorhabditis Elegans Vulval Induction Encodes a Tyrosine Kinase of the EGF Receptor Subfamily." *Nature* 348: 693–99.

Bachoo, R M et al. 2002. "Epidermal Growth Factor Receptor and Ink4a/Arf: Governing Terminal Differentiation and Transformation Stem Cell to Astrocyte Axis." *Cancer Cell* 1(3): 269–77.

Barker, Nick et al. 2009. "Crypt Stem Cells as the Cells-of-Origin of Intestinal Cancer." *Nature* 457(7229): 608–11.

Bernardos, R L, L K Barthel, J R Meyers, and P A Raymond. 2007. "Late-Stage Neuronal Progenitors in the Retina Are Radial Muller Glia That Function as Retinal Stem Cells." *J Neurosci* 27(26): 7028–40.

Blanpain, Cédric, and Elaine Fuchs. 2006. "Epidermal Stem Cells of the Skin." *Annu Rev Cell Dev Biol* 22: 339–373.

Blechinger, Scott R. et al. 2002. "The Heat-Inducible Zebrafish hsp70 Gene Is Expressed during Normal Lens Development under Non-Stress Conditions." *Mechanisms of Development* 112(1–2): 213–15.

Blobel, Carl P. 2005. "ADAMs: Key Components in EGFR Signalling and Development." *Nature reviews. Molecular cell biology* 6(1): 32–43.

Boomsma, R a, H Scott, and K Walters. 2001. "Immunocytochemical Localization of Epidermal Growth Factor Receptor in Early Embryos of the Japanese Medaka Fish (Oryzias Latipes)." *The Histochemical journal* 33(1): 37–42.

Boucher, Shayne-Emile M, and Peter F Hitchcock. 1998. "Insulin-Related Growth Factors Stimulate Proliferation of Retinal Progenitors in the Goldfish." *The Journal of Comparative Neurology* 394(3): 386–94.

Breitfeld, P P, and W H Meyer. 2005. "Rhabdomyosarcoma: New Windows of Opportunity." *Oncologist* 10(7): 518–27.

Brucker, Cosima, Nancy J. Alexander, Gary D. Hodgen, and Bruce A. Sandow. 1991. "Transforming Growth Factor-Alpha Augments Meiotic Maturation of Cumulus Cell-Enclosed Mouse Oocytes." *Molecular Reproduction and Development* 28(1): 94–98.

Buday, László, and Julian Downward. 2017. "Epidermal Growth Factor Regulates p21ras through the Formation of a Complex of Receptor, Grb2 Adapter Protein, and Sos Nucleotide Exchange Factor." *Cell* 73(3): 611–20.

Buhrow, S A, S Cohen, and J V Staros. 1982. "Affinity Labeling of the Protein Kinase Associated with the Epidermal Growth Factor Receptor in Membrane Vesicles from A431 Cells." *J.Biol.Chem.* 257: 4019–22.

Buratini, J, and E S Caixeta. 2012. "Paracrine and Autocrine Factors in the Differentiation of the Cumulus-Oocyte Complex." 3: 414–19.

Centanin, Lazaro et al. 2014. "Exclusive Multipotency and Preferential Asymmetric Divisions in Post-Embryonic Neural Stem Cells of the Fish Retina." *Development (Cambridge, England)*: 3472–82.

Centanin, Lazaro, Burkhard Hoeckendorf, and Joachim Wittbrodt. 2011. "Fate Restriction and Multipotency in Retinal Stem Cells." *Cell stem cell* 9(6): 553–62.

Clark, Wallis H. 1982. "Fine Structure of the Envelope and Micropyles in the Eggs of the White Sturgeon , Acipenser Transmontanus." 24: 341–52.

Codega, Paolo et al. 2014. "Prospective Identification and Purification of Quiescent Adult Neural Stem Cells from Their In Vivo Niche." *Neuron* 82(3): 545–59.

Cohen, S. 1962. "Isolation of a Mouse Submaxillary Gland Protein Accelerating Incisor Eruption and Eyelid Opening in the New-Born Animal." *The Journal of biological chemistry* 237(6): 1555–62.

Cohen, S, H Ushiro, C Stoscheck, and M Chinkers. 1982. "A Native 170 000 Epidermal Growth Factor Receptor-Kinase Complex from Shed Plasma Membrane Vesicles." *Journal of Biological Chemistry* 257(3): 1523–31.

Cook, Paul W. et al. 1997. "Transgenic Expression of the Human Amphiregulin Gene Induces a Psoriasis-like Phenotype." *Journal of Clinical Investigation* 100(9): 2286–94.

Coskun, S, and Y C Lin. 1995. "Mechanism of Action of Epidermal Growth Factor-Induced Porcine Oocyte Maturation." *Mol.Reprod.Dev.* 42: 311–17.

Coskun, Serdar, and Young C. Lin. 1994. "Effects of Transforming Growth Factors and Activin-A on in Vitro Porcine Oocyte Maturation." *Molecular Reproduction and Development* 38(2): 153–59.

Dackor, Jennifer, Kathleen M. Caron, and David W. Threadgill. 2009. "Placental and Embryonic

Growth Restriction in Mice with Reduced Function Epidermal Growth Factor Receptor Alleles." *Genetics* 183(1): 207–18.

Deguchi, Tomonori et al. 2009. "Infrared Laser-Mediated Local Gene Induction in Medaka, Zebrafish and Arabidopsis Thaliana." *Development Growth and Differentiation* 51(9): 769–75.

Dekel, Nava, and Israelit Sherizly. 1985. "Epidermal Growth Factor Induces Maturation of Rat Follicle-Enclosed Oocytes." *Endocrinology* 116(1): 406–9.

Dekens, Marcus P S, Francisco J Pelegri, Hans-Martin Maischein, and Christiane Nüsslein-Volhard. 2003. "The Maternal-Effect Gene Futile Cycle Is Essential for Pronuclear Congression and Mitotic Spindle Assembly in the Zebrafish Zygote." *Development (Cambridge, England)* 130(17): 3907–16.

Dhomen, Nathalie et al. 2009. "Oncogenic Braf Induces Melanocyte Senescence and Melanoma in Mice." *Cancer cell* 15(4): 294–303.

Diaz, F J, Karen Wigglesworth, and John J Eppig. 2007. "Oocytes Determine Cumulus Cell Lineage in Mouse Ovarian Follicles." *Journal of cell science* 120(Pt 8): 1330–40.

Dimitrijevic, N et al. 1998. "Activation of the Xmrk Proto-Oncogene of Xiphophorus by Overexpression and Mutational Alterations." *Oncogene* 16(13): 1681–90.

Elinson, and R P. 1986. "Fertilization in Amphibians - the Ancestry of the Block To Polyspermy." *International Review of Cytology-a Survey of Cell Biology* 101: 59–100.

Eppig, John J. 2001. "Review Oocyte Control of Ovarian Follicular Development and Function in Mammals." : 829–38.

Fan, Qi Wen et al. 2013. "EGFR Phosphorylates Tumor-Derived EGFRvIII Driving STAT3/5 and Progression in Glioblastoma." *Cancer Cell* 24(4): 438–49.

Feitsma, Harma, and Edwin Cuppen. 2008. "Zebrafish as a Cancer Model." *Molecular cancer research : MCR* 6(5): 685–94.

Feng, Hui et al. 2007. "Heat-Shock Induction of T-Cell Lymphoma/leukaemia in Conditional Cre/lox-Regulated Transgenic Zebrafish." *British journal of haematology* 138(2): 169–75.

Feng, Yi et al. 2010. "Live Imaging of Innate Immune Cell Sensing of Transformed Cells in Zebrafish Larvae: Parallels between Tumor Initiation and Wound Inflammation." *PLoS Biology* 8(12).

Fernandez, André A., and Paul R. Bowser. 2010. "Selection for a Dominant Oncogene and Large Male Size as a Risk Factor for Melanoma in the Xiphophorus Animal Model." *Molecular Ecology* 19(15): 3114–23.

Fischer, Andy J., and Thomas A. Reh. 2003. "Growth Factors Induce Neurogenesis in the Ciliary Body." *Developmental Biology* 259(2): 225–40.

Foudi, Adlen et al. 2009. "Analysis of Histone 2B-GFP Retention Reveals Slowly Cycling Hematopoietic Stem Cells." *Nature biotechnology* 27(1): 84–90.

FregosoLomas, Mariana, Fiona Hails, Jean François Boisclair Lachance, and Laura A. Nilson. 2013. "Response to the Dorsal Anterior Gradient of EGFR Signaling in Drosophila Oogenesis Is Prepatterned by Earlier Posterior EGFR Activation." *Cell Reports* 4(4): 791–802.

Friedlander, Sharon Y Gidekel et al. 2009. "Context-Dependent Transformation of Adult Pancreatic

Cells by Oncogenic K-Ras." *Cancer Cell* 16(5): 379–89.

Fukumatsu, Y, H Katabuchi, and H Okamura. 1995. "Immunohistochemical Localization of Epidermal Growth Factor and Its Effect on Granulosa Cell Proliferation in Rat Ovary." *Endocrine journal* 42(4): 467–73.

Gabay, L, R Seger, and B Z Shilo. 1997. "In Situ Activation Pattern of Drosophila EGF Receptor Pathway during Development." *Science (New York, N.Y.)* 277(August): 1103–6.

Geissinger, Eva et al. 2002. "Autocrine Stimulation by Osteopontin Contributes to Antiapoptotic Signalling of Melanocytes in Dermal Collagen." *Cancer Research* 62(16): 4820–28.

Ginsburg, A. S. 1961. "The Block to Polyspermy in Sturgeon and Trout with Special Reference to the Role of Cortical Granules (Alveoli)." *Journal of Embryology and Experimental Morphology* 9(1): 173–90.

Ginzburg, A S. 1968. Academy of Sciences of the USSR Institute of Development Biology *Fertilization in Fishes and the Problem of Polyspermy*. ed. T A Detlaf.

Goishi, Katsutoshi et al. 2003. "Inhibition of Zebrafish Epidermal Growth Factor Receptor Activity Results in Cardiovascular Defects." *Mechanisms of Development* 120(7): 811–22.

Goll, Mary G. et al. 2009. "Transcriptional Silencing and Reactivation in Transgenic Zebrafish." *Genetics* 182(3): 747–55.

Gomes Heck, T et al. 2012. "Role of Heat Shock Proteins in Skeletal Muscle." In *Skeletal Muscle – From Myogenesis to Clinical Relations*, ed. Julianna Cseri. , 105–22.

Gómez, Ana et al. 2004. "Identification of a Second Egfr Gene in Xiphophorus Uncovers an Expansion of the Epidermal Growth Factor Receptor Family in Fish." *Molecular biology and evolution* 21(2): 266–75.

Göritz, F, K Jewgenowyer, and HHD Meyer. 1996. "Epidermal Growth Factor and Epidermal Growth Factor Receptor in the Ovary of the Domestic Cat." *Journal of Reproduction and Fertility* 106(May): 117–24.

Gossen, M et al. 1995. "Transcriptional Activation by Tetracyclines in Mammalian Cells." *Science* 268(5218): 1766–69.

Gressot, Loyola V. et al. 2015. "Signal Transducer and Activator of Transcription 5b Drives Malignant Progression in a PDGFB-Dependent Proneural Glioma Model by Suppressing Apoptosis Loyola." *Int J Cancer* 136(9): 2047–54.

Herbst, R S. 2004. "Review of Epidermal Growth Factor Receptor Biology." *Int J Radiat Oncol Biol Phys* 59(2 Suppl): 21–26.

Heron-Milhavet, Lisa, Nabil Khouya, Anne Fernandez, and Ned J Lamb. 2011. "Akt1 and Akt2: Differentiating the Aktion." *Histology and histopathology* 26(5): 651–62.

Högnason, T et al. 2001. "Epidermal Growth Factor Receptor Induced Apoptosis: Potentiation by Inhibition of Ras Signaling." *FEBS letters* 491(1–2): 9–15.

Hsieh, Minnie, Kao Thao, and Marco Conti. 2011. "Genetic Dissection of Epidermal Growth Factor Receptor Signaling during Luteinizing Hormone-Induced Oocyte Maturation." *PLoS ONE* 6(6).

Iwamatsu, Takashi. 2004. "Stages of Normal Development in the Medaka Oryzias Latipes Q."

Mechanisms of Development 121: 605–18.

Iwamatsu, Takashi, Kazuo Onitake, Yasuaki Yoshimoto, and Yukio Hiramoto. 1991. "Time Sequence of Early Events in Fertilization in the Medaka Egg. (Micropyle/exocytosis/sperm Movement/calcium Release/medaka Egg)." *Development, Growth and Differentiation* 33(5): 479–90.

Iwamatsu, T Ohta, E Oshima, and N Sakai. 1988. "Oogenesis in the Medaka Oryzias Latipes : Stages of Oocyte Development." *Zoological Science* 5: 353–73.

Jamnongjit, Michelle, Arvind Gill, and Stephen R Hammes. 2005. "Epidermal Growth Factor Receptor Signaling Is Required for Normal Ovarian Steroidogenesis and Oocyte Maturation." *Proceedings of the National Academy of Sciences* 102(45): 16257–62.

Kamei, Yasuhiro et al. 2009. "Infrared Laser-Mediated Gene Induction in Targeted Single Cells in Vivo." *Nature methods* 6(1): 79–81.

Kanda, T, K F Sullivan, and G M Wahl. 1998. "Histone-GFP Fusion Protein Enables Sensitive Analysis of Chromosome Dynamics in Living Mammalian Cells." *Current biology : CB* 8(7): 377–85.

Kassahn, Karin S et al. 2009. "Evolution of Gene Function and Regulatory Control after Whole-Genome Duplication : Comparative Analyses in Vertebrates Evolution of Gene Function and Regulatory Control after Whole-Genome Duplication : Comparative Analyses in Vertebrates." : 1404–18.

Kim, Carla F Bender et al. 2005. "Identification of Bronchioalveolar Stem Cells in Normal Lung and Lung Cancer." *Cell* 121(6): 823–35.

Kinoshita, Masato, Kenji Murata, Kiyoshi Naruse, and Minoru Tanaka. 2009. "Reproduction of Medaka." In *Medaka: Biology, Management, and Experimental Protocols*, , 72–74.

Kirchmaier, Stephan, Katharina Lust, and Joachim Wittbrodt. 2013. "Golden GATEway Cloning - A Combinatorial Approach to Generate Fusion and Recombination Constructs." *PloS one* 8(10): e76117.

Knopf, Franziska et al. 2010. "Dually Inducible TetON Systems for Tissue-Specific Conditional Gene Expression in Zebrafish." *Proceedings of the National Academy of Sciences of the United States of America* 107(46): 19933–38.

Kornblum, Harley I. et al. 1998. "Abnormal Astrocyte Development and Neuronal Death in Mice Lacking the Epidermal Growth Factor Receptor." *Journal of Neuroscience Research* 53(6): 697–717.

Kudlow, Jeffrey E et al. 1987. "Ovarian Transforming Growth Factor- a Gene Expression: Im-Munohistochemical Localization to the Theca-Interstitial Cells." *Endocrinology* 121(4): 1577–79.

Kunzevitzky, Noelia J., Monica V. Almeida, and Jeffrey L. Goldberg. 2010. "Amacrine Cell Gene Expression and Survival Signaling: Differences from Neighboring Retinal Ganglion Cells." *Investigative Ophthalmology and Visual Science* 51(7): 3800–3812.

Kuroyanagi, Yoshiko et al. 2010. "Proliferation Zones in Adult Medaka (Oryzias Latipes) Brain." *Brain Research* 1323: 33–40.

Laisney, Juliette a G C et al. 2010. "Lineage-Specific Co-Evolution of the Egf Receptor/ligand Signaling

System." *BMC evolutionary biology* 10: 27.

Lang, L, D Miskovic, M Lo, and J J Heikkila. 2000. "Stress-Induced, Tissue-Specific Enrichment of hsp70 mRNA Accumulation in Xenopus Laevis Embryos." *Cell stress & chaperones* 5(1): 36–44.

Langenau, David M. et al. 2007. "Effects of RAS on the Genesis of Embryonal Rhabdomyosarcoma." *Genes and Development* 21(11): 1382–95.

Laubichler, Manfred D., and Eric H. Davidson. 2008. "Boveri's Long Experiment: Sea Urchin Merogones and the Establishment of the Role of Nuclear Chromosomes in Development." *Developmental Biology* 314(1): 1–11.

Le, Xiuning et al. 2007. "Heat Shock-Inducible Cre/Lox Approaches to Induce Diverse Types of Tumors and Hyperplasia in Transgenic Zebrafish." *Proceedings of the National Academy of Sciences of the United States of America* 104(22): 9410–15.

Lee, Tang Cheng, and David W. Threadgill. 2009. "Generation and Validation of Mice Carrying a Conditional Allele of the Epidermal Growth Factor Receptor." *Genesis* 47(2): 85–92.

Lessman, Charles A. 2009. "Oocyte Maturation: Converting the Zebrafish Oocyte to the Fertilizable Egg." *General and Comparative Endocrinology* 161(1): 53–57.

Levkowitz, G et al. 1998. "C-Cbl/Sli-1 Regulates Endocytic Sorting and Ubiquitination O the Epidermal Growth Factor Receptor." *Genes and Development* 12: 3663–74.

Li, Zhen et al. 2012. "Inducible and Repressable Oncogene-Addicted Hepatocellular Carcinoma in Tet-on Xmrk Transgenic Zebrafish." *Journal of hepatology* 56(2): 419–25.

Linggi, Bryan, and Graham Carpenter. 2006. "ErbB Receptors: New Insights on Mechanisms and Biology." *Trends in Cell Biology* 16(12): 649–56.

Livesey, F J, and C L Cepko. 2001. "Vertebrate Neural Cell-Fate Determination: Lessons from the Retina." *Nat Rev Neurosci* 2(2): 109–18.

Livet, Jean et al. 2007. "Transgenic Strategies for Combinatorial Expression of Fluorescent Proteins in the Nervous System." *Nature* 450(7166): 56–62.

Lonergan, P et al. 1996. "Role of Epidermal Growth Factor in Bovine Oocyte Maturation and Preimplantation Embryo Development in Vitro." *Biology of reproduction* 54(6): 1420–29.

Loosli, Felix et al. 2000. "A Genetic Screen for Mutations Affecting Embryonic Development in Medaka Fish (Oryzias Latipes)." *Mechanisms of Development* 97(1–2): 133–39.

Lowenstein, E. J. et al. 1992. "The SH2 and SH3 Domain-Containing Protein GRB2 Links Receptor Tyrosine Kinases to Ras Signaling." *Cell* 70(3): 431–42.

Lubzens, Esther, Graham Young, Julien Bobe, and Joan Cerdà. 2010. "Oogenesis in Teleosts: How Fish Eggs Are Formed." *General and Comparative Endocrinology* 165(3): 367–89.

Luetteke, Noreen C. et al. 1994. "The Mouse Waved-2 Phenotype Results from a Point Mutation in the EGF Receptor Tyrosine Kinase." *Genes and Development* 8(4): 399–413.

Lundberg, C, P Horellou, J Mallet, and A Bjorklund. 1996. "Generation of DOPA-Producing Astrocytes by Retroviral Transduction of the Human Tyrosine Hydroxylase Gene: In Vitro Characterization and in Vivo Effects in the Rat Parkinson Model." *Exp Neurol* 139(1): 39–53.

Lust, K. et al. 2016. "De Novo Neurogenesis by Targeted Expression of Atoh7 to Mu Ller Glia Cells."

Development (April): 1874–83.

Maklad, A et al. 2009. "The EGFR Is Required for Proper Innervation to the Skin." *J Invest Dermatol* 129(3): 690–98.

Margolis, B et al. 1990. "Tyrosine Kinase Activity Is Essential for the Association of Phospholipase C-Gamma with the Epidermal Growth Factor Receptor." *Mol.Cell Biol.* 10(2): 435–41.

Marlow, Florence L., and Mary C. Mullins. 2008. "Bucky Ball Functions in Balbiani Body Assembly and Animal-Vegetal Polarity in the Oocyte and Follicle Cell Layer in Zebrafish." *Developmental Biology* 321(1): 40–50.

Martinez-Morales, Juan Ramon et al. 2005. "Differentiation of the Vertebrate Retina Is Coordinated by an FGF Signaling Center." *Developmental Cell* 8(4): 565–74.

Maruo, T et al. 1993. "Of Epidermal Growth Factor and Its Receptor in the Human Ovary during Follicular Growth and." *Endocrinology* 132(April): 924–31.

Mayrhofer, Marie et al. 2016. "A Novel Brain Tumour Model in Zebrafish Reveals the Role of YAP Activation in MAPK/PI3K Induced Malignant Growth." *Disease Models & Mechanisms*: 15–28.

Meyer, Axel, and Yves Van De Peer. 2005. "From 2R to 3R: Evidence for a Fish-Specific Genome Duplication (FSGD)." *BioEssays* 27(9): 937–45.

Meyers, Jason R et al. 2012. "β-catenin/Wnt Signaling Controls Progenitor Fate in the Developing and Regenerating Zebrafish Retina." *Neural development* 7(1): 30.

Miettinen, P J et al. 1995. "Epithelial Immaturity and Multiorgan Failure in Mice Lacking Epidermal Growth Factor Receptor." *Nature* 376(6538): 337–41.

Moghal, Nadeem, and Paul W. Sternberg. 2003. "The Epidermal Growth Factor System in Caenorhabditis Elegans." *Experimental Cell Research* 284(1): 150–59.

Morgillo, Floriana et al. 2006. "Heterodimerization of Insulin-like Growth Factor Receptor/epidermal Growth Factor Receptor and Induction of Survivin Expression Counteract the Antitumor Action of Erlotinib." *Cancer Research* 66(20): 10100–111.

Moscatello, D K et al. 1995. "Frequent Expression of a Mutant Epidermal Growth Factor Receptor in Multiple Human Tumors." *Cancer research* 55(23): 5536–39.

Mosimann, Christian et al. 2011. "Ubiquitous Transgene Expression and Cre-Based Recombination Driven by the Ubiquitin Promoter in Zebrafish." *Development (Cambridge, England)* 138(1): 169–77.

Murata, Kenji. 2003. "Blocks to Polyspermy in Fish : A Brief Review." *32nd Joint Meeting of the United States-Japan Cooperative Program in Natural Resource (UJNR) Aquaculture Panel Meeting*: 1–15.

Nakamura, Y, C Sotozono, and S Kinoshita. 2001. "The Epidermal Growth Factor Receptor (EGFR): Role in Corneal Wound Healing and Homeostasis." *Experimental eye research* 72(5): 511–17.

Nakashima, S; Iwamatsu, T. 1989. "Ultrastructural Changes in Micropylar Cells and Formation of the Micropyle During Oogenesis in the Medaka Oryzias Latips." *Journal of Morphology* 349(202): 339–49.

Nguyen, V et al. 1999. "Morphogenesis of the Optic Tectum in the Medaka (Oryzias Latipes): A Morphological and Molecular Study, with Special Emphasis on Cell Proliferation." *The Journal of*

comparative neurology 413(3): 385–404.

Novak, U, F Walker, and a Kaye. 2001. "Expression of EGFR-Family Proteins in the Brain: Role in Development, Health and Disease." *Journal of clinical neuroscience : official journal of the Neurosurgical Society of Australasia* 8(2): 106–11.

Pang, Yefei, and Wei Ge. 2002. "Epidermal Growth Factor and TGF ‗ Promote Zebrafish Oocyte Maturation in Vitro : Potential Role of the." *Endocrinology* 143(March): 47–54.

Park, J.-Y. 2004. "EGF-Like Growth Factors As Mediators of LH Action in the Ovulatory Follicle." *Science* 303(5658): 682–84.

Pati, D et al. 1996. "Epidermal Growth Factor Receptor Binding and Biological Activity in the Ovary of Goldfish, Carassius Auratus." *American Journal of Physiology - Regulatory, Integrative and Comparative Physiology* 270(5): R1065 LP-R1072.

Patton, E Elizabeth, and Rodney S Nairn. 2010. "Xmrk in Medaka: A New Genetic Melanoma Model." *The Journal of investigative dermatology* 130(1): 14–17.

Pelicci, Giuliana et al. 2017. "A Novel Transforming Protein (SHC) with an SH2 Domain Is Implicated in Mitogenic Signal Transduction." *Cell* 70(1): 93–104.

Porazinski, Sean R, Huijia Wang, and Makoto Furutani-Seiki. 2010. "Microinjection of Medaka Embryos for Use as a Model Genetic Organism." *Journal of visualized experiments : JoVE* (46): 5–8.

Postlethwait, John et al. 2004. "Subfunction Partitioning, the Teleost Radiation and the Annotation of the Human Genome." *Trends in Genetics* 20(10): 481–90.

Procházka, Radek et al. 2000. "Developmental Regulation of Effect of Epidermal Growth Factor on Porcine Oocyte-Cumulus Cell Complexes: Nuclear Maturation, Expansion, and F-Actin Remodeling." *Molecular Reproduction and Development* 56(1): 63–73.

Ramón Martínez-Morales, Juan, Isabel Rodrigo, and Paola Bovolenta. 2004. "Eye Development: A View from the Retina Pigmented Epithelium." *BioEssays* 26(7): 766–77.

Randlett, Owen et al. 2015. "Whole-Brain Activity Mapping onto a Zebrafish Brain Atlas." *Nature Methods* 12(September): 1–12.

Rappaport, Amy, and Leisa Johnson. 2014. "Genetically Engineered Knock-in and Conditional Knock-in Mouse Models of Cancer." *Cold Spring Harbor Protocols* 2014(9): 897–911.

Raymond, Pamela A, Linda K Barthel, Rebecca L Bernardos, and John J Perkowski. 2006. "Molecular Characterization of Retinal Stem Cells and Their Niches in Adult Zebrafish." *BMC developmental biology* 6(1): 36.

Raymond, Pamela, Linda K Barthel, Rebecca L Bernardos, and John J Perkowski. 2006. "Molecular Characterization of Retinal Stem Cells and Their Niches in Adult Zebrafish." *BMC developmental biology* 6: 36.

Reinhardt, Robert et al. 2015. "Sox2, Tlx, Gli3, and Her9 Converge on Rx2 to Define Retinal Stem Cells in Vivo." *The EMBO journal* 34(11): 1572–88.

Rothschild, B Y Lord. 1954. "Polyspermy." *University of Chicago Press*.

Rotin, Daniela et al. 1992. "Presence of SH2 Domains of Phospholipase C??1 Enhances Substrate

Phosphorylation by Increasing the Affinity toward the Epidermal Growth Factor Receptor." *Journal of Biological Chemistry* 267(14): 9678–83.

Ruff-Jamison, S et al. 1993. "Epidermal Growth Factor Stimulates the Tyrosine Phosphorylation of SHC in the Mouse." *J Biol Chem* 268(11): 7610–12.

Rush, Jamie S. et al. 2012. "Endosomal Accumulation of the Activated Epidermal Growth Factor Receptor (EGFR) Induces Apoptosis." *Journal of Biological Chemistry* 287(1): 712–22.

Sakai, Yoshi T. 1961. "Method for Removal of Chorion and Fertilization of the Naked Egg in Oryzias Latipes." *Embryologia* 5(4): 357–68.

Schartl, Manfred et al. 2010. "A Mutated EGFR Is Sufficient to Induce Malignant Melanoma with Genetic Background-Dependent Histopathologies." *The Journal of investigative dermatology* 130(1): 249–58.

Schatten, G. 1994. "The Centrosome and Its Mode of Inheritance: The Reduction of the Centrosome during Gametogenesis and Its Restoration during Fertilization." *Developmental biology* 165(2): 299–335.

Schlessinger, Joseph. 2002. "Ligand-Induced, Receptor-Mediated Dimerization and Activation of EGF Receptor." *Cell* 110(6): 669–72.

Schlöndorff, J, and C P Blobel. 1999. "Metalloprotease-Disintegrins: Modular Proteins Capable of Promoting Cell-Cell Interactions and Triggering Signals by Protein-Ectodomain Shedding." *Journal of cell science* 112 (Pt 2: 3603–17.

Schweitzer, Ronen, and Ben Zion Shilo. 1997. "A Thousand and One Roles for the Drosophila EGF Receptor." *Trends in Genetics* 13(5): 191–96.

Scurry, James P. et al. 1994. "Immunoreactivity Of Antibodies To Epidermal Growth Factor, Transforming Growth Factors Alpha And Beta, And Epidermal Growth Factor Receptor In The Premenopausal Ovary." *Pathology* 26(2): 130–33.

Sherry, Maureen M, Andrew Reeves, Wu Julian K, and Brent H Cochran. 2009. "STAT3 Is Required for Proliferation and Maintenance of Multipotency in Glioblastoma Stem Cells." *Stem Cells* 27: 2383–92.

Shilo, Ben-Zion. 2005. "Regulating the Dynamics of EGF Receptor Signaling in Space and Time." *Development (Cambridge, England)* 132(18): 4017–27.

Shilo, Ben Zion. 2003. "Signaling by the Drosophila Epidermal Growth Factor Receptor Pathway during Development." *Experimental Cell Research* 284(1): 140–49.

Sibilia, M et al. 1998. "A Strain-Independent Postnatal Degeneration in Mice Lacking the EGF Receptor." *Embo J.* 17(3): 719–31.

Sibilia, Maria et al. 2007. "The Epidermal Growth Factor Receptor: From Development to Tumorigenesis." *Differentiation* 75(9): 770–87.

Sibilia, M, and E F Wagner. 1995. "Strain-Dependent Epithelial Defects in Mice Lacking the EGF Receptor." *Science* 269(5221): 234–38.

Snook, Rhonda R., David J. Hosken, and Timothy L. Karr. 2011. "The Biology and Evolution of Polyspermy: Insights from Cellular and Functional Studies of Sperm and Centrosomal Behavior

in the Fertilized Egg." *Reproduction* 142(6): 779–92.

Stemmer, Manuel et al. 2015. "CCTop: An Intuitive, Flexible and Reliable CRISPR/Cas9 Target Prediction Tool." *PLoS ONE* 10(4).

Suster, MaximilianoL. et al. 2009. "Transgenesis in Zebrafish with the Tol2 Transposon System." In *Transgenesis Techniques SE - 3*, Methods in Molecular Biology, ed. Elizabeth J Cartwright. , 41–63.

Suwa, Kaori, and Masakane Yamashita. 2007. "Regulatory Mechanisms of Oocyte Maturation and Ovulation." In *The Fish Oocyte: From Basic Studies to Biotechnological Applications*, eds. Patrick J Babin, Joan Cerdà, and Esther Lubzens. , 323–47.

Tao, Rong-Hua, and Ichi N Maruyama. 2008. "All EGF(ErbB) Receptors Have Preformed Homo- and Heterodimeric Structures in Living Cells." *Journal of cell science* 121(Pt 19): 3207–17.

Tarin, Juan J, and Antonio Cano. 2000. *Fertilization in Protozoa and Metazoan Animals*.

Teutschbein, Janka et al. 2010. "Gene Expression Analysis after Receptor Tyrosine Kinase Activation Reveals New Potential Melanoma Proteins." 4: 1–13.

Thermes, Violette et al. 2002. "I-SceI Meganuclease Mediates Highly Efficient Transgenesis in Fish." *Mechanisms of Development* 118(1–2): 91–98.

Thomas, Gareth M, and Richard L Huganir. 2004. "MAPK Cascade Signalling and Synaptic Plasticity." *Nature Reviews Neuroscience* 5(3): 173–83.

Threadgill, D W et al. 1995. "Targeted Disruption of Mouse EGF Receptor: Effect of Genetic Background on Mutant Phenotype." *Science* 269(5221): 230–34.

Todd, Levi et al. 2015. "Heparin-Binding EGF-like Growth Factor (HB-EGF) Stimulates the Proliferation of Müller Glia-Derived Progenitor Cells in Avian and Murine Retinas." *Molecular and Cellular Neuroscience*.

Trinh, Ryan, Brian Gurbaxani, Sherie L. Morrison, and Manouchehr Seyfzadeh. 2004. "Optimization of Codon Pair Use within the (GGGGS) 3 Linker Sequence Results in Enhanced Protein Expression." *Molecular Immunology* 40(10): 717–22.

Tropepe, V. 2000. "Retinal Stem Cells in the Adult Mammalian Eye." *Science* 287(5460): 2032–36.

Überall, I. et al. 2008. "The Status and Role of ErbB Receptors in Human Cancer." *Experimental and Molecular Pathology* 84(2): 79–89.

Urlinger, Stefanie et al. 2000. "Exploring the Sequence Space for Tetracycline- Dependent Transcriptional Activators : Novel Mutations Yield Expanded Range and Sensitivity." 97(14): 7963–68.

Ushiro, H., and S. Cohen. 1980. "Identification of Phosphotyrosine as a Product of Epidermal Growth Factor-Activated Protein Kinase in A-431 Cell Membranes." *Journal of Biological Chemistry* 255(18): 8363–65.

Vaughn, T J, J C Pascall, P S James, and K D Brown. 1991. "Expressionof Epidermal Growth Factor and Its mRNA in Pig Kidney, Pancreas and Other Tissues." *Biochemical Journal* 279: 315–18.

van der Veeken, J et al. 2009. "Crosstalk between Epidermal Growth Factor Receptor- and Insulin-like Growth Factor-1 Receptor Signaling: Implications for Cancer Therapy." *Curr Cancer Drug*

Targets 9(6): 748–60.

Wagner, Bettina et al. 2006. "Neuronal Survival Depends on EGFR Signaling in Cortical but Not Midbrain Astrocytes." *The EMBO journal* 25(4): 752–62.

Wallace, RA, and K Selman. 1981. "Cellular and Dynamic Aspects of Oocyte Growth in Teleosts." *Amer Zool* 21(2): 325–43.

Wan, Jin, Rajesh Ramachandran, and Daniel Goldman. 2012. "HB-EGF Is Necessary and Sufficient for Müller Glia Dedifferentiation and Retina Regeneration." *Developmental Cell* 22(2): 334–47.

Wang, Yajun, and Wei Ge. 2004. "Cloning of Epidermal Growth Factor (EGF) and EGF Receptor from the Zebrafish Ovary: Evidence for EGF as a Potential Paracrine Factor from the Oocyte to Regulate Activin/follistatin System in the Follicle Cells." *Biology of reproduction* 71(3): 749–60.

Wayne, Chad M, Heng-Yu Fan, Xiaodong Cheng, and Joanne S Richards. 2007. "Follicle-Stimulating Hormone Induces Multiple Signaling Cascades: Evidence That Activation of Rous Sarcoma Oncogene, RAS, and the Epidermal Growth Factor Receptor Are Critical for Granulosa Cell Differentiation." *Molecular endocrinology (Baltimore, Md.)* 21(8): 1940–57.

Weis, Silke, and Manfred Schartl. 1998. "The Macromelanophore Locus and the Melanoma Oncogene Xmrk Are Separate Genetic Entities in the Genome of Xiphophorus." *Genetics* 149(4): 1909–20.

Wellbrock, C et al. 1998. "Signalling by the Oncogenic Receptor Tyrosine Kinase Xmrk Leads to Activation of STAT5 in Xiphophorus Melanoma." *Oncogene* 16(23): 3047–56.

Wellbrock, Claudia et al. 2002. "Activation of p59Fyn Leads to Melanocyte Dedifferentiation by Influencing MKP-1-Regulated Mitogen-Activated Protein Kinase Signaling." *Journal of Biological Chemistry* 277(8): 6443–54.

Wellbrock, Claudia, Petra Fischer, and Manfred Scharti. 1998. "Receptor Tyrosine Kinase Xmrk Mediates Proliferation in Xiphophorus Melanoma Cells." *International Journal of Cancer* 76(3): 437–42.

Wilson, Edmund B. 1897. XXXIII Uma ética para quantos? *The Cell in Development and Inheritance*. ed. Henry F Osborn.

Wilson, Kristy J et al. 2009. "Functional Selectivity of EGF Family Peptide Growth Factors: Implications for Cancer Kristy." *Pharmacol Ther* 122(1): 1–8.

Winkler, C et al. 1994. "Ligand-Dependent Tumor Induction in Medakafish Embryos by a Xmrk Receptor Tyrosine Kinase Transgene." *Oncogene* 9(6): 1517–25.

Winnemoeller, Dirk, Claudia Wellbrock, and Manfred Schartl. 2005. "Activating Mutations in the Extracellular Domain of the Melanoma Inducing Receptor Xmrk Are Tumorigenic in Vivo." *International journal of cancer. Journal international du cancer* 117(5): 723–29.

Wittbrodt, Joachim et al. 1989. "Novel Putative Receptor Tyrosine Kinase Encoded by the Melanoma-Inducing Tu Locus in Xiphophorus." *Nature* 341(6241): 415–21.

Wolff, J A et al. 1989. "Grafting Fibroblasts Genetically Modified to Produce L-Dopa in a Rat Model of Parkinson Disease (Tyrosine." *PNAS* 86(November): 9011–14.

Xiong, Hua et al. 2009. "Inhibition of STAT5 Induces G1 Cell Cycle Arrest and Reduces Tumor Cell Invasion in Human Colorectal Cancer Cells." *Laboratory investigation; a journal of technical*

methods and pathology 89(6): 717–25.

Yarden, Y, and M X Sliwkowski. 2001. "Untangling the ErbB Signalling Network." *Nature reviews. Molecular cell biology* 2(2): 127–37.

Yefei, Pang, and G. Wei. 2002. "Epidermal Growth Factor and TGF?? Promote Zebrafish Oocyte Maturation in Vitro: Potential Role of the Ovarian Activin Regulatory System." *Endocrinology* 143(1): 47–54.

Yeh, J, G Y Lee, and E Aanderson. 1993. "Presence of Transforming Growth Factor-Alpha Messenger-Ribonucleic-Acid (Messenger-Rna) and Absence of Epidermal Growth-Factor Messenger-Rna in Rat Ovarian Granulosa-Cells, and the Effects of These Factors on Steroidogenesis Invitro." *Biology of Reproduction* 48(5): 1071–81.

Zambrowicz, B P et al. 1997. "Disruption of Overlapping Transcripts in the ROSA Beta Geo 26 Gene Trap Strain Leads to Widespread Expression of Beta-Galactosidase in Mouse Embryos and Hematopoietic Cells." *Proceedings of the National Academy of Sciences of the United States of America* 94(8): 3789–94.

Zhang, Xianrong et al. 2011. "Epidermal Growth Factor Receptor Plays an Anabolic Role in Bone Metabolism in Vivo." *Journal of Bone and Mineral Research* 26(5): 1022–34.

Zhang, Zhao et al. 2010. "Targeted Inactivation of EGF Receptor Inhibits Renal Collecting Duct Development and Function." *Journal of the American Society of Nephrology : JASN* 21(4): 573–78.

Zheng, Weiling et al. 2014. "Xmrk, Kras and Myc Transgenic Zebrafish Liver Cancer Models Share Molecular Signatures with Subsets of Human Hepatocellular Carcinoma." *PloS one* 9(3): e91179.

Zieske, James D, Hiroshi Takahashi, Audrey E K Hutcheon, and Ana C Dalbone. 2000. "Corneal Epithelial Migration AND." *Investigative Ophthalmology* 41(6): 1346–55.

VI. Acknowledgements

The last five years were an interesting journey with many ups and downs. Many people joined me on this ride, and I want to express my deep appreciation for them.

First of all, I want to thank Jochen for being my PhD-supervisor, believing in me and trusting me, for always being encouraging and motivating, for being fair and understanding and most of all for giving me the opportunity to become a scientist and a mother at the same time. I really appreciate what you did for me when you brought me back to science. Thank you!

Next, I want to thank Lázaro Centanin for being my second supervisor and permanent TAC member, for welcoming me in his starting group, homing me in the box, teaching me the "Wittbrodt Lab"-basics, for his great sense of humor, for caring and being there whenever needed. Thank you!

I also want to thank my other TAC and defense members for listening and giving feedback: Jan Felix Evers, Lucia Poggi, Steffen Lemke, Michael Boutros and Herbert Steinbeisser.

Of cause I want to thank the entire Wittbrodt and Centanin group, present and former members, for being great companions, critics, discussion-partners, team members and friends and for making the last five years good years.

Very special thanks go to my ladies from Bay 4: Katharina Lust, Clara Becker, and Alicia Perez Saturino. You three have been awesome colleagues and even better friends. Thanks so much for standing my moods during my rollercoaster-PhD, for listening, encouraging and pushing me and also for laughing and celebrating with me. You girls are the best, and it was so much fun to share the way with you and see you grow! I will miss you!

Another huge Thank You to Katha and Clara for reading, correcting and commenting my thesis! Without you, I would not have made it!

I am grateful for Clara Baader and Clara Becker, who were brave and patient enough to do their Bachelor and Master practical with me and who contributed valuable work to this thesis. I learned a lot with you and it was a great pleasure to see you develop. Weiter so!

I also want to thank all the people who did little things for me when I had to rush out to the childcare: Isa, Liz, Manuel, Alicia, Clara, Clara, Janina, Katha, Maria … you saved me!

Special thanks also to Tanja and Frederike, you are great women doing an excellent job! You were always there when I needed something be it an antibody, a document or a glass of Sekt.

For their valuable technical and scientific input and support and their companionship, I thank Narges, Thomas, Manuel, Stephan K., Lazaro, Beate, Daigo, Tina, Eva, Jan-Felix Evers, Manfred Schartl, Franz, Silvi and of cause Bay 4.

I am very grateful to the HBIGS graduate school for their training offers, career advice and family and financial support.

To all COS and especially my co-COS-PhD speakers Amaya, Borja, and Rik: it was an incredible experience to work with you and be part of the "COS-spirit." Thank you!

I feel very grateful for my family and friends, for all their love and help and for showing me what is important in life, they are the soil on which it all grew.

And last but not least I want to thank the two most important people in my live: Ricardo and Olivia (de) Carvalho. Ricardo, amongst many other things you are my true friend, you support me and help me, you are honest with me, believe in me and make me laugh; all of this was very important for this work, and I am deeply thankful to have you by my side and be the best father Olivia could wish for. Olivia, you are my sunshine, you are my life. My greatest joy is to watch you grow! I love you both with all my heart! Thank you!